Positron Annihilation Lifetime Spectroscopy Studies of Amorphous and Crystalline Molecular Materials

Dissertation

zur Erlangung des akademischen Grades
Dr. rerum naturalium (Dr. rer. nat.)

vorgelegt der
Mathematisch-Naturwissenschaftlich-Technischen Fakultät
(mathematisch-naturwissenschaftlicher Bereich)
der
Martin-Luther-Universität Halle-Wittenberg

von Frau
Dipl.-Phys. Yang Yu
geb. am 13.07.1982 in Changchun, Jilin, PR China

Gutachter:
(1) Prof. Dr. R. Krause-Rehberg (Martin-Luther-Universität Halle-Witterberg)
(2) Prof. Dr. Thurn-Albrecht (Martin-Luther-Universität Halle-Witterberg)
(3) Prof. Dr. Klaus Rätzke (Kiel Universität)

Halle (Saale), Juli 11th. 2011

Verteidigt am October 12th. 2011

Table of contents

1 Introduction

The relationship between the macroscopic properties and microscopic structure of the material is a main research topic in molecular material science. Free volume that exists due to static and dynamic disorder of the structure influences the substance properties such as viscosity [1], structure relaxation, physical aging, molecular transport [2], mobility, permeability etc. Free volume is more a geometric and descriptive concept than energetic. The combination of the free volume concept with dynamics can give a complete understanding of molecular material. So the quantitative measurement is requested to describe free volume properly, including its total amount and size, structure, distribution of its local constituents. There are several methods to detect the free volume. Among them, one of the most extensively and successfully applied techniques for determining the distribution of local free volume is the positron annihilation lifetime spectroscopy (PALS) [3, 4].

Over the past half century, the positron method plays an important role in material research, especially in defect characterization of semiconductors [5] and metals. It can investigate defect types and their relative concentrations through the analysis of the emitted γ rays coming from the annihilation of the positron with an electron with respect to their time distribution and energy or angle of emission. Depending on the analysis type, we can apply different positron measurement techniques [5], such as PALS (positron annihilation lifetime spectroscopy), DBAR (Doppler broadening of annihilation radiation), ACAR (angular correction of annihilation radiation), and special techniques such as the slow positron beam and so on.

From the "Spur" model [6, 7] and the Tao-Eldrup theory [8, 9], we obtain qualitative and quantitative information on the formation and annihilation of positronium in condensed matter and relate them to material parameters. For positron techniques applied to molecular matter, it is the lifetime of ortho-positronium, which reflects the nature of the electronic environment around it and, therefore, structural inhomogeneities and density fluctuations. Combined with other techniques such as PVT (pressure-volume-temperature) experiments, researchers try to characterize the free volume as completely as

possible. That is the aim of this work for selected molecular materials.

In this work, an effort goes to a comprehensive understanding of free volume in all structures (amorphous, crystalline, solid, liquid) of molecular material.

This thesis is subdivided into the following chapters:

In chapter 2, after a brief introduction of the definition of free volume, the focus is on the molecular properties depending on free volume. The first empirical free-space dependence of viscosity was established by Doolittle [1, 10-12]. Cohen and Turnbull [2, 13-15] deducted theoretically the relationship between molecular transport and free volume, using a hard sphere model and the assumption that molecular transport may happen when redistribution of the free volume opens up voids having a volume larger than a critical value, and the redistribution requires no energy. Molecular dynamics and ionic conductivity that have relationship with free volume are also introduced in chapter 2.

Chapter 3 presents the equation of state methods used to obtain specific free volume. The pressure-volume-temperature (PVT) experiment that supplies data for the analysis is also introduced in this chapter.

Chapter 4 exhibits the theoretical methods and molecular modeling used to calculate microscopic subnanometer scale local free (hole) volume and its size distribution.

Chapter 5 shows experimental technique to investigate local free volume: positron annihilation lifetime spectroscopy (PALS). The analysis of positron lifetime spectra and the calculation of the local free volume are revealed in this chapter.

Chapter 6 discusses the PALS experimental results of high molecular-weight organic materials: polymers. It includes the amorphous polymers 1,2-poly(butadiene) (PBD) and c-1,4-poly(isoprene) (PIP), as well as semicrystalline polymers with long self-assembled semifluorinated side chains. Other techniques such as pressure-volume-temperature (PVT), broadband dielectric spectroscopy (BDS), electron spin resonance (ESR), differential scanning calorimetry (DSC) and temperature-dependent small-angle X-ray scattering (T-SAXS) experiments are employed for comparison.

Chapter 7 represents PALS, DSC, PVT, and BDS experimental results of

ionic liquids, a class of low molecular-weight organic materials. Six samples with the same cation but different anions with different volumes are compared. Positron lifetimes in different phases (crystalline solid, amorphous supercooled and normal liquid) are explained. Systematic correlations between local free volume and molecular volume of ionic liquid particles are exhibited and discussed.

1.1 Reference

1. Doolittle, A.K., *Studies in Newtonian Flow .2. The Dependence of the Viscosity of Liquids on Free-Space.* Journal of Applied Physics, 1951. **22**(12): p. 1471-1475.
2. Cohen, M.H. and D. Turnbull, *Molecular Transport in Liquids and Glasses.* Journal of Chemical Physics, 1959. **31**(5): p. 1164-1169.
3. Dlubek, G., et al., *The free volume and its recovery in pressure-densified and CO2-swollen heterocyclic-ring-containing fluoropolymers.* Macromolecular Chemistry and Physics, 2008. **209**(18): p. 1920-1930.
4. Dlubek, G., et al., *The free volume in two untreated, pressure-densified, and CO2 gas exposed polymers from positron lifetime and pressure-volume-temperature experiments.* E-Polymers, 2007: p. -.
5. R. Krause-Rehberg, H.S.L., *Positron Annihilation in Semiconductors.* Springer Verlag: Heidelberg, 1999.
6. Mogensen, O.E., *Spur reaction model of positronium formation.* The Journal of Chemical Physics, 1974. **60**(3): p. 998-1004.
7. Tao, S., *The formation of positronium in molecular substances.* Applied Physics A: Materials Science & Processing, 1976. **10**(1): p. 67-79.
8. Tao, S.J., *Positronium Annihilation in Molecular Substances.* Journal of Chemical Physics, 1972. **56**(11): p. 5499-&.
9. Eldrup, M., D. Lightbody, and J.N. Sherwood, *The temperature dependence of positron lifetimes in solid pivalic acid.* Chemical Physics, 1981. **63**(1-2): p. 51-58.
10. Doolittle, A.K., *Studies in Newtonian Flow .3. The Dependence of the Viscosity of Liquids on Molecular Weight and Free Space (in Homologous Series).* Journal of Applied Physics, 1952. **23**(2): p. 236-239.
11. Doolittle, A.K., *Studies in Newtonian Flow .4. Viscosity Vs Molecular Weight in Liquids - Viscosity Vs Concentration in Polymer Solutions.* Journal of Applied Physics, 1952. **23**(4): p. 418-426.
12. Doolittle, A.K. and D.B. Doolittle, *Studies in Newtonian Flow .5. Further Verification of the Free-Space Viscosity Equation.* Journal of Applied Physics, 1957. **28**(8): p. 901-905.
13. Turnbull, D. and M.H. Cohen, *Free-Volume Model of Amorphous Phase - Glass Transition.* Journal of Chemical Physics, 1961. **34**(1): p. 120-&.
14. Cohen, M.H. and D. Turnbull, *Metastability of Amorphous Structures.* Nature, 1964. **203**(494): p. 964-&.
15. Turnbull, D. and M.H. Cohen, *On Free-Volume Model of Liquid-Glass Transition.* Journal of Chemical Physics, 1970. **52**(6): p. 3038-&.

2 Free volume, molecular transport and dynamics

2.1 Introduction to free volume

2.1.1 Definition

The definition of "free volume" V_f is connected with empty microscopic space that exists between molecules. Specific free volume equals the specific total volume V (cm^3/g) subtracted by the specific occupied volume, V_{occ}:

$$V_f = V - V_{occ} \qquad (2.1)$$

If we define V_{occ} as van der Waals volume V_w, that is the space occupied by a molecule, which is impenetrable to other molecules with normal thermal energies, then V_f represents the total free volume. In a crystal, this free space is well known as interstitial volume V_{fi}. In amorphous molecular material, an additional or excess free volume appears in form of irregularly subnanometer size local free volumes due to the structural disorder. This decreases the density of the material by about 10% compared with the corresponding crystal. These local free volumes are frequently termed "holes". They form the hole free volume, which can be calculated from Eq. (2.1). $V_{fh} \equiv V_f = V - V_{occ}$, here V_{occ} involves now not only the van der Waals volume but also the interstitial free volume, $V_{occ} = V_W + V_{fi}$. The hole free volume governs the diffusion of small molecules through molecular materials and also the molecular mobility [1, 2]. The occupied volume corresponds closely to the crystalline volume, $V_{occ} \approx V_c \approx$ 1.45 V_W [3].

The van der Waal volume can be calculated following Bondi's method [4].The calculation requires the knowledge of the size of each atom in a molecule as well as the bond length, angles etc. to take into account the overlap of atoms covalently bound for forming the molecular unit. Van Krevelen compiled tables of the contributions of many common polymer groups of V_w [3].

The subnanometer scale local free (hole) volume can be defined as follows:

$$V_f = v_h \times N_h{}' \qquad (2.2)$$

where $N_h{}'$ (unit g^{-1}) is the specific hole number density and v_h is the average hole volume.
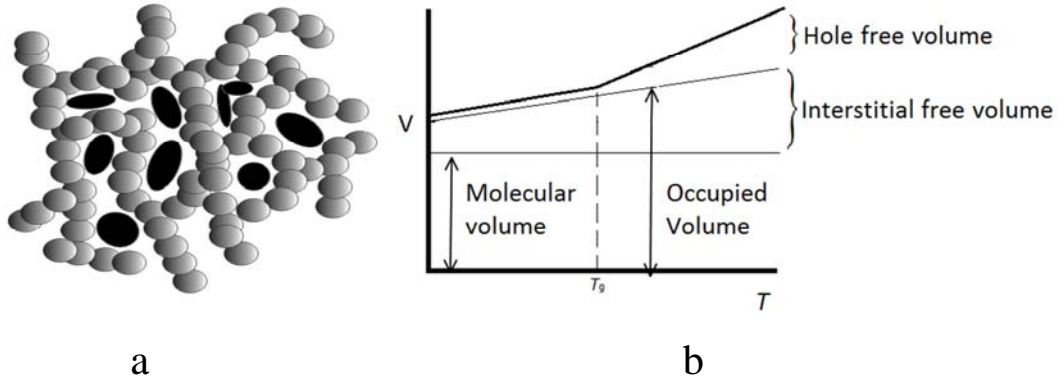
Figure 2.1 Schematic representation of a. hole volume (black ellipsoids) concept; and b. respective volumes.

Another parameter required in free volume concept is the (hole) free volume fraction (denoted as *f* or *h*):

$$h = V_f/V \tag{2.3}$$

with
$$y = 1 - h \tag{2.4}$$

is the corresponding occupied fraction.

For a point-like probe, the local free volume does not appear as discrete individual holes, but is continuous with strong local fluctuations in size, shape and number density of the local free spaces (compare Figure 2.1a). It can be modeled by individual holes connected by narrow channels, for example. Probe atoms of finite size such as the positronium atom or gas atoms can be localized in a single hole. Then the free volume appears as a sum of isolated holes.

2.1.2 Simha-Boyer model

The Simha-Boyer [5] model is a way to describe and classify the free volume and the occupied volume. It is based on an iso-free volume model [6]. As seen from Figure 2.2, below and above glass transition temperature T_g, the specific volume linearly expands with temperature. The expansion coefficient jumps at T_g. So we can write the specific volume changes with temperature as follows:

$$V_g(T) = V_g(0) + \eta_g \times T \quad T < T_g \tag{2.5}$$

$$V_r(T) = V_r(0) + \eta_r \times T \quad T > T_g \tag{2.6}$$

where $V_g(0)$ and $V_r(0)$ are the volume of $V_g(T)$ and $V_r(T)$ extrapolated to absolute 0 K. $\eta_g = (\partial V/\partial T)_{T<T_g}$ and $\eta_r = (\partial V/\partial T)_{T>T_g}$ are expansivities of glass and rubbery phase, respectively. In this model, $V_r(0)$ is the hypothetical

occupied volume at absolute 0 K. And the free volume is $\Delta V_g(0) = V_g(0) - V_r(0) = V_g(T_g) - V_r(T_g) = \Delta V_g(T_g)$, which means the free volume doesn't change below T_g. So the expansion of the specific volume is mainly due to the occupied volume. That is due to inharmonic oscillations of the chains as in crystalline materials. When the temperature is higher than T_g, the expansion of the specific volume is mainly determined by the free volume. That's due to the movement of chain segments, which is 'frozen' at glassy state. The expansivity is assumed to be the same for the occupied volume in the whole temperature range.
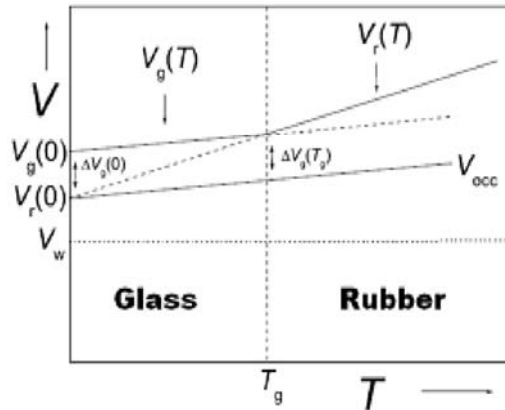
Figure 2.2 Simha-Boyer model of expansion of an amorphous polymer with temperature.

In this model, a relationship between the coefficient of cubical expansion for a 100% amorphous polymer $\alpha = \eta/V$ and T_g is also established:

$$(\alpha_r - \alpha_g) \times T_g = K_1 \tag{2.7}$$

$$\alpha_r \times T_g = K_2 \tag{2.8}$$

where $K_1 = 0.113$ and $K_2 = 0.164$ [5] are constant for a wide variety of polymers differing in cohesive energy density, chain stiffness and geometry.

2.2 Free volume dependency of molecular liquid properties

Free volume appears due to the structural, static and dynamic disorder. It has important influence on molecular properties, such as viscosity [7-10], molecular transport [1, 2, 11], structural relaxation and physical aging. Fox and Flory [12, 13] attributed the glass transition to the falling of the free volume below some critical value.

2.2.1 Viscosity of molecular liquids

Vogel-Fulcher-Tammann (VFT) equation

The famous empirical VFT equation is first proposed by Vogel [14], later applied in various liquids by Tammann, Hesse [15] and Fulcher [16]. The VFT equation connects viscosity with temperature.

$$\ln \eta = A + \frac{B}{T-T_0} \qquad (2.9)$$

η represents the viscosity of the fluid in question; T is the temperature; A, B and T_0 (the Vogel temperature) are constants. The VFT equation is not only applied in viscosity, but also in molecular dynamics.

Doolittle

Doolittle connects the free volume with the viscosity of molecular liquids [7]:

$$\eta = A \times e^{B/(v_f/v_0)}, \text{ or } \ln\eta = B(v_0/v_f) + \ln A \qquad (2.10)$$

here, η is the coefficient of viscosity; v_f/v_0 is the relative free space for a single substance; A and B are constants for a single substance.

The idea behind his work is that the resistance to flow in a liquid depends upon the relative volume of molecules present per unit of free-space.

Doolittle compared the viscosity relationship of the free volume with that of the temperature. He concluded that the relative free-space is the direct variable, instead of absolute temperature, that defines the viscosity of molecular liquids as precisely as the accuracy of the measurements themselves.

2.2.2 Molecular transport

Cohen-Turnbull

Cohen and Turnbull [1, 2, 11, 17] gave a theoretical deduction of the free volume influence of the transport property in liquids. They assumed a hard sphere model and treated diffusion as translation of a molecule across the void within its cage, not as a result of activation but rather as a result of redistribution of the free volume within the liquid. Their basic ideas are: molecular transport may occur only when voids having a volume greater than some critical value v^* formed by the statistical redistribution of the free volume, and no energy is required for free volume redistribution. Based on these ideas they obtained an expression which relates the diffusion constant with the free volume (in this work, the free volume is in fact microscopic

volume in subnanometer scale):

$$D = ga^*u \, exp[-(\gamma v^*)/v_f]$$ (2.11)

here: D is the diffusion constant; g is a geometrical factor; a^* is approximately equal to the molecular diameter; u is the average speed of molecules; γ is constant for a single substance and has a physical meaning that represents the overlap of free volume, so its value limits from 0.5 to 1; v^* is the minimum required volume of the void; v_f is the average free volume for one molecule.

Cohen and Turnbull fitted this equation for several van der Waals liquids (carbon tetrachloride; 2,3-dimethylbutane; 2,2-dimethylbutane and i-butyl bromide) [1], and the magnitudes of the constants are reasonable in all cases: the critical void v^* is near the van der Waals volume v_0. For the two limits of the γ values: $\gamma = 1$, $0.66v_0 \leq v^* \leq 0.86v_0$; $1.32v_0 \leq v^* \leq 1.7v_0$ with $\gamma = 1/2$. For liquid metals (Na, Hg, Ag, Pb, Sn, In, Ga), v^* is in most cases near the volume of the ion core.

They also draw a conclusion: liquid and glassy states together comprise a single thermodynamically well-defined phase and glass transition results ideally from the freezing out of free volume [17].

If the free volume is assumed to have a linear expansion with temperature, one obtains the VFT equation from the Cohen-Turnbull theory.

2.2.3 Molecular dynamics

Williams-Landel-Ferry (WLF) equation

The empirical WLF equation was derived by Williams, Landel and Ferry [18]:

$$\ln\alpha_T = \frac{-c_1^r(T-T_r)}{(c_2^r + T - T_r)}$$ (2.12)

T is the temperature; α_T is the ratio of the mechanical or dielectric relaxation times (τ) at temperature T to their values at a reference temperature T_r, so $\alpha_T = \tau_T/\tau_{T_r}$; c_1^r, c_2^r and c are constants. The WLF equation (2.12) is equivalent to VFT equation (2.9) with $c_2^r = T_r - T_0$ and $c_1^r = B/c_2^r$.

If T_r lies about 50 K above the glass transition temperature T_g, over a temperature range of $T_r \pm 50$, $c_1^r = 8.86$, $c_2^r = 101.6$. This applies to a wide variety of polymers, polymer solutions, organic glass-forming liquids and

inorganic glasses. If, alternatively, the reference temperature is chosen as T_g, then $c_1^r = 17.44$, $c_2^r = 51.6$. Above $T_r + 50$ (or $T_g + 100$) the equation fails because different systems show specific properties such as apparent activation energy, which are no longer dominated by the non-specific behavior associated with supercooling and vitrification.

By modification of Doolittle's free-space equation for viscosity and relating it with the WLF equation, they obtained:

$$\log \alpha_T = \left(\frac{1}{2.303}\right)\left(\frac{1}{f} - \frac{1}{f_g}\right) \tag{2.13}$$

here, f_g is the fractional free volume at T_g. Substitution of $f = f_g + \alpha_2(T - T_g)$ in (2.13), α_2 is the thermal expansion coefficients, yields:

$$\log \alpha_T = \left(\frac{T - T_g}{2.303 f_g}\right) / \left(\frac{f_g}{\alpha_2} + T - T_g\right) \tag{2.14}$$

which is identical with (2.12), by comparing the constants: $\alpha_2 = 4.8 \times 10^{-4}$ K^{-1} and $f_g = 0.025$. Both values are in good agreement with experiment result.

They concluded that temperature dependence of properties in supercooled, glass-forming liquids arises from the fact that the rates of all such processes depend on temperature primarily through their dependence on free volume.

2.2.4 Ionic conductivity

The relationship of the ionic conductivity with the free volume has been researched extensively [19-22].

Using the Nernst-Einstein conductivity-diffusion equation:

$$\sigma = \frac{nq^2 D}{kT} \tag{2.15}$$

where n is the concentration of charge carriers and q the charge; k and T are Boltzmann constant and absolute temperature, respectively. D is the diffusion coefficient and can be substituted by the Cohen-Turnbull equation (2.11):

$$\sigma = \frac{nq^2 ga^* u}{kT} exp[-(\gamma v^*)/v_f] \tag{2.16}$$

From the kinetic theory, u, which represents the molecular average speed, varies as $\sqrt{T}$, and the remaining terms are temperature independent or the dependence can be neglected compared with free volume change, so:

$$\sigma = \frac{C}{\sqrt{T}} exp[-(\gamma v^*)/v_f] \tag{2.17}$$

Bamford et al. [19] compared the relationship between ionic conductivity and free volume from positron annihilation spectroscopy of two polymeric samples: neat poly[(ethylene glycol)$_{23}$dimethacrylate][poly((EG)$_{23}$DMA)] and the same polymer doped with 0.6 mol/kg LiCF$_3$SO$_3$. The result is shown in Figure 2.3:
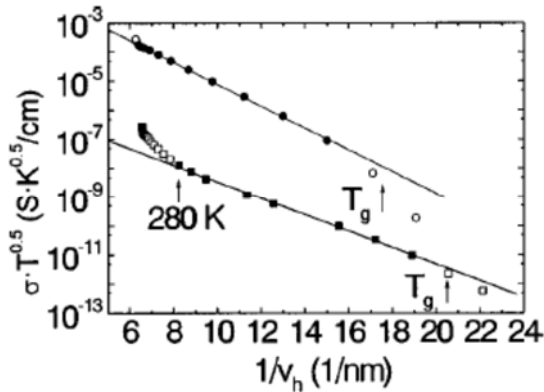

Figure 2.3 Variation of $\sigma T^{0.5}$ with the reciprocal mean local free volume $1/v_h$ in doped (circles with 0.6 mol/kg LiCF$_3$SO$_3$) and pure (squares) poly[(EG)$_{23}$DMA] [19].

From equation (2.17), $\sigma T^{0.5}$ should have a linear dependence with $1/v_h$. The experiment has a perfect agreement with the conduction - free volume relationship (2.17) in the temperature range 250 K to 350 K for the doped sample and 240 K to 285 K for the pure sample. Actually the high temperature limit is the knee temperature T_k for positron annihilation lifetime spectroscopy, at which the positron lifetime no longer represents the local free volume correctly because of the high vibration of segmental movement of the polymer. But if we employ the total free volume from pressure-volume-temperature experiment, we could obtain the conclusion that the local free volume increases linearly with temperature as the range below the knee temperature, so when we extrapolate the hole volume above knee temperature, the agreement between experiment and equation (2.17) is still valid as figure 2.4 [20] shows. In this case, the free volume relationship of the conductivity has a larger valid temperature range than the temperature relationship from the Vogel-Tamman-Fulcher equation [14-16].

The low temperature limit is around the glass transition of the polymer, since the Cohen-Turnbull theory considers the diffusion as the result of redistribution of free volume, which only happens in liquids. So after the glass transition, equation (2.17) is no longer valid.
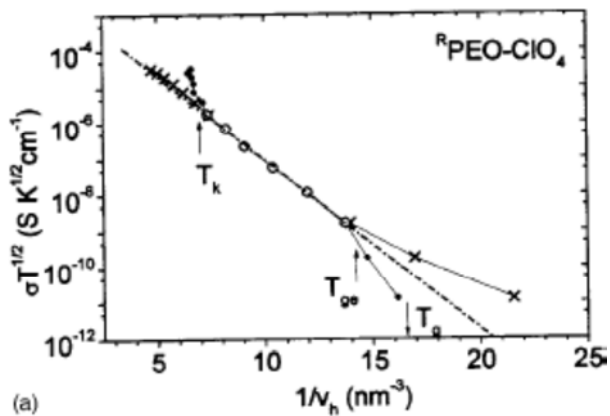
Figure 2.4 Variation of $\sigma T^{0.5}$ with the reciprocal mean local free volume $1/v_h$ in poly(ethylene oxide) doped with LiClO$_4$. Dash-dotted line: Cohen-Turnbull fit. Crosses: v_h as obtained from extrapolation of the linear fit in the range T<T$_k$. [20]

2.3 Reference

1. Cohen, M.H. and D. Turnbull, *Molecular Transport in Liquids and Glasses.* Journal of Chemical Physics, 1959. **31**(5): p. 1164-1169.
2. Turnbull, D. and M.H. Cohen, *Free-Volume Model of Amorphous Phase - Glass Transition.* Journal of Chemical Physics, 1961. **34**(1): p. 120-&.
3. Krevelen, D.v., *Properties of polymers, their estimation and correlation with chemical structure.* 2nd ed. 1976: Elsevier, Amsterdam-Oxford-New York.
4. Bondi, A., *van der Waals Volumes and Radii.* The Journal of Physical Chemistry, 1964. **68**(3): p. 441-451.
5. Simha, R. and R.F. Boyer, *On a General Relation Involving the Glass Temperature and Coefficients of Expansion of Polymers.* The Journal of Chemical Physics, 1962. **37**(5): p. 1003-1007.
6. Thomas G. Fox, J. and P.J. Flory, *Second-Order Transition Temperatures and Related Properties of Polystyrene. I. Influence of Molecular Weight.* Journal of Applied Physics, 1950. **21**(6): p. 581-591.
7. Doolittle, A.K., *Studies in Newtonian Flow .2. The Dependence of the Viscosity of Liquids on Free-Space.* Journal of Applied Physics, 1951. **22**(12): p. 1471-1475.
8. Doolittle, A.K., *Studies in Newtonian Flow .3. The Dependence of the Viscosity of Liquids on Molecular Weight and Free Space (in Homologous Series).* Journal of Applied Physics, 1952. **23**(2): p. 236-239.
9. Doolittle, A.K., *Studies in Newtonian Flow .4. Viscosity Vs Molecular Weight in Liquids - Viscosity Vs Concentration in Polymer Solutions.* Journal of Applied Physics, 1952. **23**(4): p. 418-426.
10. Doolittle, A.K. and D.B. Doolittle, *Studies in Newtonian Flow .5. Further Verification of the Free-Space Viscosity Equation.* Journal of Applied Physics, 1957. **28**(8): p. 901-905.
11. Turnbull, D. and M.H. Cohen, *On Free-Volume Model of Liquid-Glass Transition.* Journal of Chemical Physics, 1970. **52**(6): p. 3038-&.
12. Flory, P.J. and T.G. Fox, *Treatment of Intrinsic Viscosities.* Journal of the American Chemical Society, 1951. **73**(5): p. 1904-1908.
13. Fox, T.G. and P.J. Flory, *The Glass Temperature and Related Properties of Polystyrene - Influence of Molecular Weight.* Journal of Polymer Science, 1954. **14**(75): p. 315-319.
14. Vogel, H., *Temperatur-abhängigkeitsgesetz der Viscosität von Flüssigkeiten (The law of Temperature Dependence of the Viscosity of Fluids).* Phys. Z., 1921. **22**: p. 645.
15. Tammann, G. and W. Hesse, *Die Abhängigkeit der Viscosität von der Temperatur bie unterkühlten Flüssigkeiten.* Zeitschrift für anorganische und allgemeine Chemie, 1926. **156**(1): p. 245-257.
16. Fulcher, G.S., *ANALYSIS OF RECENT MEASUREMENTS OF THE VISCOSITY OF GLASSES.* Journal of the American Ceramic Society, 1925. **8**(6): p. 339-355.
17. Cohen, M.H. and D. Turnbull, *Metastability of Amorphous Structures.* Nature, 1964. **203**(494): p. 964-&.
18. Williams, M.L., R.F. Landel, and J.D. Ferry, *The Temperature Dependence of Relaxation Mechanisms in Amorphous Polymers and Other Glass-forming Liquids.* Journal of the American Chemical Society, 1955. **77**(14): p. 3701-3707.
19. Bamford, D., et al., *The local free volume, glass transition, and ionic conductivity in a polymer electrolyte: A positron lifetime study.* Journal of Chemical Physics, 2001. **115**(15): p. 7260-7270.
20. Bamford, D., et al., *Ionic conductivity, glass transition, and local free volume in poly(ethylene oxide) electrolytes: Single and mixed ion conductors.* Journal of Chemical Physics, 2003. **118**(20): p. 9420-9432.
21. Bendler, J.T., J.J. Fontanella, and M.F. Shlesinger, *A New Vogel-Like Law: Ionic Conductivity, Dielectric Relaxation, and Viscosity near the Glass Transition.* Physical Review Letters, 2001. **87**(19): p. 195503.
22. Bendler, J.T., et al., *The need to reconsider traditional free volume theory for polymer electrolytes.* Electrochimica Acta, 2003. **48**(14-16): p. 2267-2272.

3 Free volume from the equation of state

3.1 Introduction

The free volume has an influential relation with molecular material properties. It is important to obtain accurate value of the free volume. It can be calculated from fitting the pressure-volume-temperature (PVT) experiment data from equation of state. When dealing with gas molecular problem, we use the ideal gas equation of state: pV=nRT. While the pressure increases and the temperature decreases, the ideal equation is no longer valid. We need a modification. Then comes the van der Waals equation, which includes two parameters concerning only the substance. We can get them from the fitting of the equation of state with PVT data. This method is also applied in liquids to characterize physical properties and calculate the free volume.

3.2 Tait equation

The empirical Tait equation is extensively used to fit volume data over a wide pressure and temperature range with good accuracy [1-5]. The form is:

$$V_s(P,T) = \frac{1}{\rho(P,T)} = \frac{1}{\rho(P_0,T)}\left(1 - C\ln(1 + \frac{P}{B(T)})\right) \tag{3.1}$$

$$\frac{1}{\rho(P_0,T)} = a_0 + a_1 \times T + a_2 \times T^2 \tag{3.2}$$

$$B(T) = b_0 \times \exp(-b_1 \times T) \tag{3.3}$$

here: V_s is the specific volume that represents the volume of unit mass, so it is the reverse of density ρ; P and T are pressure and temperature respectively; C, a_0, a_1, a_2, b_0, and b_1 are six parameters that need to be fitted from pressure-volume-temperature experiment. When the parameters are known, the equation can be used to interpolate or extrapolate the volume data. The thermal expansion and isothermal compressibility can be obtained from the relations:

$$\alpha_p = \left(\frac{\partial \ln V_s(P,T)}{\partial T}\right)_P = \frac{a_1 + 2a_2 T}{a_0 + a_1 \times T + a_2 \times T^2} - \frac{b_1 \times C \times P}{(B(T)+P)\times(1-\ln(1+P/B(T)))} \tag{3.4}$$

$$\beta_T = -\left(\frac{1}{V_s}\right)\left(\frac{\partial V_s}{\partial P}\right)_T = \left\{(P+B)\left[\frac{1}{C} - \ln\left(1 + \frac{P}{B}\right)\right]\right\}^{-1} \tag{3.5}$$

3.3 The Sanchez-Lacombe equation of state

Sanchez and Lacombe established an elementary molecular theory of

classical fluids [6]. The model fluid is reduced to classical lattice gas, characterized as an Ising or lattice fluid. So this theory is also called lattice fluid (LF) theory. A mean field approximation is used in this model. As illustrated in figure 3.1, the fluid is modeled as a system of N molecules each occupied r sites (r-mer) and N_0 vacant lattice sites (holes). So the total number of lattice sites is $N_r = N_0 + rN$. Introducing the coordination number of the lattice z, the symmetry number σ, the flexibility parameter δ, which is a measure of internal degrees of freedom, the number of configurations can be calculated:

$$\Omega = (\tfrac{\delta}{\sigma})^N \frac{N_r!}{N_0!N!} (\frac{N_q!}{N_r!})^{z/2} \tag{3.6}$$

Using Sterling's approximation: $n! \cong (n/e)^n$ results in:

$$\lim_{z\to\infty} \Omega = (\tfrac{1}{f_0})^{N_0} (\tfrac{\omega}{f})^N \tag{3.7}$$

here, $\omega = \delta r / \sigma e^{r-1}$; $f_0 = N_0/N_r$, is the empty site fraction; $f = rN/N_r$, is the fraction of occupied sites.

The lattice (potential) energy is:

$$E = -N_r(z\epsilon/2)f^2 \tag{3.8}$$

Define closely packed volume $V^* = N(rv^*)$, here v^* represents the site volume of a mer/hole. The volume of the system $V = (N_0 + rN)v^* = N_r v^* = V^*/f$. So:

$$E/rN = -\epsilon^*(V^*/V) = -\epsilon^* f \tag{3.9}$$

where, $\epsilon^* \equiv z\epsilon/2$, ϵ is the nonbonded, mer-mer interaction energy.

Now we can get the configurational partition function:

$$Z(T,P) = \sum_{N_0}^{\infty} \Omega \exp[-\beta(E + PV)] \tag{3.10}$$

And Gibbs free energy G:

$$G = -kT\ln Z(T,P) = E + PV - kT\ln\Omega \tag{3.11}$$

Using (3.7) and (3.9), reducing variables dimensionless and minimizing the value of free energy, the Sanchez-Lacombe equation of state is presented as:

$$\tilde{\rho}^2 + \tilde{P} + \tilde{T}[\ln(1 - \tilde{\rho}) + (1 - 1/r)\tilde{\rho}] = 0 \tag{3.12}$$

here: $\tilde{\rho} = 1/\tilde{v}$, $\tilde{T}$, $\tilde{P}$, $\tilde{v}$ and $\tilde{\rho}$ are reduced temperature, pressure, volume and density, $\tilde{T} \equiv T/T^*$, $T^* \equiv \epsilon^*/k$; $\tilde{P} \equiv P/P^*$, $P^* \equiv \epsilon^*/v^*$; $\tilde{v} \equiv 1/\tilde{\rho} \equiv V/V^*$, $V^* \equiv N(rv^*)$.
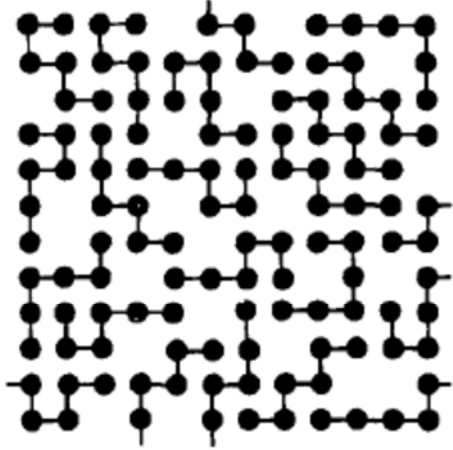
Figure 3.1 Two-dimensional example of a pure lattice fluid. Hexamers are distributed over the lattice, but not all sites are occupied. The fraction of sites occupied is denoted by $\tilde{\rho}$ [7].

In the Sanchez-Lacombe equation of state, the microscopic parameters which have specific physical meanings are connected with the macroscopic parameters P and T. In fact the model fluid can be completely characterized by three molecular parameters: ϵ^*, v^* and r. They correspond to T^*, P^* and ρ^*. The molecular weight M relates to the scale factors and r by:

$$RT^*\rho^*/P^* = v^*\rho^* = M/r \tag{3.13}$$

$$P^*v^*/RT^* = 1 \tag{3.14}$$

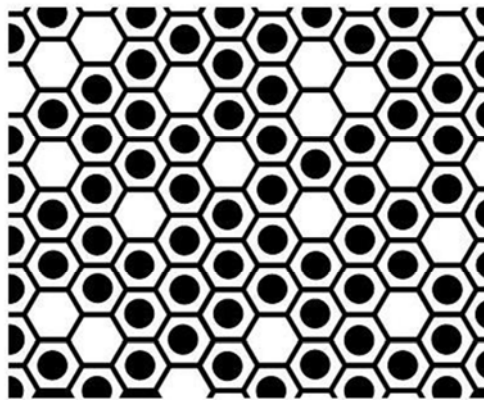## 3.4 The Simha-Somcynsky lattice-hole theory

Figure 3.2 Illustration of the lattice-hole model and arrangement of occupied as well as unoccupied cells in the Simha-Somcynsky equation of state theory [8].

The lattice-hole model of S-S eos (Simha-Somcynsky equation of state) theory [9, 10] describes the liquid as randomly distributed equal size molecules in a periodic lattice. Figure 3.2 illustrates the lattic-hole model and shows the arrangement of occupied as well as unoccupied cells in the theory. Each lattice point (cell) has 12 next neighbors and is statistically occupied with a fraction of y<1 segments (s-mers) [8]. The occupied cell is composed by van der Waals volume of the s-mers (V_w, filled circles) and empty volume inherent to packing of molecules (interstitial free volume V_{fi}). So the occupied volume can be

presented as: $V_{occ} = yV = V_w + V_{fi}$. The empty cells appear as vacancies with a typical size of 30 – 60 Å^3 and form the excess free volume: $V_f = hV$, where *h=1-y*.

We assume the occupied lattice-site fraction *y* being expressed as a function of specific volume *V* and temperature *T*: $y = y(V, T)$. Then the configurational or Helmholtz free energy *F* is a function of specific volume *V*, temperature *T* and occupied volume fraction *y*: $F = F(V, T, y)$

When the S-S theory is applied in polymers, we assume there are *N* macromolecules. Each macromolecule consisting of a number of *n* chemical repeat units, *n*-mers, with unit molecular weight M_{rep}, is divided into equivalent segments *s*-mers (the cells shown in Figure 3.2), with cell molecular weight M_0, so $sM_0 = nM_{rep}$. Then another equation of the occupied volume fraction *y* is: $= sN/(sN + N_h^{SS})$. sN is the cell number that occupied randomly by *s*-mers, $sN + N_h^{SS}$ is the number of total cell sites that is available. So N_h^{SS} is the number of unoccupied lattice sites of the S-S theory. The unoccupied fraction is denoted by $h = 1 - y$, it's also a function of *V* and *T*: $h = h(V, T)$.

From statistical thermodynamics, the configurational free energy is: $F = -k_B T ln(Z)$, where *Z* is the partition function of the system. Then we can get the first equation of state from the relationship between pressure and Helmholtz free energy $P = -(\partial F/\partial V)_T$:

$$\tilde{P}\tilde{V}/\tilde{T} = [1 - \eta]^{-1} + 2yQ^2(AQ^2 - B)/\tilde{T} \qquad (3.15)$$

where $Q = (y\tilde{V})^{-1}$ and $\eta = 2^{1/6}yQ^{1/3}$ are dimensionless quantities, *A*=1.011 and *B*=1.2045. $\tilde{P}$, $\tilde{V}$ and $\tilde{T}$ are reduced variables: $\tilde{P} = P/P^*$, $\tilde{V} = V/V^*$, $\tilde{T} = T/T^*$, where *P**, *V**, and *T** are characteristic scaling parameters:

$$P^* = \frac{zq\varepsilon^*}{sv^*} \qquad (3.16a)$$

$$T^* = \frac{zq\varepsilon^*}{Rc} \qquad (3.16b)$$

$$V^* = \frac{v^*}{M_0} \qquad (3.16c)$$

here: *s* is the number of segments per chain of molar mass *M*; 3*c* is the number of external degrees of freedom per chain; M_0 is the segmental molar mass *M/s*; *v** is the molar repulsion volume of segments; ε^* is the molar attraction energy between segments; *qz=s(z-2)+2* is the number of intermolecular contacts, *z* equals 12 in this model. Furthermore, by eliminating:

$$\frac{P^*V^*}{RT^*} = \left(\frac{1}{M_0}\right)\left(\frac{c}{s}\right) \tag{3.17}$$

By minimizing the Helmholtz free energy with respect to y, $(\partial F/\partial y)_{V,T} = 0$, assuming for polymers $s \to \infty$ and a flexibility ratio of $s/3c = 1$, we get the second equation of state:

$$[1 + y^{-1}\ln(1-y)] = [y(2^{1/2}y\tilde{V})^{-1/3} - 1/3] \times [1 - y(2^{1/2}y\tilde{V})^{-1/3}]^{-1} +$$

$$\frac{y}{6\tilde{T}}[2.409(y\tilde{V})^{-2} - 3.033(y\tilde{V})^{-4}] \tag{3.18}$$

By pressure-volume-temperature (PVT) experiments, which will be described in detail in the next section, we apply a pressure P at a temperature T, and measure the specific volume V. Substituting these values in the coupled equations (3.17) and (3.18), in theory, we can solve the y value. Then the occupied volume: $V_{occ}=yV$, and the free volume: $V_f=V-V_{occ}=hV=(1-y)V$ can be obtained. But since the form of the two equations is complicated, in practice, we use other simplified method to determine the y value [11].

It was shown that both S-S equations may be replaced in the temperature and pressure ranges $\tilde{T}$ = 0.016 to 0.071 and $\tilde{P}$ = 0 to 0.35 by the universal interpolation expression [11]:

$$\ln\tilde{V}(P,T) = a_0 + a_1\tilde{T}^{3/2} + \tilde{P}[a_2 + (a_3 + a_4\tilde{P} + a_5\tilde{P}^2)\tilde{T}^2] \tag{3.19}$$

where a_0 = -0.10346, a_1 = 23.854, a_2 = -0.1320, a_3 = -333.7, a_4 =1032.5, and a_5 = -1329.9. The usual way of analysis is to fit equation (3.19) to the experimental data from PVT experiments in the temperature range $T > T_g$ to obtain the scaling parameters V^*, T^*, and P^*. With the scaling parameters and the known specific volume V one can calculate the fractions of occupied sites, y, and hole sites, h = 1- y, from a numerical solution of equation (3.18). We remark that for the zero pressure equation (3.19) modifies to the simple expression $\ln(V/V^*) = a_0 + a_1(T/T^*)^{3/2}$.

3.5 Pressure-volume-temperature (PVT) experiment

In this work PVT experiments [4, 12] are applied to determine the temperature and pressure dependence of the specific volume. These data are analysed by the Tait, Simha-Somcynsky and Sanchez-Lacombe equation of state in order to estimate the fraction of free volume holes, h, and the specific hole free volume, $V_{fh} \equiv V_f = hV_{sp}$. These data will be correlated with the local free volume from positron annihilation lifetime spectroscopy and the number

density of holes is determined. This approach was first employed by the Cleveland group and their guests [13-17], later used by Maurer and co-workers [18, 19] and our group in Halle [3, 20, 21]. In this work, PVT experiment data were supplied by Dr. J. Pionteck (Leibniz-Institut für Polymerforschung Dresden e.V.) and Dirk Pfefferkorn from the Institute of Chemistry of the Martin-Luther-University Halle-Wittenberg.

The PVT experiments were carried out by means of a fully automated GNOMIX high pressure mercury dilatometer [22]. Figure 3.3 shows a scheme of the machine. The apparatus is described in detail in Ref. [23, 24]. The principle of the GNOMIX-PVT apparatus is the confining fluid technique. In this technique the material studied is surrounded by a confining fluid, which ensures that the material is under hydrostatic pressure at all times. The apparatus is able to collect PVT data in the range from 10 MPa to 200 MPa in typical increments of 10 MPa, and from room temperature up to 400 °C. In the isothermal standard runs the values for 0 MPa (actually the value for atmospheric pressure) are obtained by extrapolation of the values for 10 MPa to 30 MPa in steps of 1 MPa according to the Tait equation for each temperature using the standard PVT software [23].
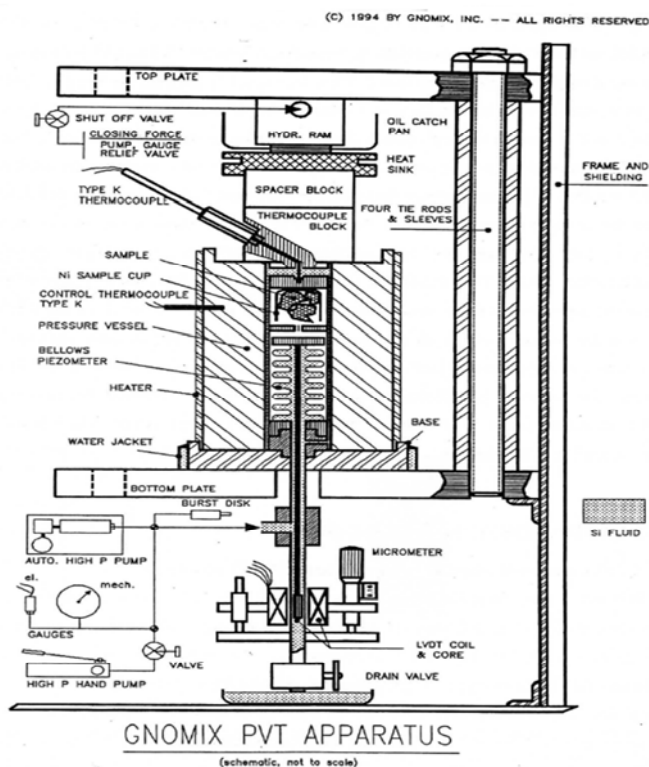

Figure 3.3 Schematic representation of a Gnomix machine for PVT-measurements. For details see Refs. [22-24].

While the accuracy limit for the absolute values of the specific volume is within 0.002 cm^3/g (above 240°C 0.004 cm^3/g), volume changes as small as 0.0002 cm^3/g can be resolved reliably. For the measurements, mercury is used as the confining fluid. About 1.5 mL of the material embedded in a nickel foil cup was used for the PVT studies. The nickel cup ensures that the material does not stick to the wall of the cell and that at all times the hydrostatic pressure is maintained on the sample [25]. The overall volume of the sample cell is about 7.1 cm^3.

To evaluate the PVT data it is necessary to know the specific volume of the material at ambient conditions, which is normally determined pycnometrically. In this work a Helium pycnometer is usually used.

3.6 Reference

1. Dymond, J.H. and R. Malhotra, *The Tait equation: 100 years on.* International Journal of Thermophysics, 1988. **9**(6): p. 941-951.
2. Dymond, J.H., et al., *(p, [varrho], T) of n-heptane, toluene, and oct-1-ene in the range 298 to 373 K and 0.1 to 400 MPa and representation by the Tait equation.* The Journal of Chemical Thermodynamics, 1988. **20**(5): p. 603-614.
3. Dlubek, G., et al., *Temperature and pressure dependence of the free volume in the perfluorinated polymer glass CYTOP: A positron lifetime and pressure-volume-temperature study.* Journal of Polymer Science Part B-Polymer Physics, 2007. **45**(18): p. 2519-2534.
4. Machida, H., Y. Sato, and R.L. Smith, *Pressure-volume-temperature (PVT) measurements of ionic liquids ([bmim(+)] [PF6-], [bmim(+)][BF4-], [bmim(+)][OcSO(4)(-)]) and analysis with the Sanchez-Lacombe equation of state.* Fluid Phase Equilibria, 2008. **264**(1-2): p. 147-155.
5. Tome, L.I.N., et al., *Measurements and correlation of high-pressure densities of imidazolium-based ionic liquids.* Journal of Chemical and Engineering Data, 2008. **53**(8): p. 1914-1921.
6. Sanchez, I.C. and R.H. Lacombe, *Elementary Molecular Theory of Classical Fluids - Pure Fluids.* Journal of Physical Chemistry, 1976. **80**(21): p. 2352-2362.
7. Sanchez, I.C. and R.H. Lacombe, *Statistical Thermodynamics of Polymer-Solutions.* Macromolecules, 1978. **11**(6): p. 1145-1156.
8. Dlubek, G., D. Kilburn, and M.A. Alam, *Temperature and pressure dependence of alpha-relaxation and free volume in poly(vinyl acetate).* Macromolecular Chemistry and Physics, 2005. **206**(8): p. 818-826.
9. Simha, R. and Somcynsk.T, *On Statistical Thermodynamics of Spherical and Chain Molecule Fluids.* Macromolecules, 1969. **2**(4): p. 342-&.
10. Simha, R., *Configurational Thermodynamics of the Liquid and Glassy Polymeric States.* Macromolecules, 1977. **10**(5): p. 1025-1030.
11. Utracki, L.A. and R. Simha, *Analytical representation of solutions to lattice-hole theory.* Macromolecular Theory and Simulations, 2001. **10**(1): p. 17-24.
12. Simha, R. and L.A. Utracki, *PVT properties of linear and dendritic polymers.* Journal of Polymer Science Part B: Polymer Physics, 2010. **48**(3): p. 322-332.
13. Kobayashi, Y., et al., *Free volume and physical aging of poly(vinyl acetate) studied by positron annihilation.* Macromolecules, 1989. **22**(5): p. 2302-2306.
14. Yu, Z., et al., *Molecular weight-dependence of free volume in polystyrene studied by positron annihilation measurements.* Journal of Polymer Science Part B: Polymer Physics, 1994. **32**(16): p. 2637-2644.
15. Srithawatpong, R., et al., *Positron annihilation lifetime studies of changes in free volume on cross-linking cis-polyisoprene, high-vinyl polybutadiene, and their miscible blends.* Journal of Polymer Science Part B: Polymer Physics, 1999. **37**(19): p. 2754-2770.
16. Consolati, G., et al., *On the relation between positron annihilation lifetime spectroscopy and lattice-hole-theory free volume.* Journal of Polymer Science Part B: Polymer Physics, 2005. **43**(16): p. 2225-2229.
17. Consolati, G., *On the Thermal Expansion of Nanohole Free Volume in Perfluoropolyethers.* The Journal of Physical Chemistry B, 2005. **109**(20): p. 10096-10099.
18. Schmidt, M., M. Olsson, and F.H.J. Maurer, *Macroscopic pressure--volume--temperature properties versus free-volume characteristics of isotropic pressure-densified amorphous polymer glasses.* The Journal of Chemical Physics, 2000. **112**(24): p. 11095-11106.
19. Schmidt, M. and F.H.J. Maurer, *Relation between free-volume quantities from PVT-EOS analysis and PALS.* Polymer, 2000. **41**(23): p. 8419-8424.
20. Dlubek, G., et al., *The free volume and its recovery in pressure-densified and CO2-swollen heterocyclic-ring-containing fluoropolymers.* Macromolecular Chemistry and Physics, 2008. **209**(18): p. 1920-1930.
21. Dlubek, G., et al., *Temperature dependence of the free volume in fluoroelastomers from positron lifetime and PVT experiments.* Macromolecules, 2004. **37**(17): p. 6606-6618.
22. *GNOMIX INC., 3809 Birchwood Drive, Boulder, CO 80304, USA.*
23. Y.A. Fakhreddin, P.Z., Society of Plastic Engineers ANTEC '91, 1991(36): p. 1642.
24. P. Zoller, D.W., *Standard Pressure-Volume-Temperature Data for Polymers.* Technomic, Lancaster, PA 1995.
25. He, J., Y.A. Fakhreddine, and P. Zoller, *Maintaining hydrostatic conditions during*

solidification of polymers in a high-pressure dilatometer. Journal of Applied Polymer Science, 1992. **45**(4): p. 745-747.

4 Local free volume concentration and size distribution

4.1 Introduction

The role of free volume in molecular material properties is influential. The specific free volume can be obtained by fitting pressure-volume-temperature (PVT) experiment data to the equation of state. Nevertheless, to understand the underlying mechanism about the free volume dependence of molecular properties, we need to characterize the free volume configuration as completely as possible.

To have a comprehension of free volume structure, several parameters of subnanometer scale local free (hole) volume are needed: mean size, size distribution and its number density. There are theoretical methods to calculate these parameters as well as molecular modeling methods to obtain the hole size concentration.

Although the quantitative total specific volume can be connected with molecular properties, it is in fact the microscopic hole volume which has a fundamental effect to the physics. Hole size and shape play an influential role in the solvation [1, 2] and mixing processes [3], small molecular permeation through hole volume is important in membrane research [4], and most important, accurately characterizing hole size distribution and its concentration is essential to understand the microscopic structure of molecular materials.

4.2 Fürth's hole theory of liquids

The idea behind the classical hole theory of Fürth [5] is very simple and descriptive: the hole forming energy is equal to the sum of work to be done against surface tension and pressure:
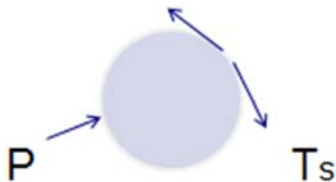

Figure 4.1 Forces that applied to a hole.

$$E_q = \frac{4}{3}\pi r^3(p - p_0) + 4\pi r^2 \sigma \qquad (4.1)$$

here, p is the external pressure, $p_0(T)$ is the pressure of the saturated vapor and $\sigma(T)$ is the surface tension of the liquid. Through a series assumptions

and classical thermodynamic statistical mechanics calculation, he got the single hole volume distribution and the average single hole volume in relation with the surface tension:

$$W_0(r)dr = C_0 e^{-\frac{r^2}{R^2}} r^6 dr \tag{4.2}$$

$$v_0 = 0.68(\frac{kT}{\sigma})^{\frac{3}{2}} \tag{4.3}$$

here, $R = \sqrt{kT/4\pi\sigma}$, $C_0 = \frac{16}{15\sqrt{\pi}}R^{-7}$, k is the Boltzmann constant and T is the temperature.

From above, we obtain the single hole volume distribution and its mean size. But the holes are not individual without interaction with other holes. Like particles, the holes can congregate together and form groups or clusters through thermal movement of the particles. This coalesce procedure is totally random and follows thermodynamic mechanical laws.

Figure 4.2 shows n-fold holes frequency function for A and C type (size of a single hole is either much smaller or larger compared with the size of a particle, respectively) [5]. From this graph, we see a maximum at n=11, which means most of the holes in A and C conditions [5] are complex holes buildup of 11 single holes.
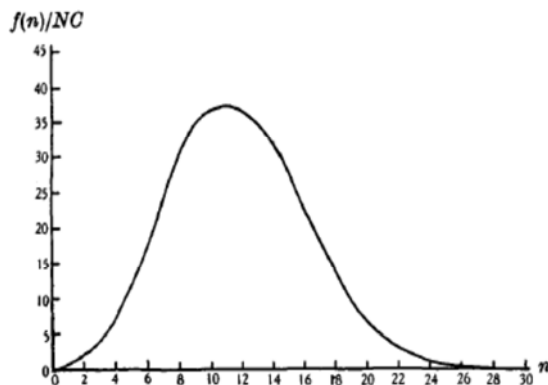

Figure 4.2 Frequency of n-fold holes distribution for type A and C [5].

Figure 4.3 is from one of our publications [6] that compare the hole volume distribution from Fürth theory [5] and positron annihilation lifetime spectroscopy. They are in good agreement and show a Poisson like distribution.

Figure 4.4 is also from our work [6]. It shows the temperature dependence of the average hole volume. The local mean free volumes from Fürth theory and positron lifetime are in the same trend and magnitude. After melting, positron lifetime can no longer represent the correct hole volume because of intense molecular motion. But from the specific free volume (right axis) obtained from

the pressure-volume-temperature experiment, we see the Fürth theory is still valid and both, the specific free volume and the mean hole volume increase with temperature linearly and the hole number density is constant.
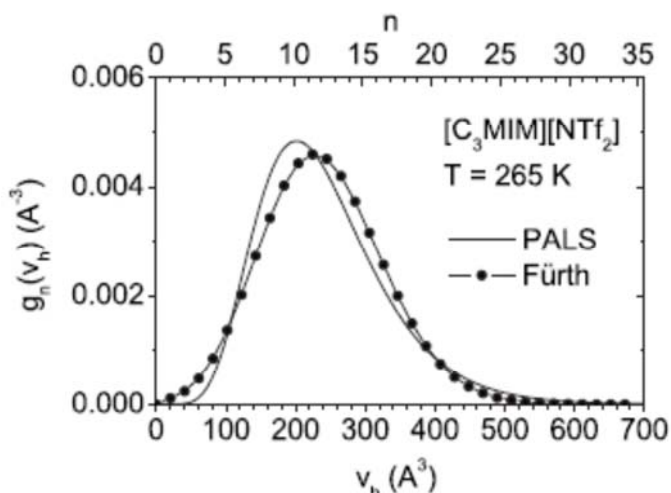

Figure 4.3 Comparison of volume distribution between Fürth theory and positron annihilation lifetime spectroscopy for the ionic liquid [C₃MIM][NTf₂] [6].
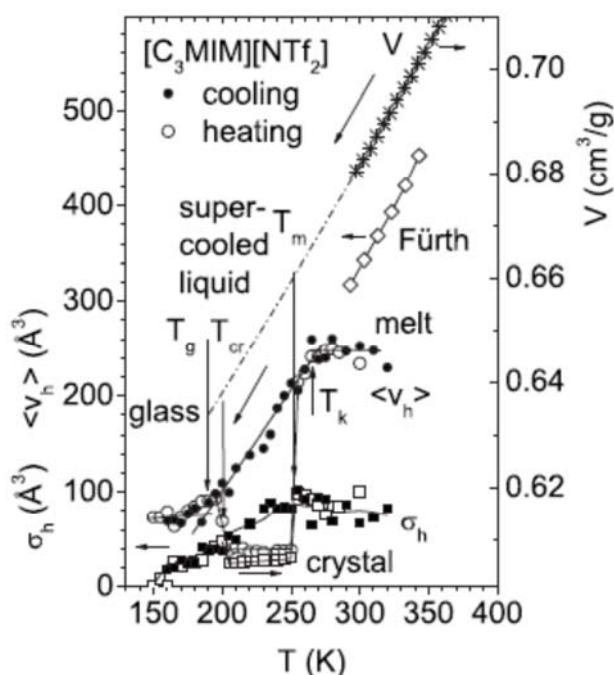

Figure 4.4 Temperature dependence of mean local free volume from Fürth theory and positron annihilation lifetime spectroscopy. The specific free volume (right axis) is from pressure-volume-temperature experiment.

4.3 Hirai-Eyring hole theory

Hirai and Eyring [7] derived an equation for the number of holes in a liquid in a way similar as Schottky for crystals. In the Hirai-Eyring model, a mixing system with N_0 molecules and N_h holes behaving the same way as for N_0 polymer molecules and N_h solvent molecules is assumed. It is not necessary that the volume of a hole, v_h, is the same as the molecular volume v_0. Usually it is smaller. The mixing entropy for this system is [8]:

$$\Delta S_M = k\{N_h \ln[N_h/(nN_0 + N_h)] + N_0 \ln[nN_0/(nN_0 + N_h)]\} \tag{4.4}$$

here, $n = v_0/v_h$, the ratio of molecular volume to hole volume; k is the Boltzmann's constant. The total entropy increase due to introduction of holes is:

$$\Delta S = \Delta S_M + N_h S_h \tag{4.5}$$

S_h is the entropy, which relates to each hole. The enthalpy of hole introduction is:

$$\Delta H = N_h H_h = N_h(\epsilon_h + Pv_h) \tag{4.6}$$

H_h and ϵ_h are enthalpy and energy of hole formation, respectively. P is the pressure.

Minimizing the Gibbs free energy $\Delta G = \Delta H - T\Delta S$ with respect to N_h, $\partial \Delta G / \partial N_h = 0$, one obtains the Hirai-Eyring equation:

$$\ln\sigma + \ln g - \left(1 - \frac{1}{n}\right)g + \frac{\epsilon_h + Pv_h}{kT} = 0 \tag{4.7}$$

$$g = N_h/(nN_0 + N_h) \tag{4.8}$$

$$\ln\sigma = 1 - 1/n - S_k/k \tag{4.9}$$

Hirai and Eyring made the approximation of neglecting N_h in the denominator, then (4.7) can be written as:

$$\frac{N_h}{nN_0} = \frac{1}{\sigma}\exp(-\frac{\epsilon_h + pv_h}{kT}) \tag{4.10}$$

The volume is:

$$V = N_0 v_0 + N_h v_h = V_0[1 + (N_h/nN_0)] \tag{4.11}$$

$V_0 = N_0 v_0$. When putting (4.10) into (4.11), the equation of state is obtained:

$$V = V_0[1 + \frac{1}{\sigma}\exp\left(-\frac{\epsilon_h + pv_h}{kT}\right)] \tag{4.12}$$

Smith [9] fitted the Hirai-Eyring equation of state for 5 different materials and got the parameters for equation (4.12): V_0, σ, ϵ_h and v_0. Figure 4.5 shows the fitting results for polystyrene and the fitted parameters for different polymers.

The fitting is in good agreement with the experimental data at low pressure and temperature, but large deviation at high pressure and temperature is obtained. That is because of the assumption of the temperature/pressure independence of v_0 of the author [9]. Ignoring this factor, the fitting parameters obtained are very reasonable. The occupied volume V_0 for PMMA is 0.79 cm^3/g, that value is similar to the positron lifetime result. The v_h for PMMA is 19 cm^3/mol, that is 31.56 Å^3. This is also in the same magnitude of

the local free volume from positron annihilation lifetime spectroscopy [10].
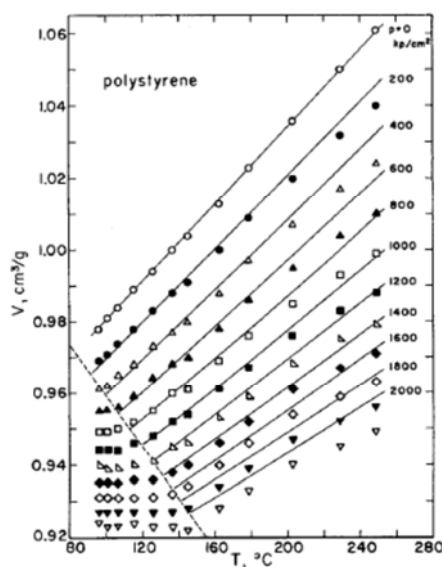
Material	V_3, cm²/g	σ	$N_A\epsilon_3$, kcal/mole	$N_A v_3$, cm³/mole
PS	0.89	1.065	1.65	20.0
PVC	0.67	1.225	1.55	15.0
PMMA	0.79	0.975	1.81	19.0
Butyl	0.98	1.455	1.18	—
PE	1.10	0.679	1.79	—

Figure 4.5 Left: Points: experiment data; Lines: fitting result from Hirai-Eyring equation of state. Right: fitting parameters [9].

4.4 Molecular modeling

Besides theory and experiment, numerical calculation and simulation methods introduce great contributions in physics with the explosive development of computation technology. Molecular modeling can be used to research free volume and provide a descriptive demonstration of its structure, different aspects and deeper physical insight.

Veld et al. [11] developed a new algorithm using energetic rather than geometric consideration. They applied this method to hard sphere (HS) fluids, Lennard-Jones (LJ) fluids, SPC/E water and two isomeric polyimides to show the universal application of this computational method to any liquid structure. In their model, a cavity is a spherical volume with a local minimum center in a repulsive particle energy field.
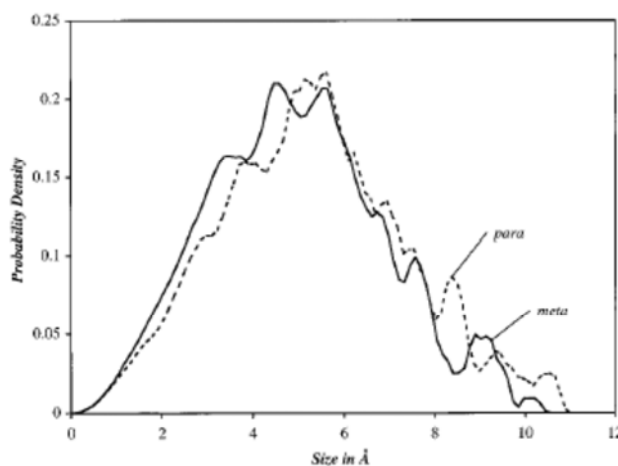

Figure 4.6 Cavity size distribution for para- and meta-polyimide isomers [11].

At first, they use Monte Carlo or molecular dynamic simulation to generate liquid or glass structure; Then fix the particles in their equilibrium position and substitute repulsive force field from Lennard-Jones interaction; A trial repulsive particle is randomly inserted into the repulsive force field to determine local minimum for the cavity center; At this time, attractive part of Lennard-Jones interaction is turned on to decide the cavity diameter, and then the volume distribution is determined. Figure 4.6 shows the size distribution of two isomers (para and meta polyimide). We can see that although the chemical components are identical, apparent difference in size distribution and mean value is obtained from this molecular model. The average cavity size is 5.0 Å for meta isomer, smaller than the para isomer with a value of 5.4Å. These values are close to the value from the positron annihilation lifetime [12] experiment. They tested the result with carbon dioxide diffusion in these isomers. The diffusion is faster in para isomer, which is in agreement with the modeling outcome.

Hofmann et al. [13] used packing model and COMPASS force field [14, 15]. They utilize the Amorphous Cell module of the InsightII/Discover Software of Molecular Simulations Inc.

This model structure is verified by the Gusev-Suter Monte Carlo method and experimental parameters of diffusivity and solubility.
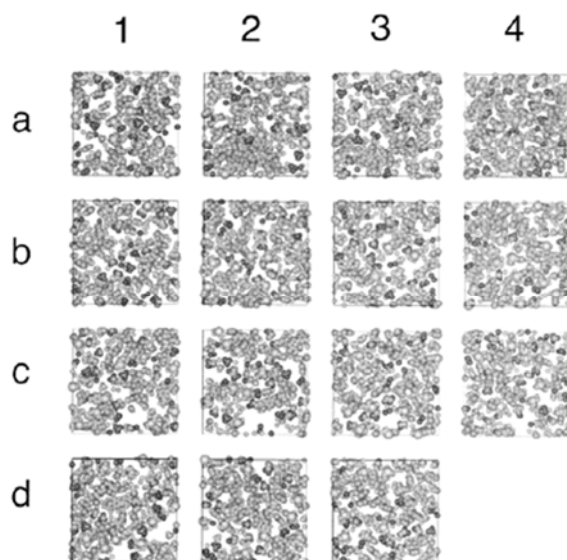

Figure 4.7 Visualization of free volume from simulation for PFPDMSS sample in equilibrated state. From a1 to d3 are 3.05 Å thick slices cut perpendicular to the z-axis from 3D packing model cubes [13].

Figure 4.7 is the visualization of a 3 dimension packing model by 3.05 Å

thickness slices cut perpendicular to z-axis for a poly(p- γ - trifluoropropyldimethyl silylstyrene) (PFPDMSS) sample. The sequence is from a1 to d3.

To determine the fractional free volume (FFV) and free volume elements (FVE), they assume that the atoms of the polymer chain are hard spheres with van der Waals radius, and utilize a test particle (in this case, positronium with 1.1 Å radius to compare with positron annihilation lifetime spectroscopy). To decide the FVE, two connect styles are considered as shown in figure 4.8: V-connect method takes all connected volumes together as one free volume element; R_max separates them into individual element. To compare with a positron lifetime experiment, R_max is more suited.
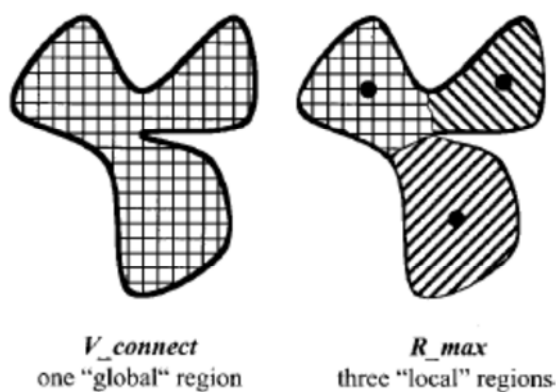

V_connect
one "global" region

R_max
three "local" regions

Figure 4.8 V-connect (left) and R_max (right) view of a large hole of complex topology [13].

Figure 4.9 shows the size distribution of free volume elements for the sample PFPDMSS from the R_max method.
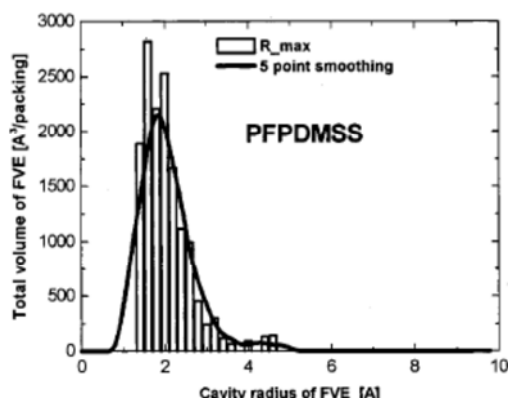

Figure 4.9 Size distribution of free volume elements (FVE) for PFPDMSS from R_max method [13].

Figure 4.10 is the size distribution of free volume elements from positron lifetime spectroscopy. Both size distributions from molecular modeling and positron lifetime experiment show a single Gaussian peak. A peak shift is observed between the molecular model (2 Å) and the positron lifetime experiment (3.6 Å). This may be caused by the random movement of the

positronium in three dimensions, so there is the possibility that Ps moves through neighboring volumes and count it as one free volume element.
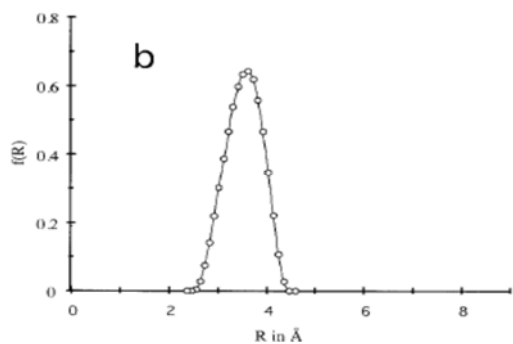

Figure 4.10 Size distribution of free volume element (FVE) from positron lifetime experiment for PFPDMSS.

Besides the peak discrepancy, the size distribution from modeling and the positron lifetime results are in good agreement for a series of polymer samples [13, 16].

4.5 Reference

1. Floris, F.M., et al., *Free energy and entropy for inserting cavities in water: Comparison of Monte Carlo simulation and scaled particle theory results.* The Journal of Chemical Physics, 1997. **107**(16): p. 6353-6365.

2. Matyushov, D.V. and B.M. Ladanyi, *Cavity formation energy in hard sphere fluids: An asymptotically correct expression.* The Journal of Chemical Physics, 1997. **107**(15): p. 5815-5820.

3. Gordon, P.A. and E.D. Glandt, *Liquid--liquid equilibrium for fluids confined within random porous materials.* The Journal of Chemical Physics, 1996. **105**(10): p. 4257-4264.

4. Nagel, C., et al., *Free volume and transport properties in highly selective polymer membranes.* Macromolecules, 2002. **35**(6): p. 2071-2077.

5. Fürth, R., *On the theory of the liquid state.* Mathematical Proceedings of the Cambridge Philosophical Society, 1941. **37**(03): p. 252-275.

6. Dlubek, G., et al., *Free volume in imidazolium triflimide ([C₃MIM][NTf₂]) ionic liquid from positron lifetime: Amorphous, crystalline, and liquid states.* The Journal of Chemical Physics, 2010. **133**(12): p. 124502-10.

7. Hirai, N. and H. Eyring, *Bulk Viscosity of Liquids.* Journal of Applied Physics, 1958. **29**(5): p. 810-816.

8. Mueller, C.R. and D.C. Stupegia, *Lattice Vacancy Theory of the Liquid State.* Journal of Chemical Physics, 1957. **26**(6): p. 1522-1525.

9. Smith, R.P., *Equation of state and the thermodynamic properties of liquid polymers: Application of the Hirai-Eyring model.* Journal of Polymer Science Part A-2: Polymer Physics, 1970. **8**(8): p. 1337-1360.

10. Kilburn, D., et al., *Free volume in poly(n-alkyl methacrylate)s from positron lifetime and PVT experiments and its relation to the structural relaxation.* Polymer, 2006. **47**(22): p. 7774-7785.

11. in 't Veld, P.J., et al., *Liquid Structure via Cavity Size Distributions.* The Journal of Physical Chemistry B, 2000. **104**(50): p. 12028-12034.

12. Dlubek, G., et al., *Water in local free volumes of polyimides: A positron lifetime study.* Macromolecules, 1999. **32**(7): p. 2348-2355.

13. Hofmann, D., et al., *Free Volume Distributions in Ultrahigh and Lower Free Volume Polymers: Comparison between Molecular Modeling and Positron Lifetime Studies.* Macromolecules, 2002. **35**(6): p. 2129-2140.

14. Sun, H. and D. Rigby, *Polysiloxanes: ab initio force field and structural, conformational and thermophysical properties.* Spectrochimica Acta Part A: Molecular and Biomolecular Spectroscopy, 1997. **53**(8): p. 1301-1323.

15. Rigby, D., H. Sun, and B.E. Eichinger, *Computer simulations of poly(ethylene oxide): force field, pvt diagram and cyclization behaviour.* Polymer International, 1997. **44**(3): p. 311-330.

16. Hofmann, D., et al., *Molecular Modeling Investigation of Free Volume Distributions in Stiff Chain Polymers with Conventional and Ultrahigh Free Volume: Comparison between Molecular Modeling and Positron Lifetime Studies.* Macromolecules, 2003. **36**(22): p. 8528-8538.

5 Positron annihilation studies of the free volume

5.1 Introduction

The positron (e$^+$) was discovered by Carl D. Anderson as a constituent of cosmic rays in 1932 [1], while its existence was postulated by Paul Dirac four years earlier [2]. The discovery of positron is a great event in physics since it's the first evidence of antimatter existence. It represents a reform of physics concept and theory.

The significance of positron is not only in theory but also in application. PET (Positron Emission Tomography) is a nuclear medical imaging technique, producing three-dimensional images of functional processes in the body. Like the electron, positron can also be used in microscopic techniques (Scanning Positron Microscopy SPM, Transmission Positron Microscopy TPM) but exhibits different aspect of material information. There are also other techniques like ACAR (Angular Correction of Annihilation Radiation), Positron Diffraction technique, PAES (Positron-annihilation induced Auger Electron Spectroscopy), which are important experimental methods to investigate materials. Among these applications, the most traditional and conventional methods in material research are PALS (Positron Annihilation Lifetime Spectroscopy), CDB (Coincidence Doppler Broadening) and Slow Positron Beam technique [3, 4].

5.2 Positron generation

There are mainly two ways to generate positron: pair production and radioactive decay.

When a photon reaches energy exceeding twice the rest mass of electron (1.022 MeV), according to the Einstein's Mass-Energy equivalence $E=mc^2$, it can produce an electron and a positron. This process is called pair production.

Apart from the conservation law of energy, this process should also follow the conservation law of momentum, angular momentum and charge.

Almost all the elements known have β^+ radioactive isotopes, but only few of them can be used in the positron annihilation lifetime spectroscopy (PALS) experiment. For this usage, the isotope should have proper half-life and it

should emit a signal when the positron is ejected from the source as a start (time zero) sign. The economic aspect should also be considered. ^{22}Na fits our requirement quite well, so normally, the researchers use it as the radioactive source in the lifetime experiment. Figure 5.1 is the decay scheme of ^{22}Na.
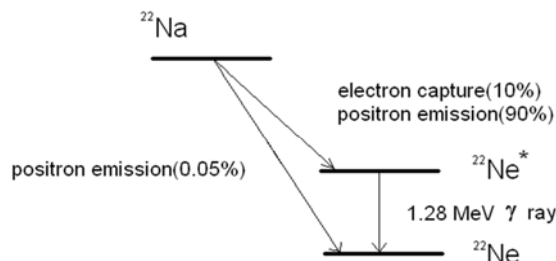

Figure 5.1 Decay scheme of sodium 22 to neon.

The half-life of sodium 22 is 2.602 years. After one of the protons in ^{22}Na emits a positron and becomes a neutron, the ^{22}Na transforms to excited state of ^{22}Ne. It's not stable and emits a photon of 1.28 MeV to ground state just 3 ps later. Since this time is negligible compared to the positron lifetime in material (larger than 100 ps), the photon emission is considered simultaneous with the positron emission. This photon is applied as start signal of the PALS experiment.

5.3 Positron property

The positron is the anti-particle of the electron. It has the physical properties all identical to the electron (rest mass corresponding to 511 keV, spin: 1/2) except charge (+1electron charge). It can annihilate with an electron under emission of photons. In this process the conservation of energy, momentum and spin is required. The annihilation of the free positron occurs mainly into two photons, and, with a much lower probability (1/137), into three photons [5].

5.4 Positron annihilation lifetime spectroscopy (PALS)

When the β^+ source ^{22}Na ejects a positron, it ejects a photon of 1.28 MeV at the same time, which is applied as a start signal for the lifetime measurement. After the positron annihilates with an electron, it emits two photons each of 511 keV, used as stop signal. The time difference between the emission of start and stop rays corresponds to the lifetime of the annihilating positron. When positrons annihilate in a material with a constant electron density, the lifetimes of individual positrons are distributed as an exponential decreasing function.

The time constant of this function is called mean positron lifetime, or for shortness, positron lifetime. The typical value of positron lifetime in bulk of metals and semiconductors is around 100 ps to 400 ps [6]. If the positron is trapped by a vacancy, due to the decrease of the electron density, the lifetime will increase. In bulk materials the thermalization duration (about 1 ps) is short comparing to the positron lifetime and can be ignored. But in some gaseous environments (particularly noble gases), the time for a positron approaching to thermal energy is much longer, about 1-100 ns. Then the time for a positron to come to thermal equilibrium with its surroundings needs to be considered.

5.4.1 Instrument system

The lifetime spectrometer is based on conventional fast/fast coincidence system. Figure 5.2 shows the instrument system of the positron lifetime experiment, including $^{22}Na_2CO_3$ source sandwiched with two identical sample sheets, plastic scintillators, photomultiplier tubes (PMT), high voltage and electronic signal analysis modulus (differential constant fraction discriminator (DCFD), Time-to-Amplitude converter (TAC), Multichannel Analyzer (MCA), delay cables and computer). The Nuclear Instrumentation Module fits NIM standard specifications: 19 inches wide case, 12 sockets with width of 34.4 mm and the modulus fit into standard power supply bins ($\pm$24V, $\pm$12V, $\pm$6V).
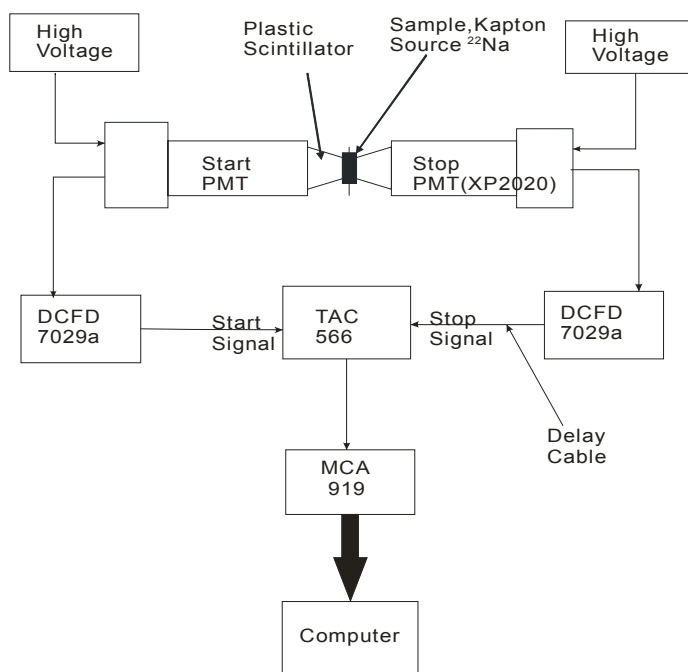

Figure 5.2 Scheme of positron annihilation lifetime spectroscopy (PALS) instrument system.

5.4.2 Positron source

In the experiment, I use 7 μm thick Kapton foil to seal the $^{22}Na_2CO_3$ positron source in a sphere of 7mm diameter. It has the advantage that Kapton has the same lifetime as the source $^{22}Na_2CO_3$ (0.38 ns). The source activity is around 10^6 Bq. The Kapton source is covered by an extra Kapton foil (7 μm) each side in order to prevent contamination of the sample, since polymer sample may melt at high temperature and stick to the source. The positrons emitted from the source will partly annihilate in the source material ($^{22}Na_2CO_3$) and Kapton covering the source, so we need a source correction which is determined using a defect-free p-type Si reference sample of known lifetime.

Since the highest kinetic energy of positrons from β^+ radioactivity is 540 keV in ^{22}Na, it will go through a long distance during thermalization and loses most of its energy by collision and ionization of surrounding molecules. So the samples need some thickness preventing the positron penetrating through it and giving information which not belongs to the samples.

The profile for penetration of positrons is expressed in the following function [7]:

$$P = \alpha \times \exp(-\alpha x) \tag{5.1}$$

$$\alpha = 16\frac{\rho}{E_{max}^{1.43}} \tag{5.2}$$

where P is the fraction of positrons stropped in the layer between x and $x+dx$, x is the distance of the layer from the surface of the solid which the positron penetrates, its unit is cm. So the parameter α has the unit cm^{-1}, density ρ in g/cm^3, maximum energy E_{max} in MeV. For ^{22}Na, E_{max}=0.54 MeV, we get:

$$\alpha[cm^{-1}] = 38.6\rho[g/cm^3] \tag{5.3}$$

For the materials Al (ρ = 2.7 g/cm^3), Cu (8.9 g/cm^3), Ti (4.54 g/cm^3), Fe (7.9 g/cm^3), Mg (1.74 g/cm^3) Si (2.33 g/cm^3), Pb (11.34 g/cm^3), polybutadiene(0.87 g/cm^3), if we need 99% of positron absorbed in the material, the thickness should be 0.44 mm (Al), 0.13 mm (Cu), 0.26 mm (Ti), 0.15 mm (Fe), 0.69 mm (Mg), 0.51 mm (Si), 0.11 mm (Pb), 1.4 mm (polybutadiene). For most solid state material, the density will be higher than 1 g/cm^3, so the thickness of the material about 1 mm ~ 1.5 mm is sufficient.

As described before, the $^{22}Na_2CO_3$ and Kapton foil will absorb some of the positrons. Therefore we need to assess the positron intensity as well as

respective lifetime for each part (0.38 ns for Kapton and $^{22}Na_2CO_3$) that annihilates in the source sandwich, which is called source correction. Usually its intensity is 10-17% in our experiments. Defect-free p-type Si is used as reference to determine the source correction. But if we consider the backscattering of emitted positrons from the sample toward the source, we still need to correct the intensity of the source component determined from Si by a factor which takes into account the atomic number of the sample under investigation. When the atomic number of the sample is higher than that of Si, the backscattering effect increases, when it is lower then it decreases compared with Si (I=11% for a Kapton foil of 7 μm thickness). We have fitted experimental source intensities determined in Ref. [8] for Mg, Al, Si and Ti by a second-order polynomial function to get a calibration curve, as shown in Figure 5.3. For polybutadiene (PBD) as the sample under investigation, the mean atomic number Z is 3, so the scaling factor is calculated to be about 0.32 (3.5/11). For the ionic liquid [BMIM][BF$_4$] (section 7.3.3.1), the mean atomic number Z is 3.93, so the scaling factor is about 0.39 (4.3/11). By these factors, the intensity of the Kapton-$^{22}Na_2CO_3$ source determined from the Si reference is lowered. These source components (lifetime and intensities) are then fixed in the data analysis, or with other words, subtracted from the measured spectrum when fitting the true lifetime components of the sample.
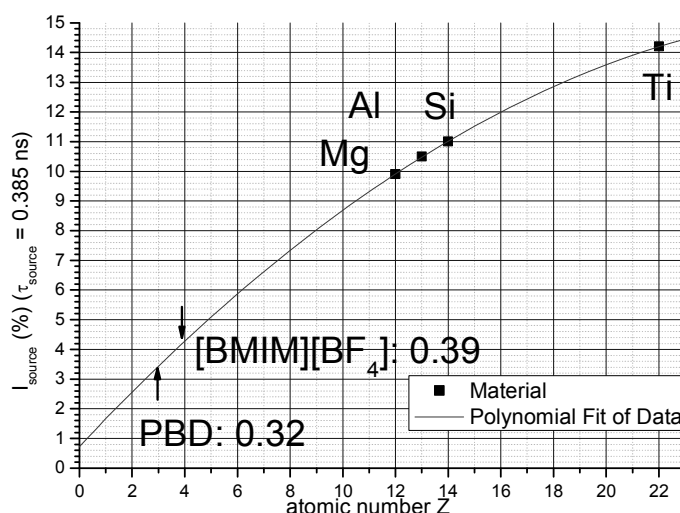

Figure 5.3 Estimation of factors for scaling the source intensity determined with Si (^{22}Na source covered with 7 μm Kapton).

5.4.3 Lifetime analysis

The annihilation rate λ of positrons is connected with the density of the

electrons around it. So the information of material structure can be obtained from the mean lifetime τ, which is the reciprocal of λ. For vacancy, hole, free volume, void and pore sites, the electron density decreases compared to the perfect crystal and the lifetime of positrons localized at these defects will increase.

The relationship between annihilation rate of positron and the electron density can be expressed by the relation [3]:

$$\lambda = \frac{1}{\tau} = \pi r_0^2 c \int d\vec{r} \, n_+(\vec{r}) n_-(\vec{r}) g(0; n_+; n_-) \tag{5.4}$$

$\vec{r}_0$ is the classical electron radius, c is the light speed in vacuum, n_+, n_- are the positron and electron density, respectively. $g(0; n_+; n_-)$ is the electron-positron correlation function, which describes the enhancement of the electron density at the position of the positron due to the Coulomb interaction.

We use the software Lifetime9 (LT9) to analyze the spectrum [9]. More detailed analysis of positron lifetime in polymer material will be presented (section 5.6).

5.5 Sample chamber

In our lab, the sample chamber system includes chamber holder, cold head (closed-cycle He cryo-system), temperature controller and vacuum accessory. The cold head is connected to a compressor (Coolpak 4000D, Leybold). Combining with the temperature controller (Model 2204e, Eurotherm) and the heating part, the temperature range is 40 K to at least 500 K. And the accuracy can reach 0.1K. The vacuum of the system is about 10^{-3} Pa with the help of a pre-pump and a Turbo-pump.

5.6 PALS method applied in molecular materials

After the positron is ejected from the source, it suffers thermalization and diffusion processes. It can either annihilate with an electron directly or being trapped by a hole (local free volume) in the molecular matters and then form positronium. After the annihilation of positronium, a long lifetime component appears in the PALS experiment. From that lifetime, free volume information of the material is obtained.

The PALS experiment makes snapshots of the hole volume structure, which in the rubbery state of the polymer fluctuates in space and time, since the

positronium lifetime (about 1-4 ns) is shorter than the relaxation time of the segmental movement (from ns to μs and finally 100 s at the glass transition temperature T_g).

5.6.1 Thermalization

The "thermalization" is a process during which a high energetic positron reaches thermal equilibrium state with the surrounding molecules in the material. Positrons emanate from the radioactive source sodium 22 with a continuous energy spectrum, which is a characteristic of the beta decay. The end-point energy is 0.54 MeV. After the introduction of the positron into the solid, at higher energy, positron loses its energy rapidly by ionization process during collision with molecules. Each inelastic collision costs about 100 eV of the hot positron in average. That process creates electron-ion pairs along the trajectory of injected positron. The ionized electron (secondary electron) with mean kinetic energy of 10-50 eV [10] extends around, losing energy by ionization, excitation, phonon scattering etc. and finally recombines with another ion to form a neutral molecule. At lower positron energy, excitation of atoms takes over. Eventually, molecule vibration and phonon scattering take the energy of the inelastic collision of positron with molecules and allow the positron to come into thermal equilibrium with the material.

5.6.2 Diffusion

After thermalization, positron with environmental thermal energy randomly travels around before it annihilates or meets a hole and falls into a localized state. This process is called diffusion. The collision with host atoms is quasi-elastic, its momentum conserves in the collision.

5.6.3 Positronium

The existence of a bound state of a positron and an electron, which is called positronium, was postulated not long after the discovery of the positron in 1932. Experimental evidence of it was first published by Deutsch in 1951 [11]. Positronium is a hydrogen-like bound state composed by a positron and an electron. They circulate a common center. The atomic mass is 0.0011 amu. The diameter (distance of the two particles) is $3a_0$ (a_0 - classical Bohr radius).

The ionization energy in vacuum is 6.803 eV. There are two possible configurations depending on the relative spin orientations of the electron and the positron of positronium: para-Positronium (*p*-Ps), denoted $^1S_0$ with opposite spin direction, so the spin angular momentum is zero; and ortho-Positronium (*o*-Ps), denoted $^3S_1$ with the same spin direction, so the spin angular momentum is unit [3]. The result of the annihilation for *p*-Ps is the appearance of two photons emitted into opposite direction. For *o*-Ps (self-annihilation in vacuum), due to the conservation of spin and momentum, the annihilation result is three photons.
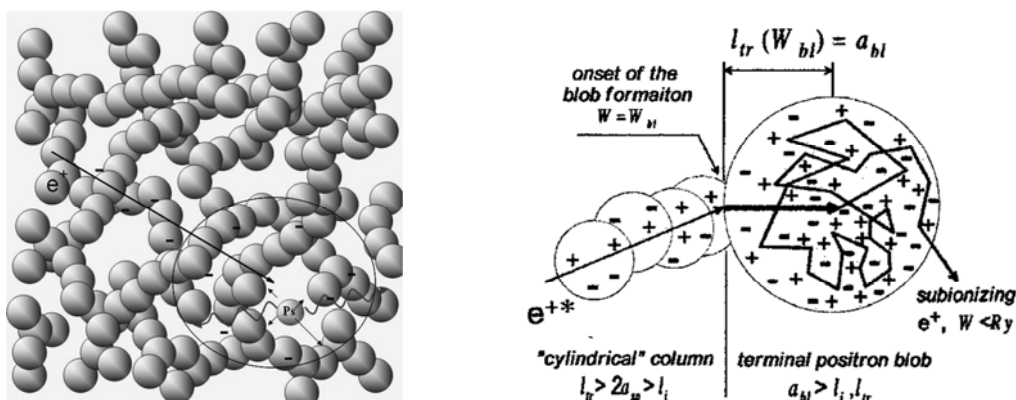
Figure 5.4 Scheme of the Positronium formation in molecular matter [12].

Positronium plays an important role when PALS experiment was applied in polymer science. Positronium can be formed in insulators with no free electrons, such as ionic crystals (KCl), inorganic glasses and polymers, but not in metals and semiconductors. Formation of Positronium can be described by the blob model [12-15], which is an extension of the traditional spur model [10]. As illustrated in figure 5.4 right, through ionizing collisions (the spur, cylindrical column), a positron with several hundred keV kinetic energy will lose most of its energy within 10^{-12} s [16]. When the positron energy falls between 0.5 keV and ionization threshold of several eV, $n_0 \approx 30$ electron-ion pairs are generated within a blob with radius $a_{b1} \approx 40$ Å. Faster subionizing positrons may diffuse out of the blob. The positron thermalized within the blob cannot escape and will encounter one of the thermalized ionized intrablob electron, forming a weakly bound $e^+ \cdots e^-$ pair. The pair transforms to quasi-free Ps (qf-Ps) and finally localized in one of the local free volumes due to repulsive exchange interaction between electrons in molecules and Ps:

$$e^+_{qf} + e^-_{blob} \rightarrow (e^+ \cdots e^-) \rightarrow qf\text{-Ps} \rightarrow \text{Ps localized} \qquad (5.5)$$
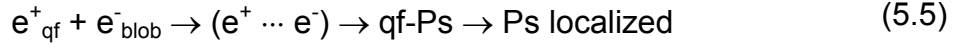
In vacuum, the self-annihilation lifetime of *p*-Ps is 124 ps and for *o*-Ps is 142 ns. But since the *o*-Ps is in the material and there are electrons around, the positron in the pair will annihilate with another electron with opposite spin direction nearby other than its partner, and emit two photons instead of three. This kind of phenomenon is called pick-off annihilation. And its lifetime is influenced greatly by the electron density, which means by the size of the open volume (hole) where *o*-Ps is localized. Correspondingly, we can get the hole dimension by the pick-off annihilation lifetime of *o*-Ps.
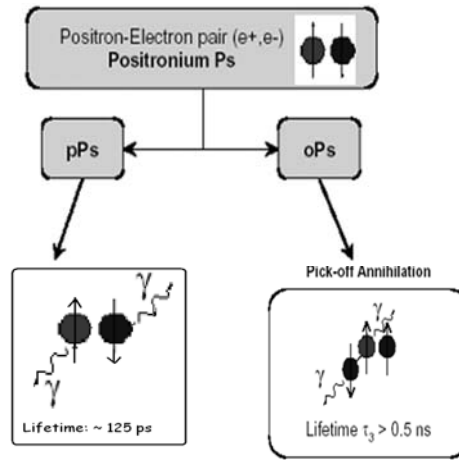
Figure 5.5 Scheme of two species of Positronium and Pick-off annihilation.

5.6.4 Positron lifetime analysis in molecular materials

In molecular materials usually Ps is formed from a fraction of positrons. Then three lifetime components with time constant (mean lifetime) and intensity for each, from three decay channels are expected: para-Ps (*p*-Ps, channel 1), positrons having not formed Ps (e⁺, channel 2) and ortho-Ps (*o*-Ps, channel 3).

Their typical values are shown below:

$$\tau_{p-Ps} = \frac{1}{(\eta/\tau^0_{p-Ps} + 1/\tau_{po})}, \tau^0_{p-Ps} = 125 \text{ ps} \qquad (5.6a)$$

$$\tau_{free} = \tau_p \approx 350 \text{ to } 500 \text{ ps} \qquad (5.6b)$$

$$\tau_{o-Ps} = \frac{1}{(\eta/\tau^0_{o-Ps} + 1/\tau_{po})} \approx 1 \text{ to } 4 \text{ ns} \qquad (5.6c)$$

$$I_{free} = 1 - (I_{p-Ps} + I_{o-Ps}) \qquad (5.6d)$$

τ is the mean lifetime which is reciprocal of the annihilation rate λ. τ^0_{p-Ps} and τ^0_{o-Ps} are self-annihilation lifetimes of *p*-Ps and *o*-Ps in vacuum with the value

124 ps, 142 ns respectively. η is the so-called contact density or relaxation parameter. It describes the relaxation of Ps in material compared with the state in vacuum and its value is estimated in polymers from magnetic quenching experiments between 0.5 and 1 [17, 18]. More recent calculations give values close to 1, or even larger than 1 if Ps is localized at very small holes [19, 20]. τ_{po} is the pick-off annihilation lifetime. I_i is the intensity of the i-th component of the annihilation spectrum (area below the exponential decay curves). So a naive spectrum can be expressed by the formula:

$$s(t) = \sum_i (I_i/\tau_i)\exp(-t/\tau_i) = \sum_i (I_i\lambda_i)\exp(-t\lambda_i) \tag{5.7}$$

here, we assume that there are three decay terms (i=3) and the mean lifetimes appear discrete, i.e. there is no dispersion (distribution) of the mean lifetimes.
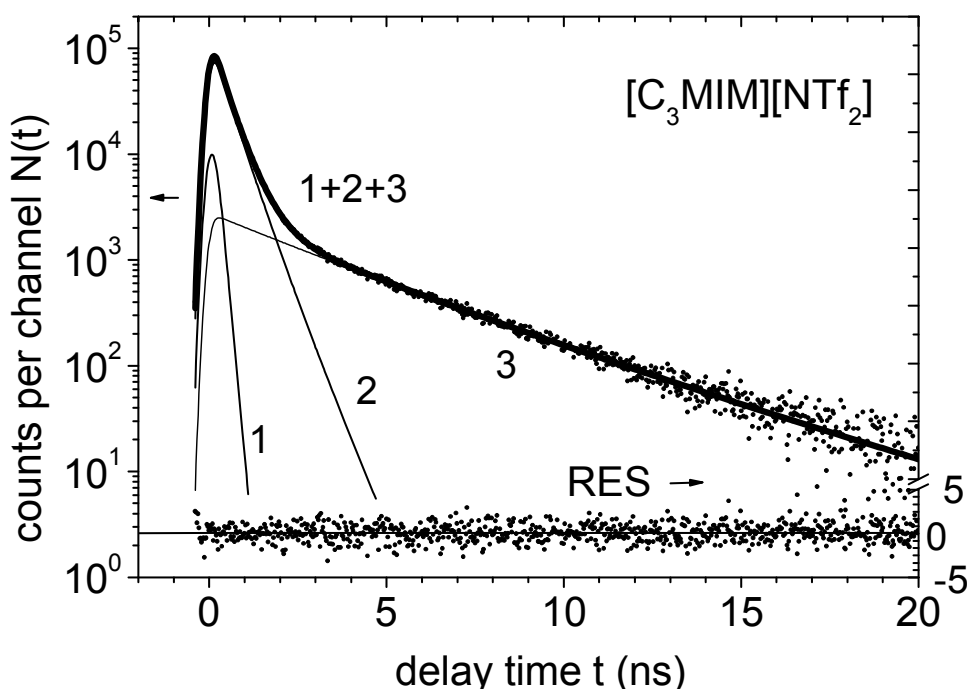
Figure 5.6 The positron decay spectrum (dots) of [C$_3$MIM][NTf$_2$] at 300 K after subtracting the source components and the background B [21]. The top thick line shows the LT-9.0 fit to the spectrum, which was decomposed into the components p-Ps (1), e$^+$ (2), and o-Ps (3, all curves are convoluted with the resolution function). RES shows the weighted residuals.

Positron annihilation lifetime instrument system described in section 5.4.1 is used to get the experimental original data. The software LT9 [9, 22] is employed to analyze the data. Figure 5.6 shows the deconvolution of the spectrum from lifetime of the ionic liquid [C$_3$MIM][NTf$_2$] [21] into three components.

The observed spectrum can be expressed by:

$$y(t) = R(t) \otimes (N_t s(t) + B) \tag{5.8}$$

R(t) is the resolution function (a single Gaussian or a sum of two Gaussians) which is determined by the PALS instrument system. *B* is the background due to random coincidence. N_t is the total counts in the spectrum. $\otimes$ denotes a convolution of the decay integral.

In polymers or low molecular glass formers, the mean free and *o*-Ps lifetimes have a dispersion due to the dispersion of hole sizes. So the spectrum is expressed as:

$$s(t) = \sum_i I_i \int_0^\infty \alpha_i(\lambda)\lambda \exp(-\lambda t)\,d\lambda \qquad (5.9a)$$

where $\alpha(\lambda)$ is the annihilation rate distribution (probability density function). The routine LifeTime, version 9.0 (LT9.0) was developed based on experiences with the program CONTIN-PALS [23] (a numerical Laplace inversion) and assumes from the beginning that the distributions $\alpha_i(\lambda)$ follow a logarithmic Gaussian function, where $\alpha_i(\lambda)$ is the distribution of the annihilation rate of the decay channel *i*. Compared with other routines, LT9.0 shows the most success in the analysis of positron lifetime spectra. The reason for this lies in the significant reduction of the degree of freedom compared with CONTIN-PALS and also with the routine MELT [24, 25] (a maximum entropy method) by assuming the number of different annihilation channels and the shape of the annihilation rate distributions. Moreover, because lifetime analysis is less sensitive to the particular shape of the distributions, the assumed log normal function seems to sufficiently describe the real situation.

So, the routine LT9.0 describes the annihilation rate distributions $\alpha_i(\lambda)$ by:

$$\alpha_i(\lambda)\lambda d\lambda = \frac{1}{\sigma_i^*(2\pi)^{1/2}} \exp\left[-\frac{(\ln\frac{\lambda}{\lambda_{i0}})^2}{2\sigma_i^{*2}}\right]d\lambda \qquad (5.9b)$$

$$\sum_i I_i = 1 \qquad (5.9c)$$

$$\int_0^\infty \alpha_i(\lambda)d\lambda = 1 \qquad (5.9d)$$

The distribution has a maximum position at λ_{i0} and the standard deviation σ_i^*. The routine can be applied also for a discrete term analysis by setting all width parameters σ_i^* to zero. Then it gives the same results as the traditional routine POSITRONFIT of the package PATFIT [26].
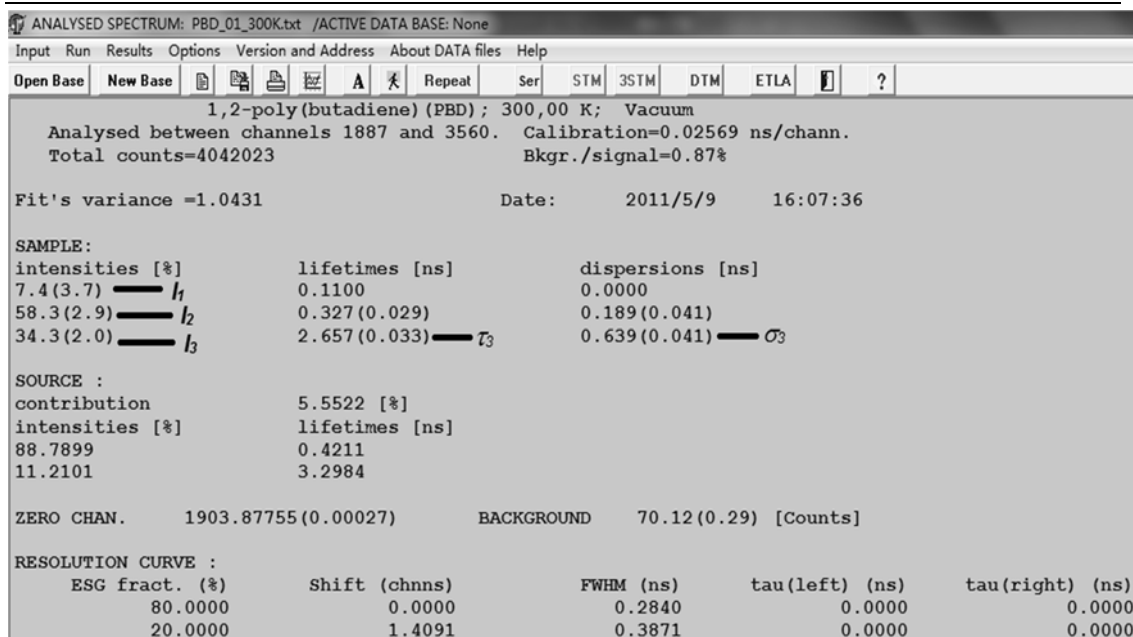
```
ANALYSED SPECTRUM: PBD_01_300K.txt  /ACTIVE DATA BASE: None
Input  Run  Results  Options  Version and Address  About DATA files  Help

Open Base   New Base  [icons]  A  [icon]  Repeat   Ser  STM  3STM   DTM   ETLA  [icon]  ?

                1,2-poly(butadiene)(PBD); 300,00 K;  Vacuum
      Analysed between channels 1887 and 3560.  Calibration=0.02569 ns/chann.
      Total counts=4042023                      Bkgr./signal=0.87%

   Fit's variance =1.0431               Date:     2011/5/9     16:07:36

   SAMPLE:
   intensities [%]          lifetimes [ns]         dispersions [ns]
   7.4(3.7) ━━ I₁           0.1100                 0.0000
   58.3(2.9)━━ I₂           0.327(0.029)           0.189(0.041)
   34.3(2.0)━━ I₃           2.657(0.033)━━ τ₃      0.639(0.041)━━ σ₃

   SOURCE :
   contribution             5.5522 [%]
   intensities [%]          lifetimes [ns]
   88.7899                  0.4211
   11.2101                  3.2984

   ZERO CHAN.    1903.87755(0.00027)      BACKGROUND    70.12(0.29) [Counts]

   RESOLUTION CURVE :
      ESG fract. (%)       Shift (chnns)       FWHM (ns)    tau(left) (ns)   tau(right) (ns)
            80.0000             0.0000            0.2840        0.0000           0.0000
            20.0000             1.4091            0.3871        0.0000           0.0000
```

Figure 5.7 Example analysis result of 1,2-poly(butadiene) sample from software LT9.

Figure 5.7 is the fitting result for 1,2-poly(butadiene) (PBD, section 6.1) sample from LT9.0. The non-linear least-squares fit method is employed to decompose the spectrum. Parameters as intensities, mean lifetime and dispersion for some of the lifetime components can be obtained.

5.6.5 The Tao-Eldrup model

A quantitative relationship which connects pick-off annihilation lifetime with the hole size or its radius R is established by the work Tao [27] and calibrated by Eldrup at al. [28], later Naganishi et al. [29]. In the Tao-Eldrup model a spherical pore (here holes of irregular shape are treated as spheres for simplicity) is described by a rectangular potential well with spherical symmetry. This rectangular potential well with radius R and a finite potential barrier ΔV is substituted by a well with an infinite potential barrier V and a size $R + \Delta R$, which is illustrated in figure 5.8. By this construction, Ps wave function occupying the ground state in the infinite potential well overlaps with bulk (electron layer in the wall of the pore) in the range between R and $R + \Delta R$.

In this model, the o-Ps pick-up annihilation rate λ equals to the multiplication of the two factors: annihilation rate in bulk and the probability P of appearance of the Ps in the area with non-zero electron density. In an infinite well, electron could not penetrate the wall. Thus, to simulate the overlap of positronium with an electron layer in sphere pore, Tao broadened the well with a layer of ΔR

thickness. So this time, the overlap area is $R \leq r \leq R + \Delta R$, it is the electron layer thickness.
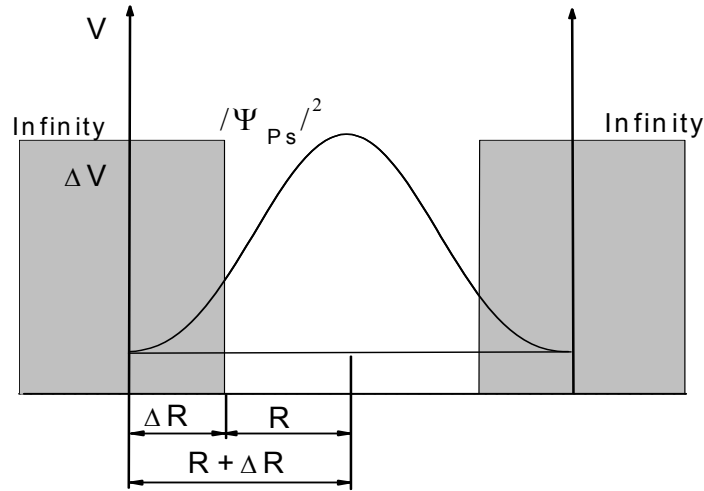

Figure 5.8 Schematic representation of the Tao-Eldrup model.

For the factor of annihilation rate in bulk, it is assumed that in the region with a high electron density, *o*-Ps annihilates with its highest possible rate, which corresponds to the spin-averaged Ps annihilation rate in vacuum with the two spin states (1/0.125 ns^{-1} and 1/142 ns^{-1}):

$$\lambda = (\lambda_{p-Ps} + 3\lambda_{o-Ps})/4 \tag{5.10}$$

and is about 2 ns^{-1}.

For the other factor of probability *P* of finding the Ps inside the electron layer range:

$$P(R) = 1 - \int_0^R |\Psi|^2 r^2 dr \,/ \int_0^{R+\Delta R} |\Psi|^2 r^2 dr \tag{5.11}$$

here, using the quantum mechanics knowledge with particle in spherical geometry well and with normalization, we could get the wave function:

$$\Psi(r) = [\frac{1}{2\pi(R+\Delta R)}]^{0.5} \sin\left(\frac{\pi r}{R+\Delta R}\right)/r \tag{5.12}$$

By integrating (5.11) with (5.12) in the range $R\sim R+\Delta R$ and multiplying with the equation (5.10), we get the Tao-Eldrup equation (here $r_h = R$ and $\delta r = \Delta R$)

$$\tau_{o-Ps\,pickoff} = \frac{0.5\,\text{ns}}{1 - \frac{r_h}{r_h+\delta r} + \frac{1}{2\pi}\sin(\frac{2\pi r_h}{r_h+\delta r})}, \quad \delta r = 1.66\,\text{Å} \tag{5.13}$$

There exist a threshold (volume of 9.2 Å^3 with radius 1.3 Å) that can be detected by PALS method. If the hole becomes smaller than that value, it cannot localize the *o*-Ps.

The overlap parameter ΔR (δr) is assumed to be the same for all materials and was empirically determined to be 1.66 Å [28, 29].

Figure 5.9 shows the comparison of the experimental data and the calculation curve following the Tao-Eldrup model. The experimental data fits the theory very well.

The Tao-Eldrup model was extended to other hole shapes (as cubes, cuboids, cylinders and large holes) as well as different potential shapes [30-34].
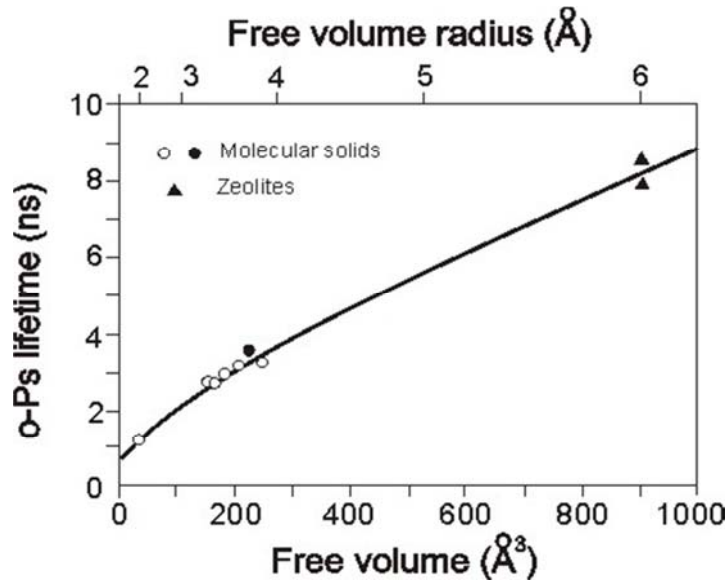
Figure 5.9 Fit of the Tao-Eldrup model to the experimental data for vacancies in molecular solids and zeolites done by Eldrup et al. [28]. Together with the experimental data of Naganishi et al. [29].

5.6.6 Hole volume calculated from positron lifetime

As described in 5.6.4, the radius of the holes shows a distribution. This can be calculated from the *o*-Ps lifetime distribution:

$$\alpha_3(\lambda) = \frac{1}{\lambda \sigma_3^*(2\pi)^{1/2}} \exp[-\frac{\left(\ln\frac{\lambda}{\lambda_{30}}\right)^2}{2\sigma_3^{*2}}]$$ (5.14)

The routine LT9 supplies as output not the annihilation rate parameters but the lifetime parameters for comparison with the conventional discrete term analysis. The distribution of lifetimes, $\alpha_3(\tau)$, is related to the distribution of annihilation rates, $\alpha_3(\lambda)$ ($\lambda = 1/\tau$), via $\alpha_3(\tau)\mathrm{d}\tau = \alpha_3(\lambda)\mathrm{d}\lambda = \alpha_3(\lambda)\lambda^2\mathrm{d}\tau$, where the mean lifetime $<\tau_3> = \tau_3 = \exp(\sigma_3^{*2}/2)/\lambda_{30}$ and the dispersion of the lifetimes (standard deviation of the distribution) is $\sigma_3 = \sigma_3(\tau) = \tau_3[\exp(\sigma_3^{*2}) -1]^{0.5}$. With τ_3 and σ_3 from the output of the LT9 routine analysis of the spectrum we can

calculate the $\alpha_3(\lambda)$. From the Tao-Eldrup model, we know the relation between λ and r. Then the hole radius distribution (pdf) is given by [23, 35]:

$$n(r_h) = -\alpha_3(\lambda)d\lambda_3/dr_h = -2\delta r\{\cos[2\pi r_h/(r_h + \delta r)] - 1\}\alpha_3(\lambda)/(r_h + \delta r)^2 \quad (5.15)$$

From the radius distribution, we get the hole volume distribution $g(v_h)$ = $n(r_h)/4\pi r_h^2$. Unfortunately, the mechanism by which o-Ps probes the holes is not well known, and it is hard to determine what a suitable weighting factor with respect to the hole size and hole shape may look like. In early works [36] it was assumed that eq. (5.15) may involve a weighting factor which increases linearly with radius and may be corrected by dividing eq. (5.15) by $k(r_h)$ = 1.0 + 8.0r_h. Our group assumes that $n(r_h)$ and $g(v_h)$ represent volume-weighted values. Indications that this picture may be warranted were discussed in several papers [37-40]. The number-weighted hole volume distribution can then be calculated from $g_n(v_h)$ = $g(v_h)/v_h$. From the statistic mathematics, the mean value and the dispersion of the hole volume are expressed by:

$$< v_h >= \int v_h g_n(v_h)dv_h \quad (5.16a)$$

$$\sigma_h = [\int (v_h - < v_h >)^2 g_n(v_h)dv_h]^{1/2} \quad (5.16b)$$

where the distribution $g_n(v_h)$ is normalized the unity area below the curve. Figure 5.10 shows the radius distribution dependence on temperature of the ionic liquid [C$_3$MIM][NTf$_2$] [21]. With increase of the temperature, the mean value of the radius as well as dispersion of lifetime distribution increase. That is coincident with the physical intuition, that when the temperature increases, the free volume expands especially above the glass transition temperature due to segmental movement of the polymer chains or the molecular groups.
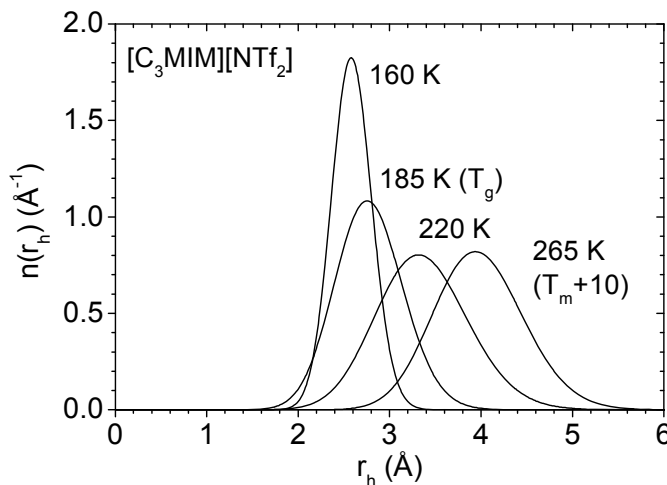
Figure 5.10 Radius distribution dependence on temperature for [C$_3$MIM][NTf$_2$] sample [21].

PALS itself is able to measure the mean volume of the holes, it can also give information of hole size distribution. But it cannot directly measure the specific hole number density and the free volume fraction. This work needs the combination of both PALS and pressure-volume-temperature (PVT, section 3.5) experiment using the following equation:

$$V_f = v_h \times N_h'$$

(5.17)

here V_f = V_{fh} is the specific hole free volume with unit cm^3/g, $<v_h>$ is the mean hole volume and N_h' is mean specific hole number density with unit g^{-1}.

5.7 Reference

1. Anderson, C.D., *The Positive Electron.* Physical Review, 1933. **43**(6): p. 491.
2. Dirac, P.A.M., *The Quantum Theory of the Electron.* Proceedings of the Royal Society of London. Series A, Containing Papers of a Mathematical and Physical Character, 1928. **117**(778): p. 610-624.
3. Y. C. Jean, P.E.M., D. M. Schrader, *Principles and Application of Positron and Positronium Chemistry.* World Scientific, Singapore, 2003.
4. R. Krause-Rehberg, H.S.L., *Positron Annihilation in Semiconductors.* Springer Verlag: Heidelberg, 1999.
5. Ore, A. and J.L. Powell, *Three-Photon Annihilation of an Electron-Positron Pair.* Physical Review, 1949. **75**(11): p. 1696.
6. Puska, M.J. and R.M. Nieminen, *Theory of positrons in solids and on solid surfaces.* Reviews of Modern Physics, 1994. **66**(3): p. 841.
7. Brandt, W. and R. Paulin, *Positron implantation-profile effects in solids.* Physical Review B, 1977. **15**(5): p. 2511.
8. Monge, M.A. and J.d. Rio, *Position annihilation in Kapton source-supporting foils.* Journal of Physics: Condensed Matter, 1994. **6**(13): p. 2643.
9. Kansy, J., *Microcomputer program for analysis of positron annihilation lifetime spectra.* Nuclear Instruments and Methods in Physics Research Section A: Accelerators, Spectrometers, Detectors and Associated Equipment, 1996. **374**(2): p. 235-244.
10. Mogensen, O.E., *Spur reaction model of positronium formation.* The Journal of Chemical Physics, 1974. **60**(3): p. 998-1004.
11. Deutsch, M., *Evidence for the Formation of Positronium in Gases.* Physical Review, 1951. **82**(3): p. 455.
12. S. V. Stepanov, V.M.B., Principles and Application of Positron and Positronium chemistry, World Scientific, Singapore, 2003: p. 117.
13. Stepanov, S.V., V.M. Byakov, and T. Hirade, *To the theory of Ps formation. New interpretation of the e+ lifetime spectrum in water.* Radiation Physics and Chemistry, 2007. **76**(2): p. 90-95.
14. Stepanov, S.V., et al., *Energy dissipation and Ps bubble growth in liquids.* Radiation Physics and Chemistry, 2007. **76**(2): p. 275-279.
15. Stepanov, S.V., V.M. Byakov, and Y. Kobayashi, *Positronium formation in molecular media: The effect of the external electric field.* Physical Review B, 2005. **72**(5): p. 054205.
16. J. Dryzek, P.H., *The Distribution of Slowing-Down Times of Positrons Emitted from ^{22}Na and ^{68}Ge\$^{68}$Ga Isotopes into Metals.* Materials Science Forum 2011. **666**: p. 10.
17. Bertolaccini, M. and et al., *Relaxed positronium in polymers.* Journal of Physics C: Solid State Physics, 1974. **7**(21): p. 3827.
18. Consolati, G., *Magnetic quenching of positronium.* Journal of Radioanalytical and Nuclear Chemistry, 1996. **210**(2): p. 273-292.
19. Amy L.R. Bug, M.M., Jillian Waldman, P.A. Sterne, *Positronium in Solids: Computer Simulation of Pick-Off and Self-Annihilation.* Materials Science Forum 2004. **Positron Annihilation - ICPA-13, 445 - 446**: p. 375.
20. Tamas Fulop, Z.F., Alfred Seeger, Janos Major, *On the inner structure of confined positronium.* [cond-mat.mtrl-sci], 2003. **arXiv:cond-mat/0304442v1**.
21. Dlubek, G., et al., *Free volume in imidazolium triflimide ([C_3MIM][NTf_2]) ionic liquid from positron lifetime: Amorphous, crystalline, and liquid states.* The Journal of Chemical Physics, 2010. **133**(12): p. 124502-10.
22. Kansy, J., *A comparison of different theoretical models of positron lifetime spectra for polymers.* Acta Physica Polonica A, 2008. **113**(5): p. 1397-1407.
23. Gregory, R.B., *Free-volume and pore size distributions determined by numerical Laplace inversion of positron annihilation lifetime data.* Journal of Applied Physics, 1991. **70**(9): p. 4665-4670.
24. Shukla, A., M. Peter, and L. Hoffmann, *Analysis of positron lifetime spectra using quantified maximum entropy and a general linear filter.* Nuclear Instruments and Methods in Physics Research Section A: Accelerators, Spectrometers, Detectors and Associated Equipment, 1993. **335**(1-2): p. 310-317.
25. Hoffmann, L., et al., *Linear and non-linear approaches to solve the inverse problem: applications to positron annihilation experiments.* Nuclear Instruments and Methods in Physics Research Section A: Accelerators, Spectrometers, Detectors and Associated Equipment, 1993. **335**(1-2): p. 276-287.

26. Peter Kirkegaard, N.J.P.a.M.E., *A Data-Processing System for Positron Annihilation Spectra on Mainfram and Personal Computers.* Risø National Laboratory, DK-4000 Roskilde, Denmark, 1989. **Tech. Rep. Risø-M-2740**.

27. Tao, S.J., *Positronium Annihilation in Molecular Substances.* Journal of Chemical Physics, 1972. **56**(11): p. 5499-&.

28. Eldrup, M., D. Lightbody, and J.N. Sherwood, *The temperature dependence of positron lifetimes in solid pivalic acid.* Chemical Physics, 1981. **63**(1-2): p. 51-58.

29. H Nakanishi, S.W., YC Jean, *Positron Annihilation Studies of Fluids.* Sharma, S. C., Ed., Word Scientific Singapore, 1988: p. 292.

30. Jasińska, B., A. Kozioł, and T. Goworek, *Ortho-positronium lifetimes in nonspherical voids.* Journal of Radioanalytical and Nuclear Chemistry, 1996. **210**(2): p. 617-623.

31. Goworek, T., et al., *Positronium in large voids. Silicagel.* Chemical Physics Letters, 1997. **272**(1-2): p. 91-95.

32. Gidley, D.W., et al., *Positronium annihilation in mesoporous thin films.* Physical Review B, 1999. **60**(8): p. R5157.

33. Dauwe, C., et al., *Trapping of positronium in a size-dependent spherical square well potential.* Radiation Physics and Chemistry, 2000. **58**(5-6): p. 681-685.

34. Bug, A.L.R., et al., *Simulation of positronium: Toward more realistic models of void spaces in materials.* Radiation Physics and Chemistry, 2007. **76**(2): p. 237-242.

35. Deng, Q., F. Zandiehnadem, and Y.C. Jean, *Free-volume distributions of an epoxy polymer probed by positron annihilation: temperature dependance.* Macromolecules, 1992. **25**(3): p. 1090-1095.

36. Liu, J., Q. Deng, and Y.C. Jean, *Free-volume distributions of polystyrene probed by positron annihilation: comparison with free-volume theories.* Macromolecules, 1993. **26**(26): p. 7149-7155.

37. Dlubek, G., et al., *Temperature dependence of the free volume in fluoroelastomers from positron lifetime and PVT experiments.* Macromolecules, 2004. **37**(17): p. 6606-6618.

38. Dlubek, G., et al., *High-pressure dependence of the free volume in fluoroelastomers from positron lifetime and PVT experiments.* Macromolecules, 2005. **38**(2): p. 429-437.

39. Kilburn, D., et al., *Microstructure of free volume in SMA copolymers I. Free volume from Simha-Somcynsky analysis of PVT experiments.* Polymer, 2005. **46**(3): p. 859-868.

40. Kilburn, D., et al., *Microstructure of free volume in SMA copolymers II. Local free volume from PALS.* Polymer, 2005. **46**(3): p. 869-876.

6 High molecular-weight organic materials: polymers

6.1 Amorphous polymers 1,2-poly(butadiene), cis-1,4-poly(isoprene)

6.1.1 Introduction

The origin of glass transition, as well as viscous and relaxation slowing down of supercooled liquids is still an elusive problem in polymer science. Compared with the static structure, which can be characterized by X-ray and neutron studies, showing a monotonous change over a wide temperature range down to the glass transition regime [1-3], dynamic parameters such as relaxation and viscosity change over some 15 decades in a relatively narrow temperature range 100 – 150 K [4, 5]. Distinct dynamical regimes that cannot be described by one Vogel-Fulcher-Tammann-Hesse (VFTH) equation are indicated by crossover temperature such as Arrhenius, Stickel or Schonehals temperatures. The absence of structural changes and the radical change in dynamics parameter arise the question: what is the basic physical factor controlling the glass formation and the dramatic relaxation parameter change in a wide temperature range of polymers: kinetics, thermodynamics or free volume.

In this work the free volume in two amorphous polymers 1,2-poly(butadiene) (PBD) and cis-1,4-poly(isoprene) (PIP) was studied. To depict the temperature dependence of the microstructure as completely as possible, positron annihilation lifetime spectroscopy (PALS) and pressure-volume-temperature (PVT) technique are employed. The free volume parameters are compared with dynamics data from broadband dielectric spectroscopy (BDS) [6] and from electron spin resonance (ESR) experiments [7].

6.1.2 Materials and experiments

Two structurally simple polymers are used in this study: 1,2-poly(butadiene) (PBD, chemical structure formula - [CH_2 - $CH(CH=CH_2)$]$_n$ -) with high fragility (m_g = 129) and cis-1,4-poly(isoprene) (PIP, chemical structure formula - [CH_2 - CH = C (CH_3) - CH_2]$_n$ -) with low fragility (m_g = 63). The PBD sample was prepared by Dr. L. Willner from the Institut für Festkörperforschung (IFF) Jülich, Germany. The PIP sample was obtained from Aldrich Inc. Both samples were supplied by Prof. Jozef Bartos from the Polymer Institute, Slovak Academy of

Sciences, Bratislava, Slovakia.

Analytical data obtained by temperature-modulated differential-scanning calorimetry (MDSC) and pressure-volume-temperature (PVT) experiments were provided by Dr. J. Pionteck (Leibniz-Institut für Polymerforschung Dresden e.V.). MDSC was performed with a DSC Q2000 V24.4 (PIP) and a DSC Q1000 V9.9 (PBD) device, respectively, both from TA Instruments and operated with a heating rate of 3 K/min and a temperature modulation ± 0.318 K in a period of 30 s.
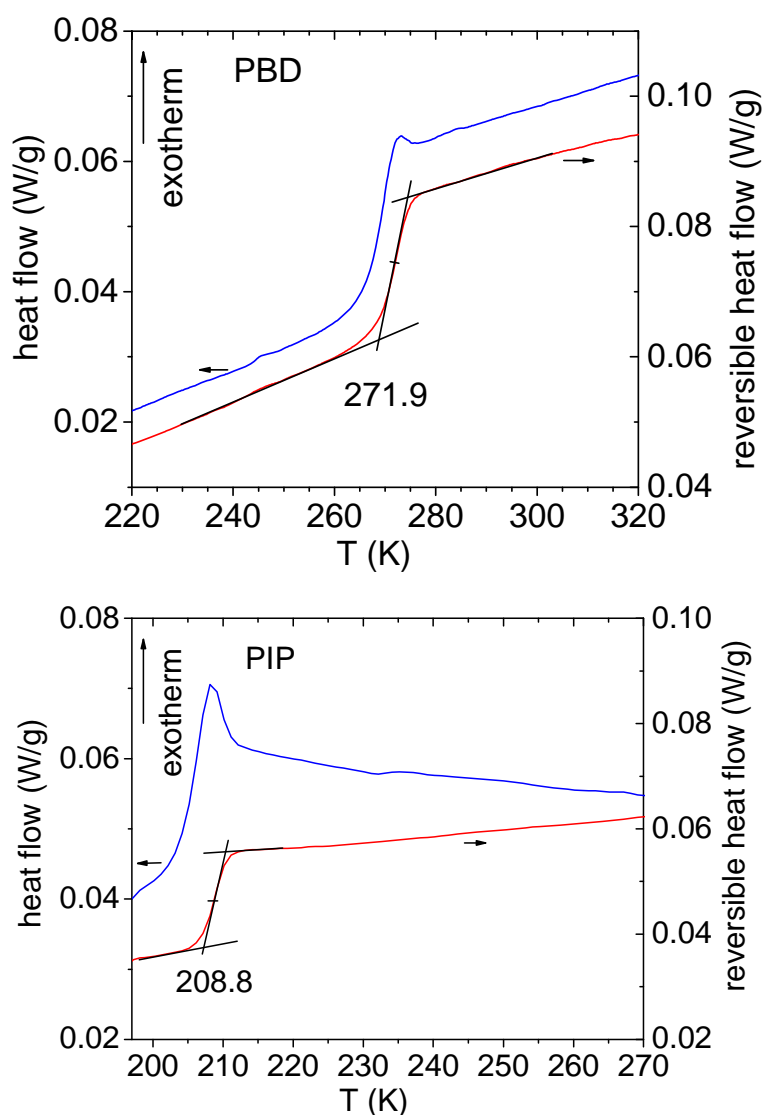
Figure 6.1 MDSC heating scan with a rate of 3 K/min (first heating). Shown are the heat flow and the reversible heat flow curves, the latter was used to determine glass transition temperature T_g. a) Top: PBD. b) Bottom: PIP

The PBD used in this work has a molecular mass of $M_n = 2 \times 10^4$ g/mol and the following isomer microstructure: 95% of 1,2-isomers and 5% of 1,4-cis + 1,4-trans-isomers (Dr. L. Willner). The heating scans of MDSC are shown in

figure 6.1 a. The analysis gives a glass transition range between 269.0 K and 274.6 K and a glass transition temperature T_g = 271.9 K was estimated from the midpoint of the reversible heat flow curve. The specific heat capacity change at T_g is ΔC_p = 0.611 J/g·K.

PIP had 97% of cis-isomers and M_n = 8x10^5 g/mol (Aldrich). The MDSC scan show a glass transition in the temperature range between 207.1 K and 210.5 K with T_g = 208.8 K and ΔC_p = 0.372 (figure 6.1 b).

6.1.3 Experiment results and discussion

6.1.3.1 PVT: temperature and pressure dependence

PVT experiments were carried out by means of a fully automated GNOMIX high-pressure mercury dilatometer. Both the polymers were measured between room temperature and 455 K in steps of 5 – 10 K in standard isothermal mode (ITS). Tait (solid lines) and Simha-Somcynski (empty symbols) equation of state (chapter 3) were used to fit the PVT experimental data (specific volume shown as solid dots) for PBD and PIP samples in this work. Figure 6.2 and 6.3 display the fitting result for both samples, respectively.
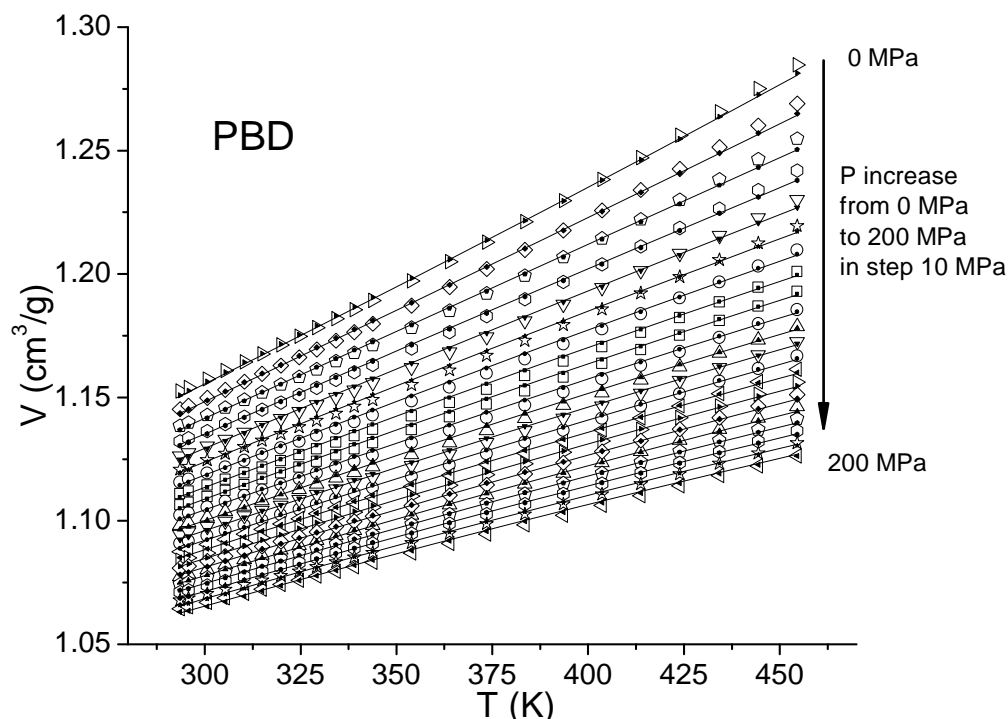
Figure 6.2 The specific total volume V(solid dots) of PBD as a function of temperature *T* at a series of constant pressure *P* (in MPa, increase from top to bottom from 0 MPa to 200 MPa in 10 MPa step). The solid lines show the fits of the Tait equation and the empty symbols those of the S-S eos to the volume data.
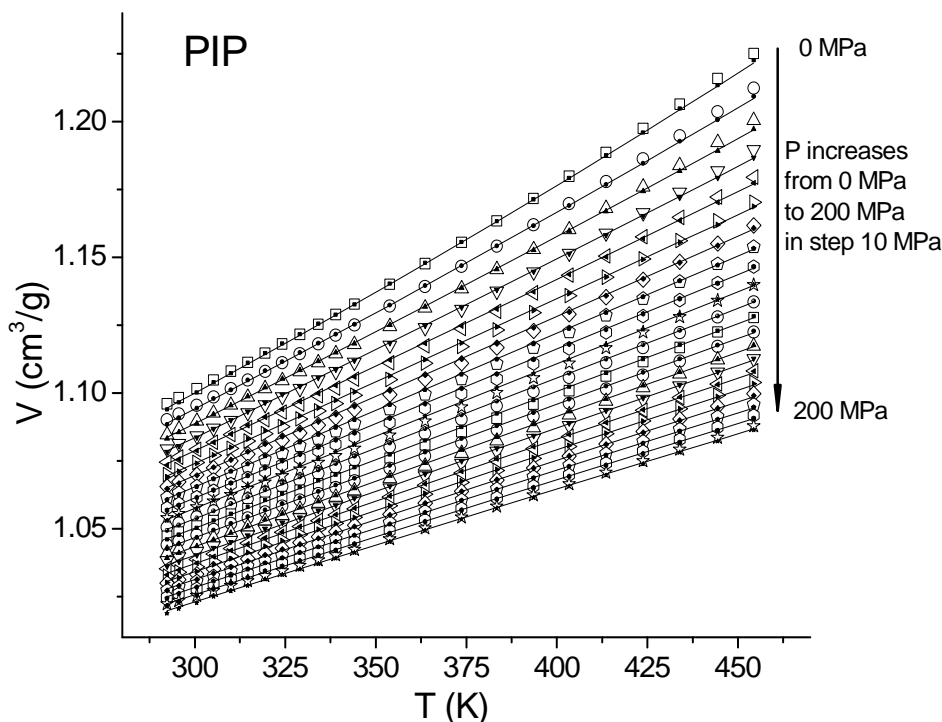
Figure 6.3 Same as figure 6.2, but for PIP sample.

The fitting parameters are summarized in table 6.1: a_0, a_1, a_2, C, b_0, b_1 are six fitting parameters in the Tait equation (section 3.2). The coefficients of determination were $R^2 = 0.99996$ (PBD) and 0.99995 (PIP). T^*, V^*, P^* are scaling parameters for temperature, volume and pressure in the Simha-Somcynsky equation of state (section 3.4). M_{rep} is the molecular mass of the chemical repeating unit. M_0 is the molecular weight of a mer of the lattice. When assuming one external degree of freedom per s-mer and infinite chain length for the polymers studied in this work, $M_0 = RT^*/(3P^*V^*)$, R is the gas constant. V_{sp} is the total specific volume, V_{occ}, V_f are the specific occupied volume and the specific free volume, respectively. The volume of a cell of the S-S lattice $v_{SS} = M_0 V_{occ}/N_A$, N_A is the Avogadro number. V_W is the molar van der Waals volume estimated from the group contributions tabulated by van Krevelen [8]. h is the free volume fraction.

For PBD at ambient pressure and 300 K, $V_{sp}/V_w = 1.682$, $V_{occ}/V_w = 1.578$, $V^*/V_w = 1.654$, and $V_{occ}/V^* = K = 0.9544$. $M_{rep}/M_0 = 1.36193$, is the number of external degrees of freedom per chemical repeat unit, a measure of the flexibility of the polymer chains.

For PIP, $V_{sp}/V_w = 1.573$, $V_{occ}/V_w = 1.475$, $V^*/V_w = 1.544$, and $V_{occ}/V^* = K = 0.9551$. $M_{rep}/M_0 = 1.98272$.

Table 6.1 Results from the Tait and the S-S eos analysis of the PVT experiment.

Tait equation				
Quantity	PBD	Uncertainty	PIP	Uncertainty
a_0 (cm^3 g^{-1})	0.94417	8.8 E-4	0.92138	8.8 E-4
a_1 (cm^3 g^{-1} K^{-1})	6.3593 E-4	4.9 E-6	4.6875 E-4	4.9 E-6
a_2 (cm^3 g^{-1} K^{-2})	2.2904 E-7	6.8 E-9	4.2218 E-7	6.8 E-9
C	0.08132	1.9 E-4	0.08433	2.6 E-4
b_0 (MPa)	523.3	2.6	648.7	3.7
b_1 (K^{-1})	0.00479	1.4 E-5	0.00478	1.5 E-5
R^2	0.99996		0.99995	
Simha-Somcynski equation of state				
Quantity	PBD	Uncertainty	PIP	Uncertainty
T^* (K)	10158.186	13.193	10031.981	11.300
V^* (cm^3/g)	1.13684	3.458 E-4	1.07951	2.958 E-4
P^* (MPa)	624.549	1.887	750.934	2.363
M_{rep} (g/mol)	54		68	
M_0 (g/mol)	39.6497	0.131	34.2963	0.115
v_{SS} (Å^3)[a]	71.4617	0.2363	62.6677	0.2101
V_{sp} (cm^3/g)[a]	1.156	0.002	1.100	0.002
V_w (cm^3/g)	0.6874		0.6992	
V_{occ} (cm^3/g)[a]	1.085	0.003	1.031	0.003
V_f (cm^3/g)[a]	0.071	0.003	0.069	0.003
h[a]	0.060	0.003	0.063	0.003
H_h (kJ/mol)	6.45	0.5	6.47	0.5
E_c (kJ/mol)[b]	18.9 - 17.1	0.1	18.7 - 16.8	0.1
δ (MPa$^{1/2}$)[b]	20.4 - 18.3	0.1	22.3 - 20.0	0.1

a: For T = 300K, P = 0 MPa.
b: For T = 295 K – 455 K, P = 0 MPa.

Figure 6.4 and 6.5 show isobars of respective specific volumes (V_{sp}, V_{occ} and V_f) for selected pressures. Although the occupied volume takes a large amount of the total volume (> 85%), the dominant volume changes come from the free volume. This fact is more evident from figures 6.6 and 6.7, which display the behavior of the isobaric thermal expansion coefficient α =

$(1/V)(dV/dT)|_p$, $\alpha_{occ}^* = (1/V)(dV_{occ}/dT)|_p$ and $\alpha_f^* = (1/V)(dV_f/dT)|_p$. More than 95% volume change comes from free volume for both polymers.
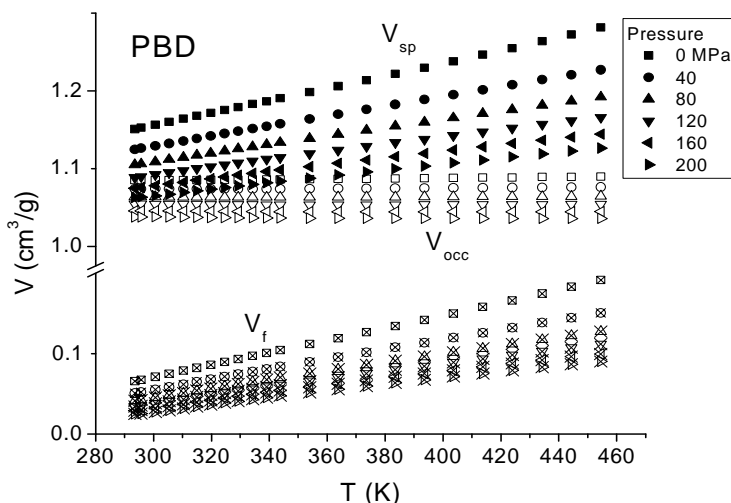
Figure 6.4 The specific total, V_{sp}, occupied, V_{occ}, and free, V_f, volume for PBD as a function of temperature T under selected pressures P.
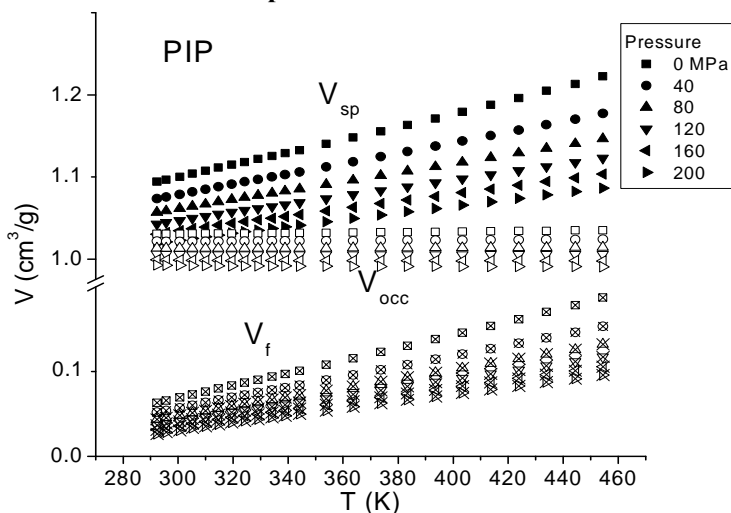
Figure 6.5 As figure 6.4, but for PIP sample.
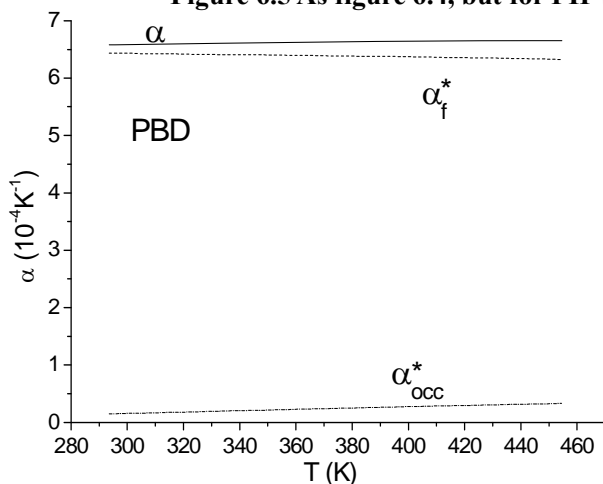
Figure 6.6 The temperature dependency of the isobaric coefficient of thermal expansion for ambient pressure of the total volume, α, and its constituents, the occupied, α_{occ}^*, and free α_f^*, volume for PBD.
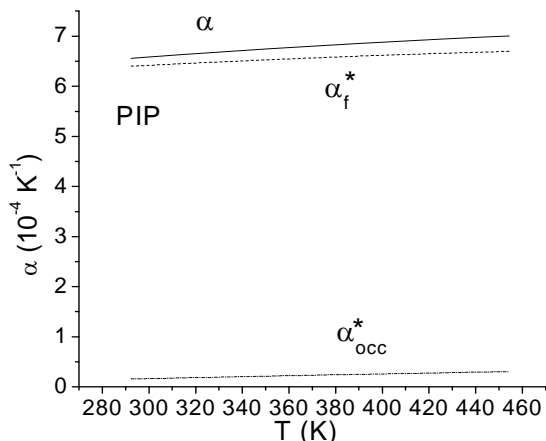
Figure 6.7 As figure 6.6, but for PIP sample.

The temperature dependences of the free volume fraction h obtained from fitting of the PVT data for selected pressures to the S-S eos are shown in figure 6.8 (PBD) and figure 6.9 (PIP). When considering the vacancies in the lattice-hole model as Schottky-point defects, the equilibrium concentration (hole fraction h in this work) can be expressed by the Schottky equation [9]:

$$h = A \exp(-H_h/k_B T) \tag{6.1}$$

here: A is a constant, k_B is the Boltzmann constant, and H_h is the hole formation enthalpy. Fitting the data in figure 6.8 at ambience delivers $A = 0.83$ and $H_h = 6.45$ kJ/mol ($R^2 = 0.9992$) for PBD. For PIP, $A = 0.85$ and $H_h = 6.47$ kJ/mol ($R^2 = 0.9995$). The cohesive energy E_c [10] in the temperature range 295 K – 455 K has the value 18.9 – 17.1 kJ/mol (PBD) and 18.7 – 16.8 kJ/mol (PIP), so the value of H_h corresponds to 0.34 – 0.38 (PBD) and 0.35 – 0.39 (PIP) of E_c. The solution parameter $\delta = $ CED$^{1/2}$ [10] (CED is cohesive energy density) equals 20.4 – 18.3 MPa$^{1/2}$ (PBD) and 22.3 – 20.0 MPa$^{1/2}$ (PIP) in the same temperature range.
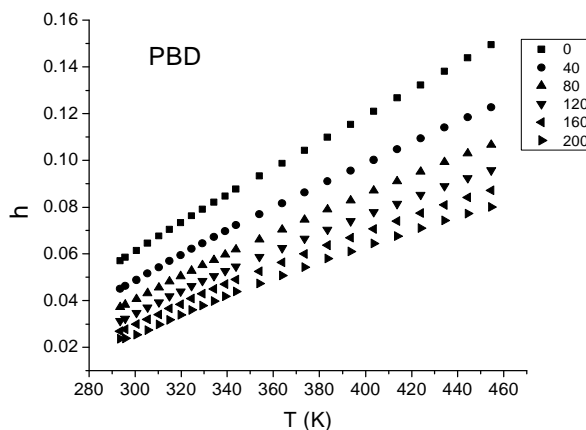
Figure 6.8 Temperature dependence of the free volume fraction h under selected pressures for PBD.
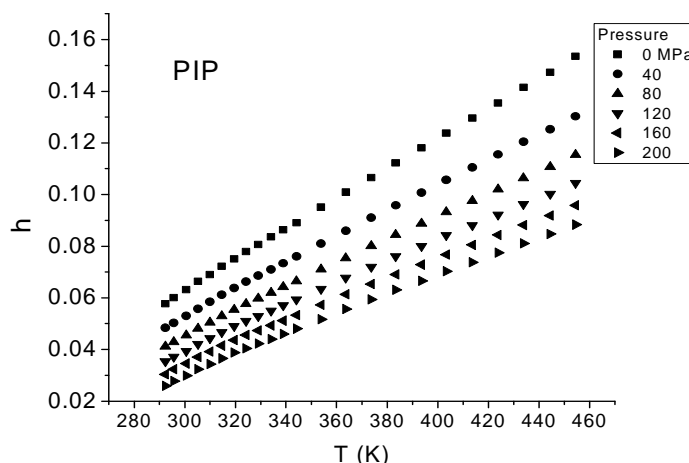
Figure 6.9 As figure 6.8, but for PIP sample.

6.1.3.2 PALS: temperature dependence

The positron lifetime parameters for the PBD sample exhibit a simple behavior similar to that known for amorphous polymers [11] or low-molecular weight glass formers [12]. Figure 6.10 shows the o-Ps lifetime parameters during a heating run. The $<\tau_3>$ and σ_3 mirror the mean size and dispersion of the hole size distribution. Two crossover temperature points T_g (265 ± 5 K) and T_k (355 ± 5 K) corresponding to glass transition and "knee" temperature can be discerned from the slope changes of the mean o-Ps lifetime $<\tau_3>$. Below T_g, o-Ps is trapped in local free volume within the glassy matrix and detects more or less static frozen holes. Above T_g, due to rapidly increasing thermal motion of polymer segments in rubbery state, the holes among them grow steeply in the heating run and show an increasingly broader distribution. With increasingly segmental mobility in frequency, the structural relaxation time decreases toward to the order of the o-Ps lifetime, which will smear the hole during the lifetime of o-Ps. Thus, $<\tau_3>$ no longer mirrors correctly the hole size. The combined effect of hole expansion and increasing hole smearing may cause the apparent constancy of $<\tau_3>$, which levels off at T_k.

Positron lifetime parameters of the PIP sample exhibit a similar behavior as PBD except one more crossover temperature denoted as Tb_1 (255 ± 5 K) between T_g (205 ± 5 K) and T_k (290 ± 5 K), such manner is often observed for strong polymers or low-molecular weight glass formers with smaller fragility, such as cis-trans-1,4-poly(butadiene) [13], glycerol [14] and propylene glycol [15]. Details of these crossover temperatures will be discussed in the structure dynamics section.
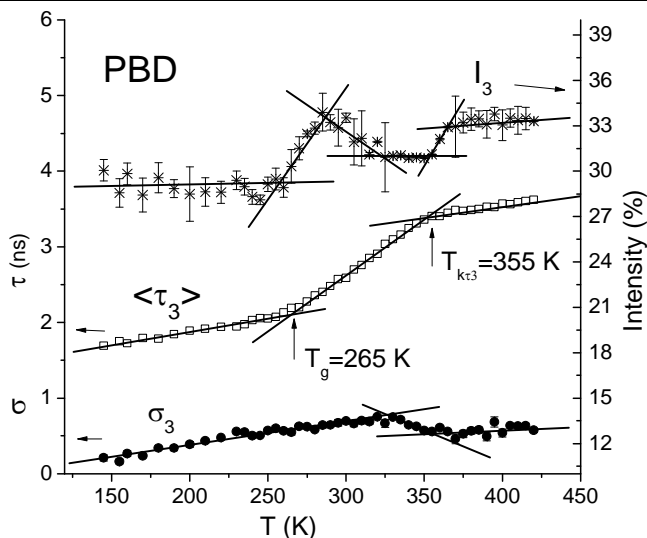
Figure 6.10 The mean, $<\tau_3>$, the standard deviation, σ_3 and the intensity I_3 of the o-Ps lifetime distribution as a function of temperature T during heating of PBD. T_g indicates the glass transition temperature and T_k the "knee" temperature.
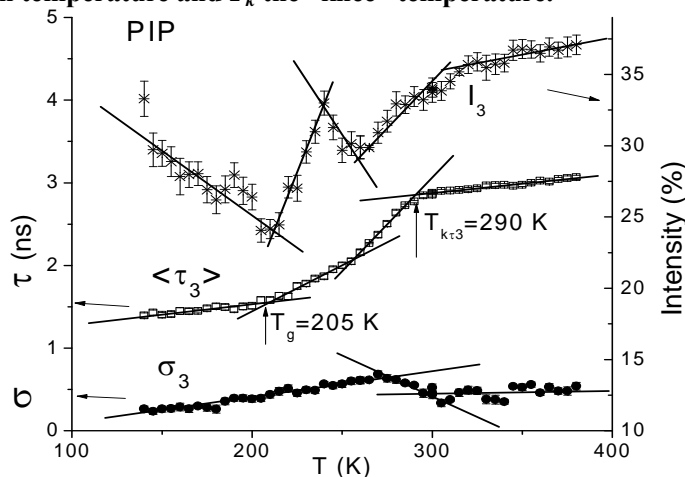
Figure 6.11 As figure 6.10, but for PIP sample.

The mean size $<v_h>$ and dispersion σ_h of the local free volume distribution is calculated from the standard Tao-Eldrup model [16, 17]. The $<v_h>$ linearly increases with temperature from 80 Å^3 to 230 Å^3 with a slope change at T_g and levels off at T_k (PBD, figure 6.12). For PIP, the $<v_h>$ changes linearly with temperature between 50 Å^3 to 170 Å^3 with slope changes at T_g, Tb_1 and levels off at T_k (PIP, figure 6.13). The $<v_h>$ shows similar features as o-Ps lifetime for both polymers in this work.

The linear fit between the specific free volume at 0 MPa, determined from PVT experiments and the mean local free volume, obtained from PALS, at supercooled regime of the form:

$$V_f = N_h' \times < v_h > \tag{6.2}$$

gives the specific hole density $N_h' = 0.45 \times 10^{21}$ g^{-1}, that is 0.39 nm^{-3} at 300 K

for PBD (figure 6.14). For PIP (figure 6.15), the fitting range is between Tb_1 and T_k, and the specific hole density $N'_h = 0.28 \times 10^{21}$ g^{-1}, that is 0.25 nm^{-3} at 300 K.
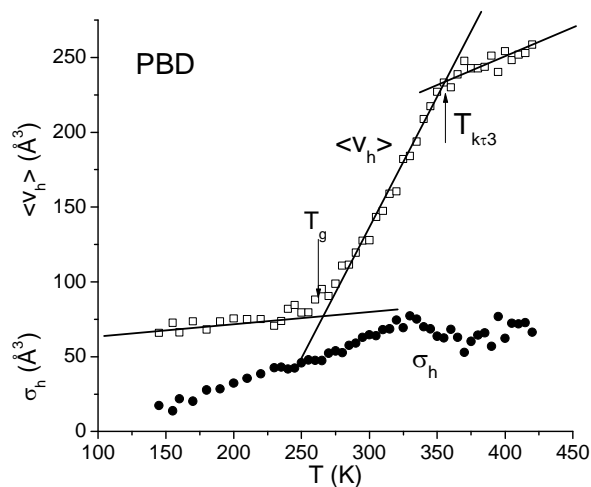
Figure 6.12 Number-weighted mean $<v_h>$ and standard deviation σ_h of the hole size calculated from positron lifetime for PBD sample.
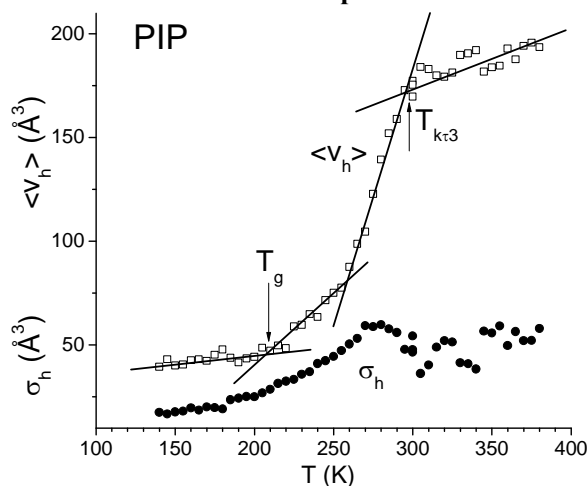
Figure 6.13 As figure 6.12, but for PIP sample.
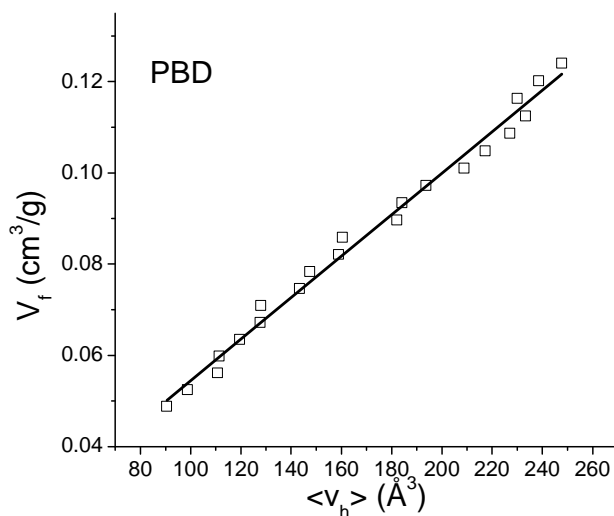
Figure 6.14 Plot of the specific free volume calculated from the fit of PVT data under 0 MPa vs the mean hole volume at the supercooled liquid state (between T_g and T_k) for PBD. The line is a linear fit of the data.
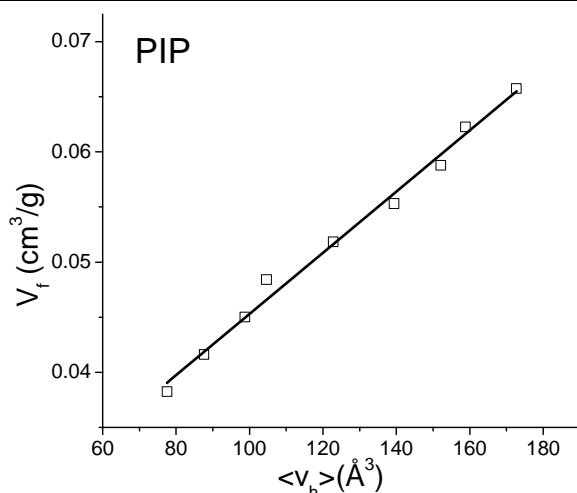
Figure 6.15 As figure 6.14, but for PIP sample, the fitting range is between Tb_1 and T_k.

All the parameters from PALS experiment are summarized in table 6.2.

Table 6.2 Result parameters from PALS experiment.

PALS				
Quantity	PBD	Uncertainty	PIP	Uncertainty
v_f (Å^3)^a	127.93		175.42	
N' (g^{-1})	0.45 E21	E19	0.28 E21	E19
N(nm^{-3})^a	0.39		0.25	
T_g(DSC)	271.9 K		208.8 K	
T_g(PALS)	265 K	5 K	205 K	5 K
Tb_1			255 K	5 K
Tb_1/T_g			1.24	
$Tb_2(T_k)$	355 K	5 K	290 K	5 K
Tb_2/T_g	1.38		1.45	

a: For T = 300K

6.1.3.3 BDS: temperature dependence

The primary (α) relaxation time τ_α determined by broadband dielectric spectroscopy (BDS) [6] (solid circle) is compared with the o-Ps lifetime (empty square) in figure 6.16 for the PBD sample. In BDS experiments, the glass transition occurs when τ_α equals 100 s. For PBD, T_g(BDS) = 269 K, corresponding to the T_g(DSC) = 271.9 K and T_g(PALS) = 265 ± 5 K. The threshold temperature for the Arrhenius region T_A is 360 K, which is in agreement with $Tb_2(T_k)$ = 355 K ± 5 K from PALS. $\tau_\alpha(T_A)$ = 7 × 10^{-9} s reaches the magnitude of the o-Ps lifetime. T_A is often found to be close to T_m, which

indicates a transition from ordinary, normal liquid to the frustrated solid-like state of a supercooled liquid [18-21]. For crystallisable polymers, T_m corresponds to the melting temperature of the crystalline phase of crystallizing non-frustrated materials.
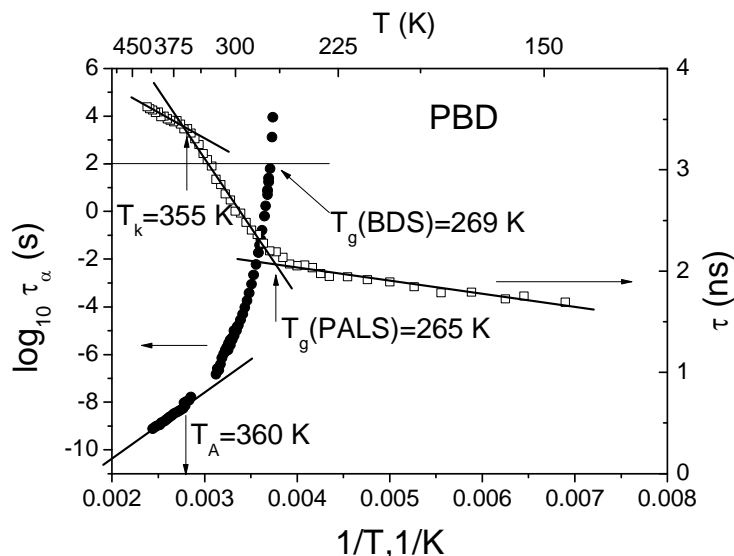
Figure 6.16 Arrhenius plot of the structural relaxation times (solid circle) vs *o*-Ps lifetime (empty square) for PBD. The characteristic Arrhenius temperature T_A = 360 K.

6.1.3.4 ESR: temperature dependence

Electron spin resonance (ESR) experiment result was supplied by Prof. Dr. Jozef Bartos from the Polymer Institute Bratislava, Slovak Academy of Sciences [7]. Two spin probes were used: 2,2,6,6-tetramethyl-1-piperidinyloxy, known as TEMPO and 4-Maleinimido-2,2,6,6-tetramethyl-1-piperidinyloxy (MI-TEMPO) from Aldrich Chemical Comp., Inc. Their chemical structure, molecular mass in g/mol and van der Waals volume in $Å^3$ are presented in figure 6.17 [22].
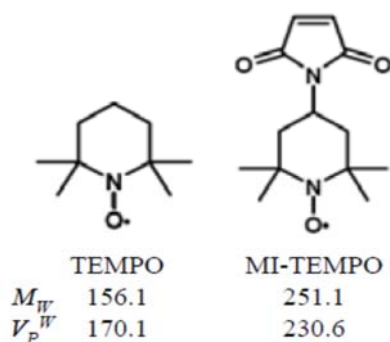
Figure 6.17 Chemical structure, molecular mass in g/mol and van der Waals volume in $Å^3$ of the two spin probes used in this work [22].

$2A_{zz'}$ is the spectral parameter of the spin probe mobility. The lower value represents a faster rotation mobility of the spin probe particle. Distinct four regions can be discerned from the comparison between the $2A_{zz'}$ and *o*-Ps

lifetime in figure 6.18. T_{50G} denotes the temperature at which the spin probe rotation mobility changes from the slow regime to the fast regime in ESR experiments. For TEMPO, T_{50G} = 255 K, corresponding to Tb_1 (255 K) from PALS. Another crossover temperature, T_{X2} = 288 K, corresponds to T_k (290 K) from PALS. For MI-TEMPO, T_{50G} = 288 K is close to T_k (290 K) from PALS.
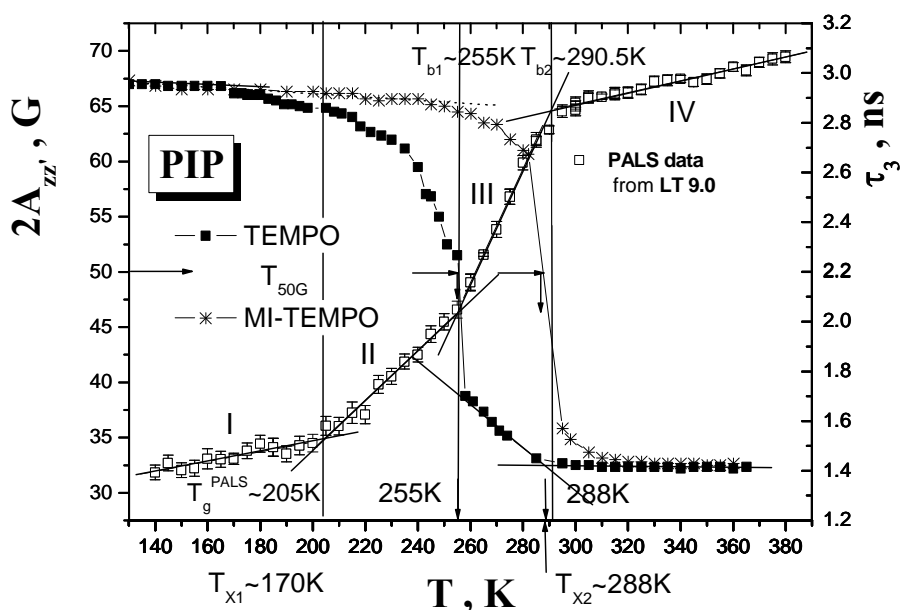
Figure 6.18 Comparison between the spectral parameter of spin probe mobility, $2A_{zz'}$, obtained from ESR experiments, and mean o-Ps lifetime, obtained from PALS experiments, for the PIP. The characteristic temperatures indicate four regions.

The number-weighted hole volume distribution $g_n(v_h)$ (section 5.6.6) at selected temperature calculated from o-Ps lifetime parameters for the PIP sample is shown in figure 6.19. The v_{ss} = 62.6677 Å^3 is the volume of a cell of the S-S lattice from PVT experiment, which is close to the van der Waals volume (78.98 Å^3) of repeat unit in the polymer chain. v_{occ_PIP} is the occupied volume of repeat unit, it equals 116.46 Å^3. The van der Waals volumes of the two spin probe particles TEMPO and MI-TEMPO are V_{W_TEMPO} = 170.1 Å^3 and $V_{W\_MI-TEMPO}$ = 230.6 Å^3.

At the Tb_1 = T_{G50} = 255 K, tail of the volume distribution covers the V_{W_TEMPO}, which means there exist holes with volume larger than V_{W_TEMPO}. That is the prerequisite for the slow to fast regime transition in the ESR experiments. But it is not the sufficient condition since at 245 K, the volume distribution also includes the V_{W_TEMPO} value. The same is found for MI-TEMPO at T_k (290 K) ~ T_{G50} (288 K). Therefore, there must be an underlying physical factor that

affects both spin probe rotation mobility and *o*-Ps lifetime at the same characteristic temperature. Further work is needed to clarify this factor.
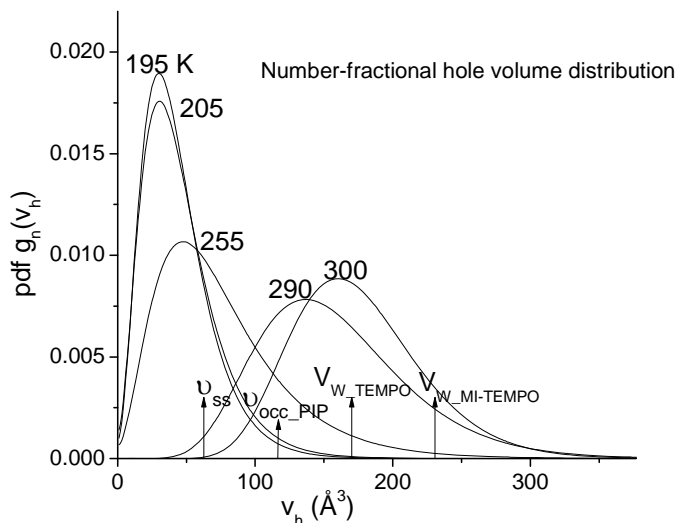
Figure 6.19 Number-weighted hole volume distribution at selected temperatures from the PALS experiment. The volume of a cell of the S-S lattice from the PVT experiment, υ_{ss}, the occupied volume of repeat unit in polymer chain of PIP, υ_{occ_PIP}, and the van der Waals volume of TEMPO and MI-TEMPO are denoted by arrows.

6.1.4 Conclusion

The thermal extension coefficient of PVT experiment shows that above T_g dominant volume change comes from free volume for amorphous polymers. A combination of the specific free volume from PVT experiment and the mean hole free volume from PALS delivers the specific number density: 0.45×10^{21} g^{-1} (PBD), 0.28×10^{21} g^{-1} (PIP). Clearly state transitions can be observed from *o*-Ps lifetime parameters. For amorphous polymers with high fragility like PBD, no obvious slope change can be observed between T_g and T_k in the PALS experiment. The crossover temperatures, which denote the state transition from PALS, are in good agreement with the characteristic bend temperatures, which denote dynamic motion mode changes in BDS and ESR experiments. This suggests the free volume origin of the change in dynamic regime of amorphous polymers.

6.2 Phase transitions in polymers containing long self-assembled CF$_2$ sequences in side chain

Semicrystalline polymers such as polyethylene and polypropylene have been studied for decades. Long main chain folding in local domains (normally 10 nm thickness) plays an important role for crystallization in these materials. Compared to the variety of studies on crystallizable main chain polymers, less is known about the side-chain polymer crystallization [23-26]. This section deals with the application of positron annihilation lifetime spectroscopy (PALS) in the study of the temperature dependence of the size of sub-nanometer local free volumes (holes) in three self-assembled semifluorinated side chain polyesters. The aim of the section is to get insights into the microstructure of these complex polymers and its changes during the phase transitions.

6.2.1 Samples

The semi-fluorinated samples selected in this work all have the same oxydecyl-perfluorodecyl side chains (R$_1$ in figure 6.20 –O-(CH$_2$)$_{10}$-(CF$_2$)$_9$-CF$_3$). Poly (*p*-phenylene-5– oxydecyl-perfluorodecyl isophthalate) is denoted as HQ; two aromatic-aliphatic polyesters with spacers R$_2$ corresponding to –(CH$_2$)$_6$- and –(CH$_2$)$_8$- are denoted as H6 and H8, respectively. These samples were synthesized by melt polycondensation as reported by Pospiech et al. [27]. The chemical characterizations of the samples used in this study are summarized in Table 6.3.
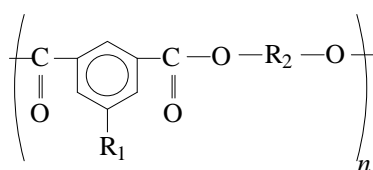
Figure 6.20 General chemical structure of the investigated polyesters. R$_1$: O-(CH$_2$)$_{10}$-(CF$_2$)$_9$-CF$_3$; R$_2$: p-phenylene for HQ, (CH$_2$)$_6$ for H6 and (CH$_2$)$_8$ for H8, respectively.

Table 6.3 Composition and chemical characterization of the semi-fluorinated polyesters studied. M$_{n,GPC}$, M$_{w,GPC}$ and η$_{inh}$ denote the number and weight averaged molecular mass and the solution viscosity.

Polymer	R$_1$	R$_2$	M$_{n,GPC}$[2) (g/mol)	M$_{w,GPC}$[2) (g/mol)	M$_w$/M$_n$ (g/mol)	η$_{inh}$[1) (dL/g)
HQ	-O-(CH$_2$)$_{10}$-(CF$_2$)$_9$-CF$_3$	Ph	28,000	57,600	2.06	0.33
H6	-O-(CH$_2$)$_{10}$-(CF$_2$)$_9$-CF$_3$	-(CH$_2$)$_6$-	12,900	63,400	4.93	0.49
H8	-O-(CH$_2$)$_{10}$-(CF$_2$)$_9$-CF$_3$	-(CH$_2$)$_8$-	14,400	86,700	6.02	0.47

[1) Solution viscosity in trifluoroacetic acid/chloroform (1/1 vol/vol), Ubbelohde viscometer at 25 °C, polymer concentration 0.5 g/dL.
[2) Knauer GPC with pentafluorophenol/chloroform (1/2 vol/vol) as eluent, RI detection, PL MiniMix-D separation column, molar masses were calculated relative to small distributed polystyrene standard.

The molecular model for the structure of HQ is shown in figure 6.21 [26]. The semi-fluorinated side chains of HQ are rigid and stretched. They are arranged in a layer between the backbones of the aromatic polyester.
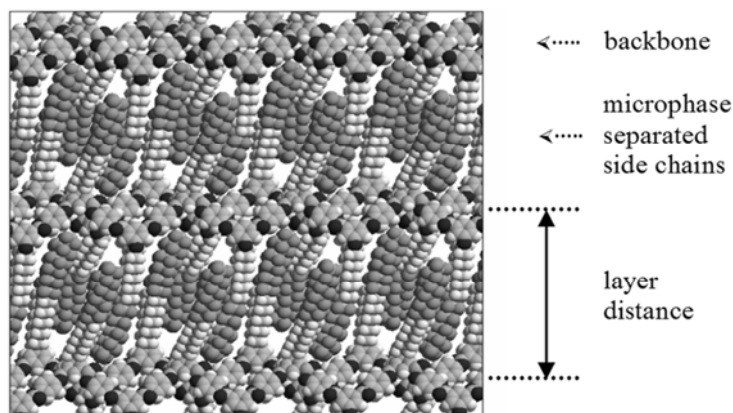

Figure 6.21 Molecular model [26] of the solid state structure of the semifluorinated aromatic polyester poly(p-phenylene-oxydecylperfluorodecyl-isophthalate) (sample HQ) based on the X-ray data of solution synthesized [28] samples.

6.2.2 Experimental results and discussion

6.2.2.1 Differential Scanning Calorimetry (DSC)

DSC was performed using a Perkin Elmer DSC 7 system at a scan rate of 10 K/min by Mrs. L. Häußler, Leibniz-Institut für Polzmerforschung Dresden e.V.. The transition temperatures were determined from the second heating run. For HQ, there are three endothermic transitions in the DSC curve (figure 6.22), assigned to side chain melting (T_m = 330 K), glass transition of the aromatic main chain (T_g = 400 K) and isotropization (T_i = 470 K). The H6 and H8 only have two visible transitions corresponding to side chain melting T_m (352 K for H6, 349 K for H8) and isotropization T_i (422 K for H6, 410 K for H8).
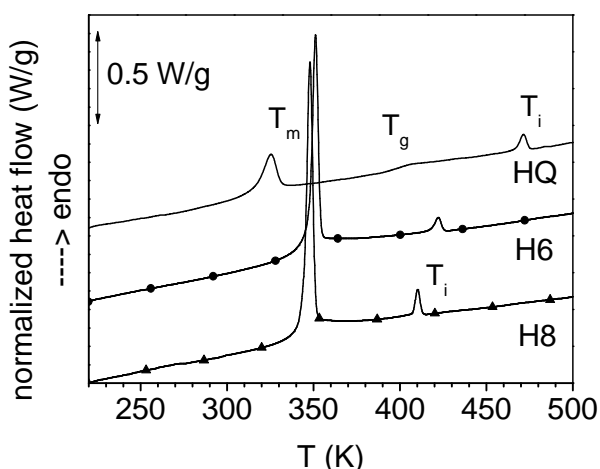
Figure 6.22 Complete 2nd heating run (DSC) of the aromatic polyester HQ (————) compared to the semifluorinated polyesters H6 (————●————) and H8 (————▲————).

6.2.2.2 Temperature-Dependent Small-Angle X-ray Scattering (T-SAXS)

T-SAXS was performed by Dr. D. Jehnichen et al., Leibniz-Institut für Polymerforschung Dresden e.V., using synchrotron radiation (SR wavelength: 0.15 nm) at DESY Hamburg, HASYLAB, beamline A2, with heating/cooling cycles from 300 K to 570 K with 3 K/min. A contour plot of SAXS curve at different temperatures in heating and cooling run for sample H8 is represented in figure 6.23.
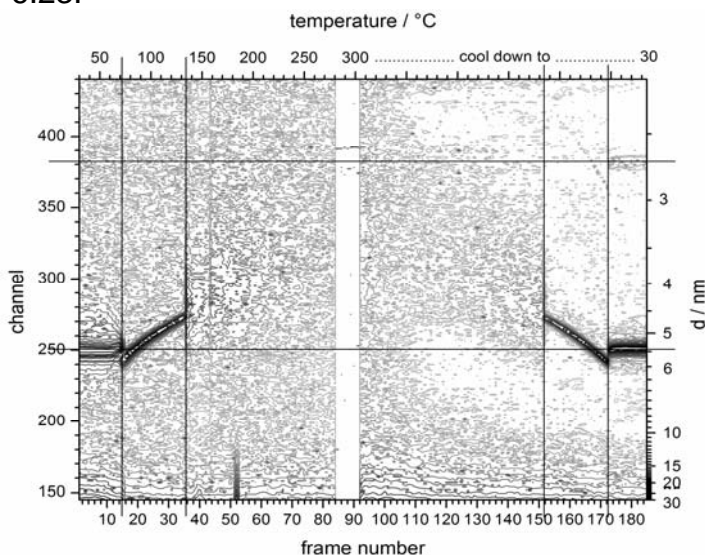
Figure 6.23 Topographic contour plot of the intensity *I* *vs.* the temperature *T* and the layer spacing *d* of T-SAXS measurements of sample H8. Here the temperature is given in °C.

Three temperature regions representing the different structure behavior of H8 can be discerned. a) From room temperature up to T_m = 345 K (75 °C), a layer structure with a constant layer spacing of d = 5.4 nm is found. At T_m a melting takes place connected with a loss of lateral correlation of the side chains, and d jumps to 5.82 nm. b) From T_m to T_i = 408 K (135 °C), d drops down to 4.65 nm continuously to T_i (referred to as isotropization) and vanishes. c) For $T > T_i$, no further structural information can be found. In the cooling regime the re-organization of all structures discussed in the heating regime takes place in the reverse order.

6.2.2.3 PVT experiment

A fully-automated GNOMIX high-pressure dilatometer (GNOMIX Inc.) was employed by Dr. J. Pionteck, Leibniz-Institut für Polymerforschung Dresden e.V., to perform pressure-volume-temperature (PVT) analysis [29]. Isothermal standard (ITS) runs were performed within the temperature range of 298 - 518 K in steps of 5 or 10 (±1) K for the H8 sample.

A distinct transition mainly attributed to the melting of semi-fluorinated side chains is marked by the T_m line in figure 6.24 a in the ITS curves. The glass transition can be seen more clearly when magnifying the temperature range from 320 K to 440 K (figure 6.24 b). At 200 MPa, for example, a change in the slope of the $V_{sp} - T$ curve occurs at 365 K.
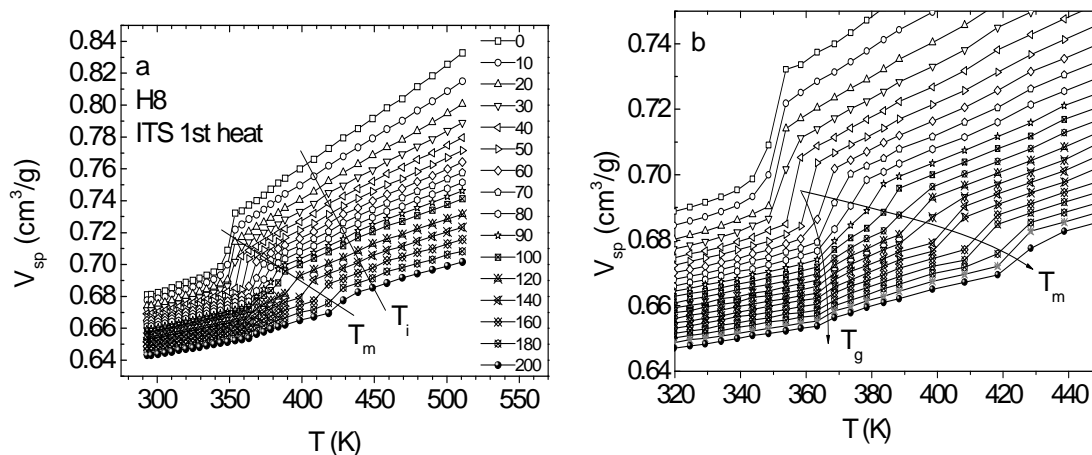
Figure 6.24 V_{sp}-T-plot of H8. a) Complete isothermal (ITS) heating run. The lines mark the pressure dependent melting (T_m, overlapped by glass transitions) and isotropization (T_i, very soft effect on V_{sp}) temperature. b) The irregular compression behavior implies that in the marked T range between 365 and 420 K two transitions, the glass transition in the main chain, characterized by a change in the slope of $V_{sp}(T)$ at T_g, and melting, characterized by a steep increase in V_{sp} at T_m, overlap.

Isotropization denoted by T_i line (figure 6.24 a) is more evident from the inset of figure 6.25. A small increase in V_{sp} of ca. 0.02% can be observed at $T_i = 409$ K. The 10 MPa isobars in figure 6.25 show the melting and crystallization transitions with a slight hysteresis between heating and cooling runs.
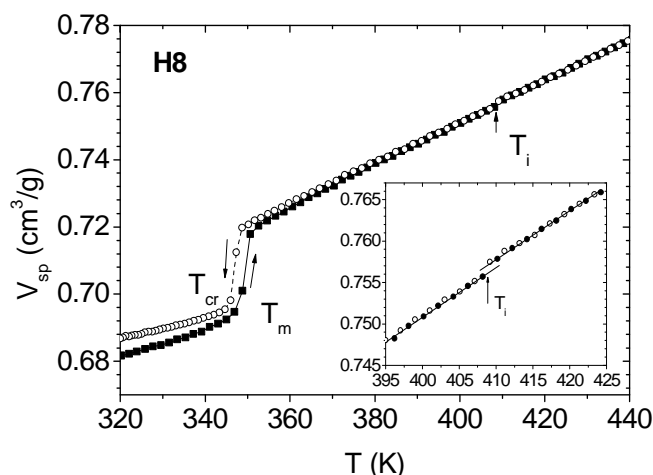
Figure 6.25 Isobars of H8 taken at 10 MPa with a heating (filled squares) and cooling (empty circles) rate of 2 K/min. The image shows clearly the melting (T_m) / crystallization (T_{cr}) of the semifluorinated chains and the reversible isotropization (T_i) of the melt. The inset is a magnification of isotropization at 409 K. The lines are a visual aid to show the step in the V_{sp} values due to isotropization. Heating and cooling curves were normalized to show the same values above T_i.

6.2.2.4 PALS experiment

The PALS experiments were performed for the three samples HQ, H6 and H8. For the semicrystalline material, we split the o-Ps lifetime into two components: the $\tau_{3(i)}$ represents crystalline or at least more ordered phase with a relatively high packing density formed by the side chains and $\tau_{3(ii)}$ a less dense amorphous phase associated with the main chain.
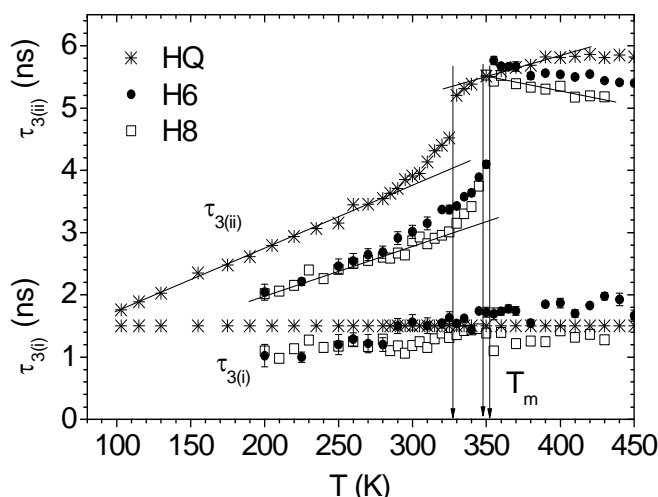
Figure 6.26 Lifetimes $\tau_{3(i)}$ and $\tau_{3(ii)}$ of o-Ps in HQ (stars), H6 (filled circle), and H8 (open squares) as a function of temperature T during heating the samples. For HQ $\tau_{3(i)}$ was fixed to 1.5 ns. The statistical errors are only shown for H6 for clarity. The lines are a guide for the eyes.

From figure 6.26, at the temperature range from 200K to 430K, $\tau_{3(i)}$ increases from 1.0 ns to 1.4 ns for H8 and 2.1 ns for H6. This lifetime shows no response to the melting transition at T_m. In case of HQ the decomposition of o-Ps into $\tau_{3(i)}$ and $\tau_{3(ii)}$ was more difficult and the fits were frequently instable. Therefore we have fixed here $\tau_{3(i)}$ to a constant value of 1.50 ns. $\tau_{3(ii)}$ shows for all of the three materials a strong step-like increase which occurs at temperature of 325K for HQ, 352K for H6 and 347K for H8 respectively. These temperatures agree well with the DSC experiment and this behaviour is attributed to the melting of the self-organized side-chains. At low temperatures $\tau_{3(ii)}$ exhibits a linear rise with a stronger continuous increase starting 30-50K below the jump at the melting transition. After side-chain melting, $\tau_{3(ii)}$ levels off and shows only a slight variation with temperature.

The intensities (figure 6.27) of the o-Ps lifetime components, $I_{3(i)}$ and $I_{3(ii)}$, mirror the probability of Ps formation in the two phases. For the sample H6, both intensities exhibit below T_m almost the same value, $I_{3(i)} \approx I_{3(ii)}$, and increase

smoothly from 6 % to 8.5 %. At T_m, $I_{3(i)}$ slumps to 3 – 4 %, while $I_{3(ii)}$ jumps to 14 % to 15 %. The behavior of $I_{3(i)}$ and $I_{3(ii)}$ shows that at T_m the fraction of the disordered, amorphous or liquid, regions increases drastically on the expenses of the ordered regions. The fact that $I_{3(i)}$ does not fall to zero can be taken as indication that after side-chain melting a small fraction of densely packed regions is conserved.
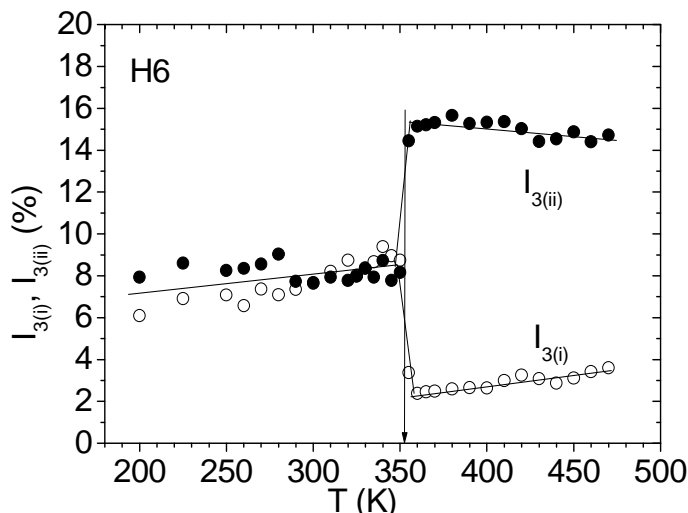
Figure 6.27 The relative intensity $I_{3(i)}$ (open circles) and $I_{3(ii)}$ (filled circles) of the *o*-Ps lifetime components for H6 as a function of temperature T. The absolute statistical errors correspond to ±0.3 %. The lines are a guide for the eyes.

Figure 6.28 shows the calculated hole free volume from $\tau_{3(ii)}$. The total variation of v_h lies between 80 Å^3 and 500-580 Å^3.
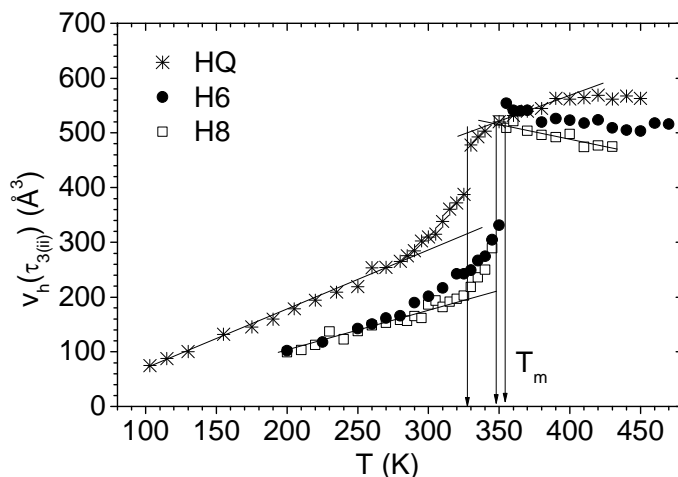
Figure 6.28 Mean hole volume v_h calculated from the lifetime $\tau_{3(ii)}$ of HQ (stars), H6 (filled circle), and H8 (open squares) as a function of temperature T during heating the samples. The lines are a guide for the eyes.

The variation in the mean hole volume from PALS, $v_h(\tau_{3(ii)})$, is compared with the specific volume from PVT experiments, V_{sp}, for HQ (figure 6.29) and H8 (figure 6.30), respectively. The scales are chosen so that the data points of

both volumes at 300 K and immediately after complete side-chain melting (melting end point temperature T_m) correspond to each other. The specific volume jumps at T_m to a higher value by a factor of 1.0184 (HQ) and 1.0625 (H8). The corresponding changes in the hole volume are 1.55 (HQ) and 2.47 (H8). The increases in v_h are extremely strong, showing that the dominating part of the volume increase at T_m, if not all, occurs in the hole free volume. In the solid v_h and V_{sp} exhibit a parallel behaviour, while in the liquid there is an increasing discrepancy with increase temperature.

Plots of $V_{sp}(T)$ vs. v_h in the temperature range between 300 K and $T_m - 10$ K can be fitted to a straight line. The specific number density can be obtained by the fitting: $N_h' = 0.11 \times 10^{-21}$ g^{-1} (HQ) and 0.17×10^{-21} g^{-1} (H8).
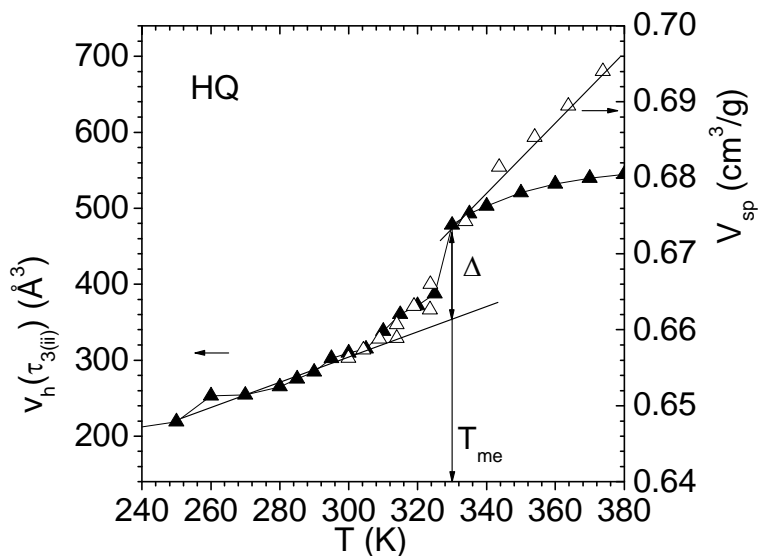
Figure 6.29 Comparison of mean local free volume from PALS, $v_h(\tau_{3(ii)})$ (solid dot), with specific volume from PVT experiments, V_{sp} (empty dot), for HQ. The scales are normalized so that the data points of both volumes at 300 K and at the end point of melting, T_{me}, concur.
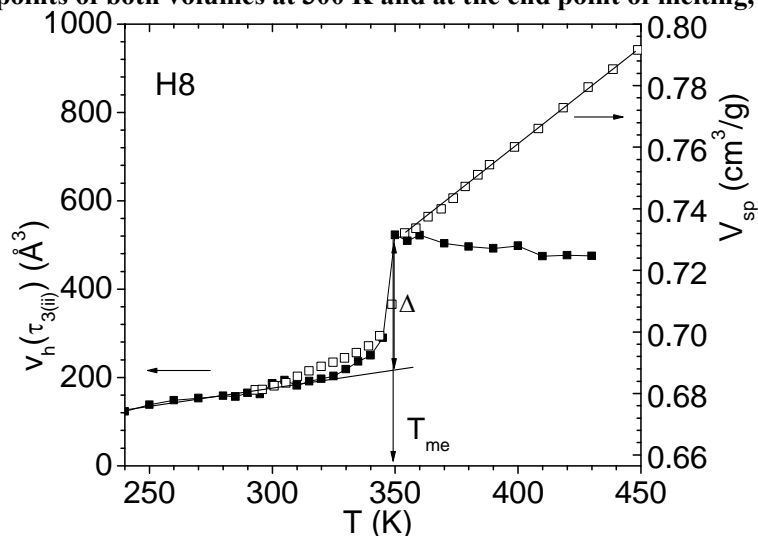
Figure 6.30 As figure 6.29, but for H8.

6.2.3 Conclusion

The PALS experiment can be applied to study phase transitions in polymers with complex structures. For side chain crystalline semifluorinated polyesters studied in this work, the o-Ps lifetime $\tau_{3(i)} = 1.0 - 2.1$ ns and $\tau_{3(ii)} = 1.9 - 6.0$ ns, corresponding to two phases: a) the densely packed crystalline structure; b) the more open amorphous structure. The hole volume v_h varies between 80 Å^3 at 100 K and 580 Å^3 at 470 K for these samples. The specific hole density is $0.1 - 0.2 \times 10^{-21}$ g^{-1} corresponding to $0.2 - 0.3$ nm^{-3}. The v_h shows an abrupt increase at T_m by a factor of $1.5 - 2.5$. V_{sp} increases at T_m by a factor of 1.018 - 1.062, much smaller than that of v_h. The o-Ps intensities $I_{3(i)}$ and $I_{3(ii)}$ show at T_m a sharp decrease and increase, respectively. $I_{3(i)} > 0$ at $T > T_m$ may show that some ordered regions survive melting. The lifetime $\tau_{3(i)}$ does not show a response to the phase transition. Above T_m there is an increasing discrepancy of v_h with T to the specific volume V_{sp}. This may be related to the structural and chemical heterogeneous nature of this polymer. $\tau_{3(ii)}$ decreases with T in good correlation with T-SAXS experiments which show that the separation width of the ordered layers decrease from 5.8 to 4.5 nm. In contrast to PALS, PVT is sensitive to isotropization, which exhibits a small volume effect at high temperature.

6.3 Reference

1. Champeney, D.C., R.N. Joarder, and J.C. Dore, *Structural studies of liquid D-glycerol by neutron diffraction.* Molecular Physics: An International Journal at the Interface Between Chemistry and Physics, 1986. **58**(2): p. 337-347.

2. Frick, B. and et al., *Structural Changes near the Glass Transition–Neutron Diffraction on a Simple Polymer.* EPL (Europhysics Letters), 1989. **9**(6): p. 557.

3. Leheny, R.L., et al., *Structural studies of an organic liquid through the glass transition.* The Journal of Chemical Physics, 1996. **105**(17): p. 7783-7794.

4. Rössler, E., *Indications for a change of diffusion mechanism in supercooled liquids.* Physical Review Letters, 1990. **65**(13): p. 1595.

5. Ngai, K.L., *Dynamic and thermodynamic properties of glass-forming substances.* Journal of Non-Crystalline Solids, 2000. **275**(1-2): p. 7-51.

6. Alegria, A., et al., *Dielectric investigation of the temperature dependence of the nonesponentiality of the dynamics of polymer melts.* Physical Review E, 1999. **59**(6): p. 6888-6895.

7. H. Švajdlenková, O.Š., G. Dlubek, J. Krištiak and J. Bartoš, *ESR study of the spin probe dynamics in relation to the free volume from PALS in a series of amorphous polymer glass-formers.* To be published, 2011.

8. Krevelen, D.v., *Properties of polymers, their estimation and correlation with chemical structure.* 2nd ed. 1976: Elsevier, Amsterdam-Oxford-New York.

9. Schottky, *Über die Drehung der Atomachsen in festen Körpern.* Physik. Zeitschr, 1922. **XXIII**: p. 448.

10. Simha, R. and Somcynsk.T, *On Statistical Thermodynamics of Spherical and Chain Molecule Fluids.* Macromolecules, 1969. **2**(4): p. 342-&.

11. Dlubek, G., et al., *The free volume and its recovery in pressure-densified and CO2-swollen heterocyclic-ring-containing fluoropolymers.* Macromolecular Chemistry and Physics, 2008. **209**(18): p. 1920-1930.

12. Dlubek, G., et al., *Temperature dependence of the free volume from positron lifetime experiments and its relation to structural dynamics: Phenylphthalein-dimethylether.* Physical Review E, 2008. **78**(5): p. -.

13. Bartos, J., et al., *Free volume factor in supercooled liquid dynamics.* Journal of Non-Crystalline Solids, 2002. **307-310**: p. 417-425.

14. Bartoš, J., *Phenomenological Description of the PALS Response in Glass-Forming Systems.* Mat. Sci. Forum, 2009. **607**: p. 48-52.

15. Bartos, J., et al., *Positron annihilation and broadband dielectric spectroscopy: A series of propylene glycols.* Journal of Non-Crystalline Solids, 2011. **357**(2): p. 376-384.

16. Tao, S.J., *Positronium Annihilation in Molecular Substances.* Journal of Chemical Physics, 1972. **56**(11): p. 5499-&.

17. Eldrup, M., D. Lightbody, and J.N. Sherwood, *The temperature dependence of positron lifetimes in solid pivalic acid.* Chemical Physics, 1981. **63**(1-2): p. 51-58.

18. Tanaka, H., *Two-order-parameter description of liquids. I. A general model of glass transition covering its strong to fragile limit.* The Journal of Chemical Physics, 1999. **111**(7): p. 3163-3174.

19. Tanaka, H., *Two-order-parameter description of liquids. II. Criteria for vitrification and predictions of our model.* The Journal of Chemical Physics, 1999. **111**(7): p. 3175-3182.

20. Tanaka, H., *Two-order-parameter model of the liquid-glass transition. II. Structural relaxation and dynamic heterogeneity.* Journal of Non-Crystalline Solids, 2005. **351**(43-45): p. 3385-3395.

21. Lunkenheimer, P. and A. Loidl, *Dielectric spectroscopy of glass-forming materials: [alpha]-relaxation and excess wing.* Chemical Physics, 2002. **284**(1-2): p. 205-219.

22. Švajdlenková, H. and J. Bartoš, *Spin probe dynamics in relation to free volume and relaxation dynamics of poly(isobutylene).* Polymers & Polymer Composites, 2008. **Chem. Listy, 102**: p. s1271.

23. Mierzwa, M., et al., *Effect of pressure on the side-chain crystallization of poly(n-octadecyl methacrylate) studied by dielectric spectroscopy.* Physical Review B, 2000. **62**(21): p. 14012.

24. Hempel, E., et al., *On the crystallization behavior of frustrated alkyl groups in poly(n-octadecyl methacrylate).* Journal of Non-Crystalline Solids, 2006. **352**(42-49): p. 5013-5020.

25. Hempel, E., et al., *Crystallization of Frustrated Alkyl Groups in Polymeric Systems*

Containing Octadecylmethacrylate, in *Progress in Understanding of Polymer Crystallization*, G. Reiter and G. Strobl, Editors. 2007, Springer Berlin / Heidelberg. p. 201-228.

26. Friedel, P., et al., *Polyesters with semifluorinated side chains: A proposal for the solid-state structure.* Journal of Polymer Science Part B: Polymer Physics, 2000. **38**(12): p. 1617-1625.

27. Pospiech, D.J., D.; Komber, H.; Voigt, D.; Häußler, L.; Friedel, P.; Grundke, K.; Busch, P.; Große, H.; Kremer, F.; Tsuwi, J.; Menzel, H.; Helmecke, O, e-Polymers, 2005. **no. E_002**: p. online publication, http://www.e-polymers.org/paris/data/L1690.pdf.

28. Pospiech, D.J., D.; Häußler, L.; Voigt, D.; Grundke, K.; Ober, C. K.; Körner, H.; Wang, J. Polymer Prepr, Am Chem Soc, Div Polym Chem 1998. **39**: p. 882-883.

29. P. Zoller, D.W., *Standard Pressure-Volume-Temperature Data for Polymers.* Technomic, Lancaster, PA 1995.

30. Yu, Y., et al., *Phase Transitions in Polymers Containing Long Self-Assembled CH2 Sequences in the Side Chain: A Psitron Lifetime Study.* Materials Science Forum, 2010. **666**: p. 71-74.

31. Dlubek, G., et al., *Temperature dependence of the free volume in fluoroelastomers from positron lifetime and PVT experiments.* Macromolecules, 2004. **37**(17): p. 6606-6618.

7 Low molecular-weight organic materials: ionic liquids

7.1 Introduction

Low molecular-weight organics, ionic liquids are organic salts with melting temperature below 100 °C or even room temperature. Compared with its variety in application [1-5], origins of several underlying physical properties are unclear. In this work, positron annihilation lifetime spectroscopy is used to study a series of ionic liquids with the same cation 1-Butyl-3-methylimidazolium ([BMIM]) and different anions with different volumes. Local free volume changes with temperature can be observed under phase transitions between amorphous, crystalline, solid and liquid states. The hole volume relationship with molecular volume is represented.

7.2 Experimental

The samples were supplied by Prof. Dr. Ingo Krossing from University of Freiburg. Preparation and purification procedures are described in the literature [6, 7]. The series of ionic liquids in this work has the same cation (1-Butyl-3-methylimidazolium, [BMIM]) and different anions (tetrafluoroborate [BF_4], bis(trifluoromethanesulfonyl)imide [NTf_2], trifluoromethanesulfonate [OTf], hexafluorophosphate [PF_6], chloride [Cl] and tetrakis (hexafluoroisop-ropoxy)borate [$B(hfip)_4$]) as displayed in figure 7.1.
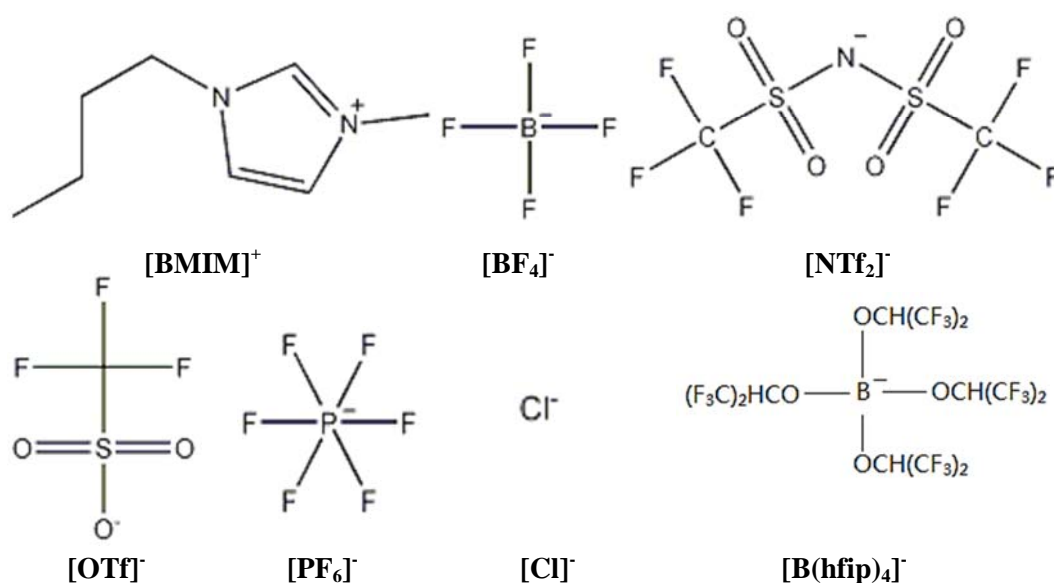
Figure 7.1 Ionic formulae of the ionic liquids studied in this work.

Due to negligible vapor-pressure, the ionic liquids can be measured in vacuum condition using positron annihilation lifetime spectroscopy (PALS). A [22]Na positron source protected by $7\mu m$ Kapton foil each side is surrounded by 2 mm thick layer ionic liquid sample (liquid or solid) in the sample holder. The holder was attached to a finger with the cooling and heating system in a chamber with a pressure of 10^{-3} Pa. A fast-fast coincidence system with 310 ps time resolution and 25.7 ps analyzer channel width is applied for the positron lifetime measurement. Cooling and heating runs were performed in the temperature range from as low as 140 K to several decades higher than the melting point for each sample in steps of 5 or 10 K. At least 4×10^6 counts were collected for each spectrum, which needs 5 – 7 hours.

Pressure-volume-temperature (PVT) experiments for [BMIM][BF$_4$] and [BMIM][Cl] were taken by Dirk Pfefferkorn from the Institute of Chemistry of the Martin-Luther-University Halle-Wittenberg. Dr. J. Pionteck (Leibniz-Institut für Polymerforschung Dresden e.V.) provided the PVT data for [BMIM][NTf$_2$] and [BMIM][PF$_6$]. Dielectric spectroscopy experiments for [BMIM][BF$_4$], [BMIM][NTf$_2$], [BMIM][PF$_6$] and [BMIM][Cl] were carried out by Professor Dr. Marian Paluch from the Institute of Physics, University of Silesia.

7.3 Results and discussion

7.3.1 1-Butyl-3-methylimidazolium tetrafluoroborate [BMIM][BF$_4$]

1-Butyl-3-methylimidazolium tetrafluoroborate [BMIM][BF$_4$] represents a classical ionic liquid with a simple temperature dependence behavior. Its chemical formula is C$_8$H$_{15}$BF$_4$N$_2$, and the molecular mass is M = 226.0 g/mol. [BMIM][BF4] does not crystallize and shows only the glass transition at T_g = 188 – 190 K [8-10] (figure 7.2).

In agreement with the differential scanning calorimetry (DSC) results, the lifetime parameters from PALS experiments exhibit a simple and transparent behavior, which is similar to that known for amorphous polymers or low-molecular weight glass formers [11]. Figures 7.3 to 7.5 show the most important lifetime parameters, which are all reversible in cooling and heating runs. During cooling the mean o-Ps lifetime $<\tau_3>$ decreases from 2.85 ns in the temperature range from 280 K - 350 K to 1.35 ns at 130 K (figure 7.3). The curve shows a characteristic change in the slope at a temperature T_g(PALS) =

190 ± 3 K. This point can be identified as the glass transition.
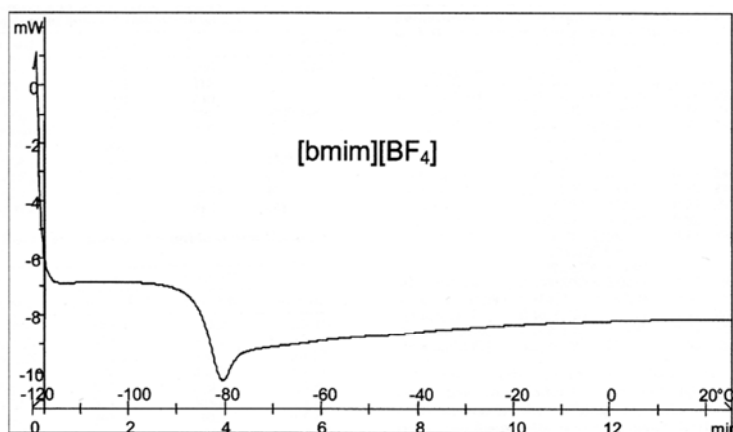
Figure 7.2 Differential scanning calorimetry (DSC) scan for [BMIM][BF4][8].

Due to increased thermal motion of ions, the holes between them grow in the heating run and show an increasingly broader distribution indicated by the increasing width of the hole size distribution σ_3. The small value of I_3 (11% - 13%) can be attributed to the solvation of free slowed-down positrons - the Ps precursor - which reduces the Ps formation probability. This process seems to occur in the true and also in the supercooled liquid.
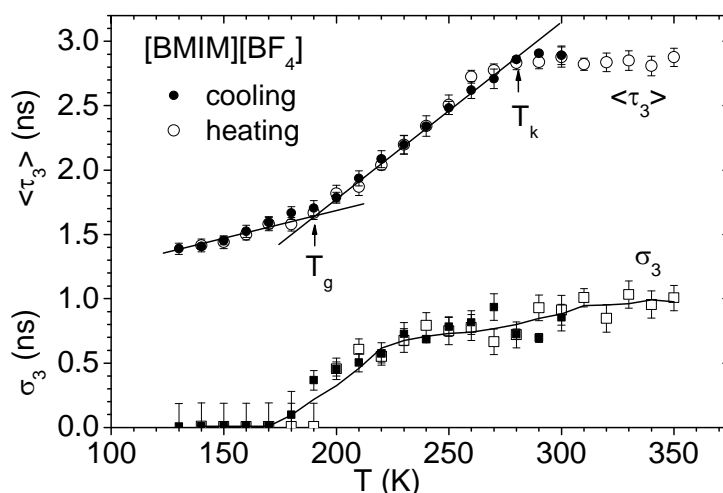
Figure 7.3 The mean, $<\tau_3>$, and the standard deviation, σ_3, of the o-Ps lifetime distribution as a function of temperature T during cooling and heating of [BMIM][BF$_4$]. T_g indicates the glass transition temperature and T_k the "knee" temperature.

There is a second characteristic point in the $<\tau_3>$ curve at $T_k = 280\pm5$ K (the "knee" temperature), which is characterized by a leveling-off of the increase in the o-Ps lifetime $<\tau_3>$. This behavior can be attributed, like for amorphous polymers, to the decreased structural relaxation time, which comes into the order of the o-Ps lifetime. Actually, from the Vogel-Fulcher-Tamman (VFT) fits

to the main or α-relaxation of [BMIM][BF4] from dielectric spectroscopy experiment, shown in figure 7.6, one can estimate a relaxation time $\tau_\alpha = \tau_{max}$ of 2.85 ns at $T = 275$ K $\approx T_k$. At this and higher temperatures, the hole walls move during the life of o-Ps, which leads to a smearing of the hole size detected by o-Ps. The combined effect of hole expansion and increasing hole smearing may cause the apparent constancy of $<\tau_3>$. The o-Ps lifetime does not anymore mirror correctly the true hole size and the true free volume structure of the liquid. Below T_k, o-Ps makes "snapshots" of a structure which fluctuates in space and time. This is mirrored in the distribution of o-Ps lifetimes (of hole sizes). Below T_g, the structural dynamics is frozen and more or less static.
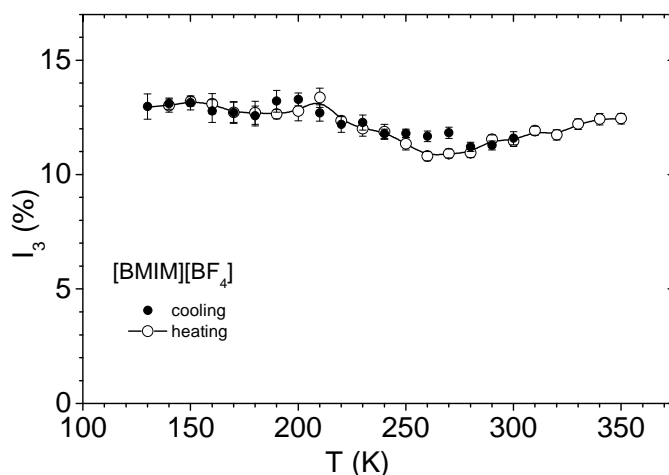
Figure 7.4 The intensity I_3 of the o-Ps lifetime as a function of temperature T during cooling and heating of [BMIM][BF$_4$].
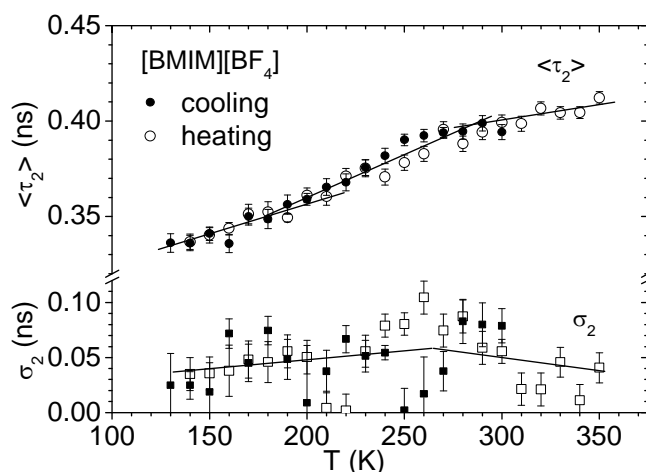
Figure 7.5 The mean, $<\tau_2>$, and the standard deviation, σ_2, of the e^+ lifetime distribution as a function of temperature T during cooling and heating of [BMIM][BF$_4$].

The mean e^+ lifetime $<\tau_2>$ shows a behavior analogous to $<\tau_3>$ (figure 7.5). The width parameter σ_2 varies only slightly around 0.05 ns.
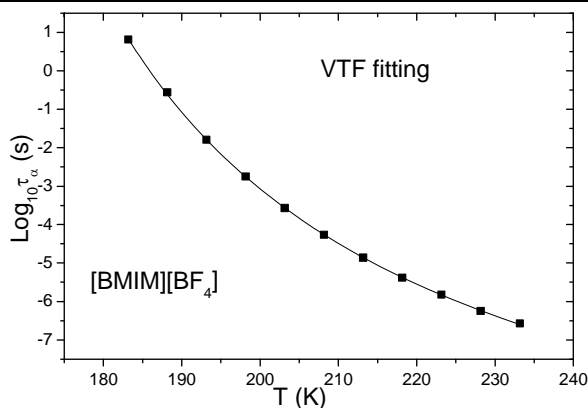
Figure 7.6 Vogel-Fulcher-Tamman (VFT) fit to the α-relaxation for [BMIM][BF4] of dielectric spectroscopy experiment data.

The dielectric spectroscopy result for [BMIM][BF$_4$] is displayed in figure 7.6 as temperature dependence of the relaxation time τ_α. The Vogel-Fulcher-Tamman (VFT) fit:

$$\log_{10}\tau_\alpha = \log_{10}\tau_0 + \frac{B'}{T-T_0} \qquad (7.1)$$

gives the parameters: $\log_{10}\tau_0$ = -12.89, B' = 581.72 and T_0 = 140.8. So the temperature $T(\tau_\alpha = \tau_{\text{max\_o-Ps}} = 2.85$ ns$) = 275$ K $\approx T_k$.
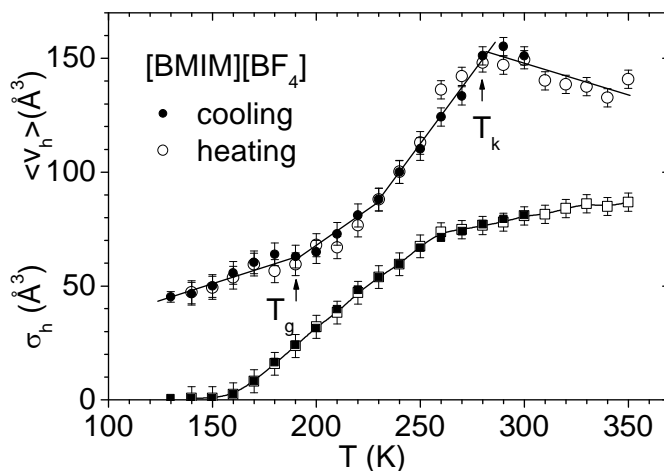
Figure 7.7 Number-weighted mean $<v_\text{h}>$ (spheres) and standard deviation σ_h (squares) of the hole size calculated from positron lifetime.

Mean local free volume and its dispersion calculated by the Tao-Eldrup model (section 5.6) from positron lifetime is shown in figure 7.7. $<v_\text{h}>$ linearly increases with temperature from 50 Å^3 to 150 Å^3 with a slope change at T_g and levels off at T_k like positron lifetime behaviour.

The pressure-volume-temperature (PVT) experiment result is shown in figure 7.8. The specific volume V_sp increase linearly with temperature in the temperature range 297 K – 474 K and decrease with increasing pressure.
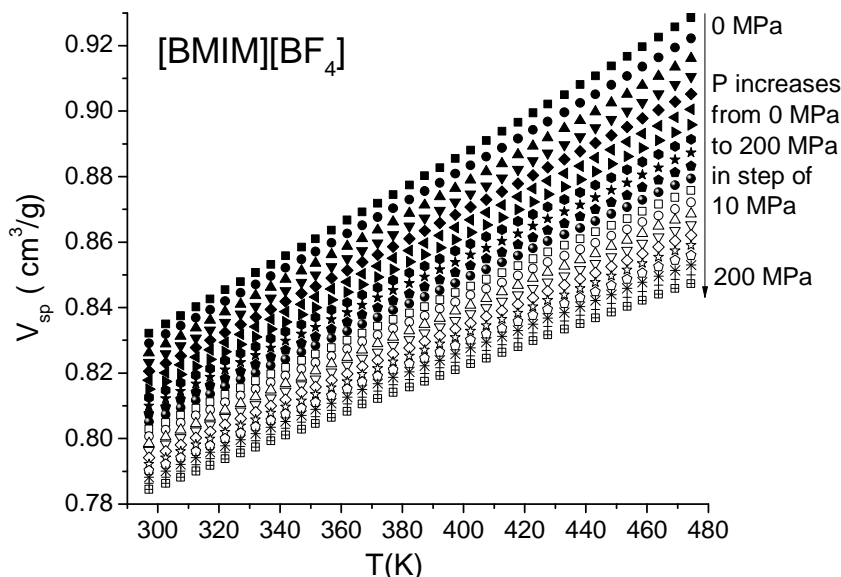
Figure 7.8 Specific total volume (V_{sp}) as a function of temperature T and pressure P from pressure-volume-temperature (PVT) standard ITS runs for [BMIM][BF$_4$].
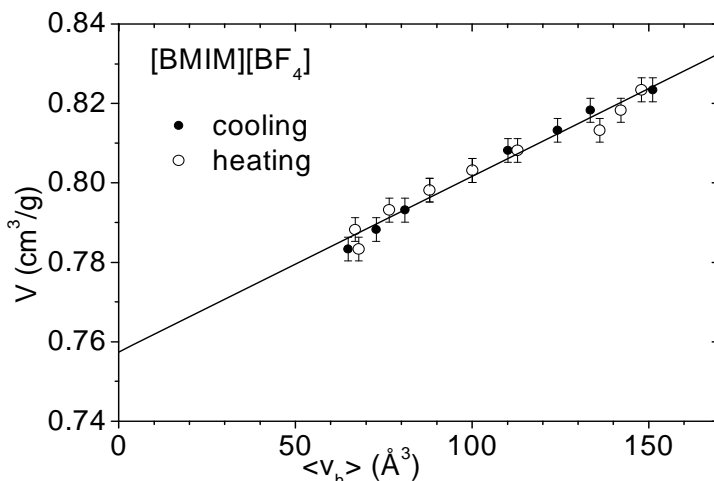
Figure 7.9 Plot of the specific volume from PVT experiment under 0 MPa vs the mean hole volume at supercooled liquid state (between T_g and T_k). The line is a linear fit of the data.

A linear fit between the specific total volume from PVT experiment under 0 MPa and mean hole volume from PALS experiment of the form:

$$V_{sp} = N_h' \times < v_h > + V_{occ} \tag{7.2}$$

gives the specific hole density $N_h' = 0.442 \times 10^{21}$ g^{-1} and the occupied volume $V_{occ} = 0.7574$ cm^3/g. The Sanchez-Lacombe (section 3.3) fitting of the PVT experiment gives $V_{occ} = 0.7799$ cm^3/g, corresponding to the fitting value with 3% difference.

The temperature dependence of the specific free volume V_f and the free volume fraction f_h calculated from comparison of PVT and PALS experiments are shown in figure 7.10. When considering the vacancies in the lattice-hole liquid model as Schottky-point defects, the equilibrium concentration (hole

fraction f_h in this work) can be expressed by the Schottky equation [12]:

$$f_h = A \exp(-H_h/k_B T) \tag{7.3}$$

A is a constant, k_B is the Boltzmann constant, and H_h is the hole formation enthalpy. Fitting with the data in figure 7.10 delivers $A = 0.61709$ and $H_h = 4.78$ kJ/mol.
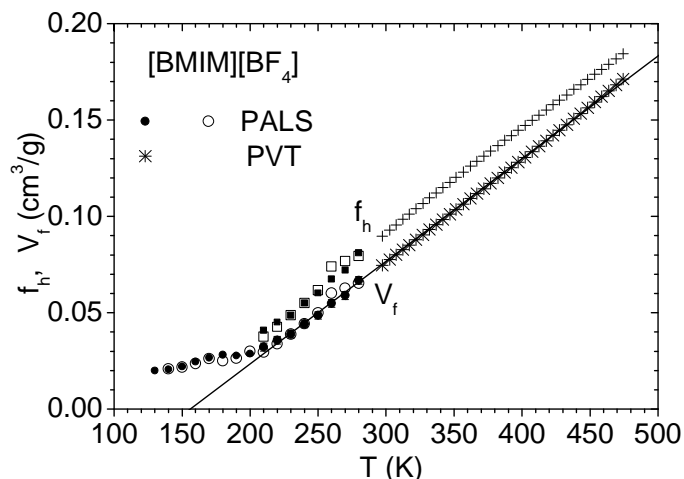
Figure 7.10 Temperature dependence of specific free volume V_f and free volume fraction f_h.

7.3.2 1-Butyl-3-methylimidazolium bis(trifluoromethanesulfonyl)imide [BMIM][NTf₂]

The chemical formula and the molecular mass for 1-Butyl-3-methylimidazolium bis(trifluoromethanesulfonyl)imide [BMIM][NTf₂] are $C_{10}H_{15}F_6N_3O_4S_2$ and 419.37 g/mol. [BMIM][NTf₂] stays in amorphous state (supercooled liquid and glassy with T_g = 186 K) during cooling, but shows crystallization (T_{cr} = 232 K) and melting (T_m = 271 K) during heating as in DSC experiments [10]. In correspondence with DSC results, the lifetime parameters from PALS experiments exhibit phase transitions with temperature change. In the cooling procedure, the mean o-Ps lifetime $<\tau_3>$ decreases from 3.5 ns in the temperature range 270 K – 350 K to 1.6 ns at 140 K (figure 7.11) and shows glass transition behavior at T_g(PALS) = 190 ± 5 K. The leveling off of the curve gives T_k = 270 ± 5 K. Due to decreased thermal motion of ions, hole size distribution σ_3 steadily decrease. I_3 decreases from 18% at glass state to 13 % at true liquid (figure 7.12). The mean e^+ lifetime $<\tau_2>$ shows a steadily decrease during cooling, while the width parameter σ_2 varies only slightly around 0.07 ns as indicated in figure 7.13.
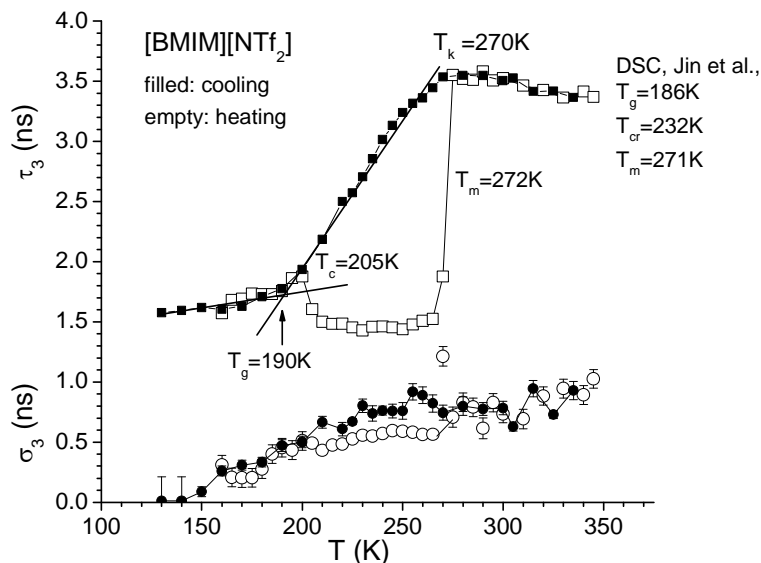
Figure 7.11 The mean, $<\tau_3>$ (squares), and the standard deviation, σ_3 (spheres), of the o-Ps lifetime distribution as a function of temperature T during cooling and heating of [BMIM][NTf$_2$].
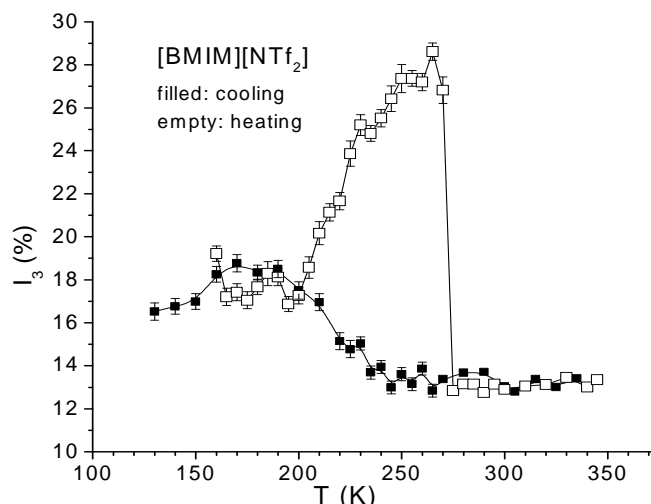
Figure 7.12 As for figure 7.11, but the o-Ps intensity I_3.

The heating curve overlaps the cooling one below crystallization temperature T_{cr}(PALS) = 205 ± 5 K and above melting temperature T_m(PALS) = 270 ± 5 K (in correspond to T_k) for all the lifetime parameters ($<\tau_3>$, σ_3, I_3, $<\tau_2>$ and σ_2). T_{cr}(PALS) is around 20 K lower than in DSC experiment, that may be due to the different time scale of the experiments (10 K/min in DSC and 6 hours for one temperature point in PALS). Between T_{cr}(PALS) and T_m(PALS), a sharp transition can be observed for all parameters: $<\tau_3>$ drops down from 1.9 ns to 1.5 ns, indicating crystallization of the supercooled liquid and stays at that value until melting, jumping to 3.5 ns. σ_3 also descends at crystalline state. The extraordinary large value of σ_3 in the heating curve at 270 K is due to the

two-phase character of the sample at this point (partially crystallized). $<\tau_2>$ and σ_2 decrease at crystalline state during heating and jump to the value of cooling in true liquid after melting. I_3 rapidly increase at crystalline state and drops to a low value of 13% after melting. This behavior can be attributed to a solvation of e^+ by the anions, which reduces the Ps formation probability in the true and supercooled liquid.
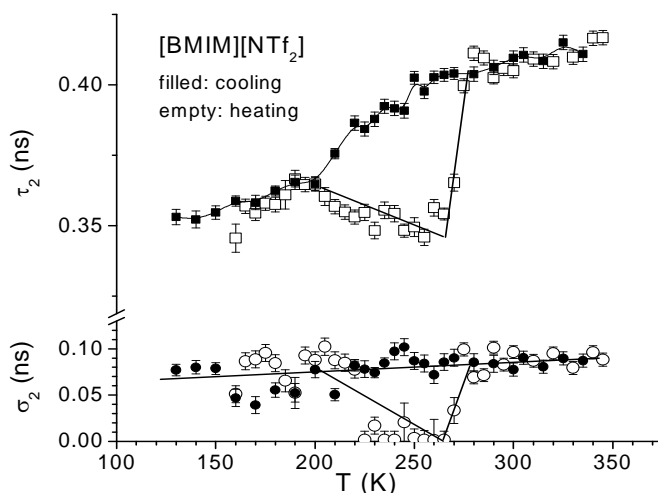
Figure 7.13 As for figure 7.11, but the mean, $<\tau_2>$ (squares), and the standard deviation, σ_2 (spheres), of the e^+ lifetime distribution.
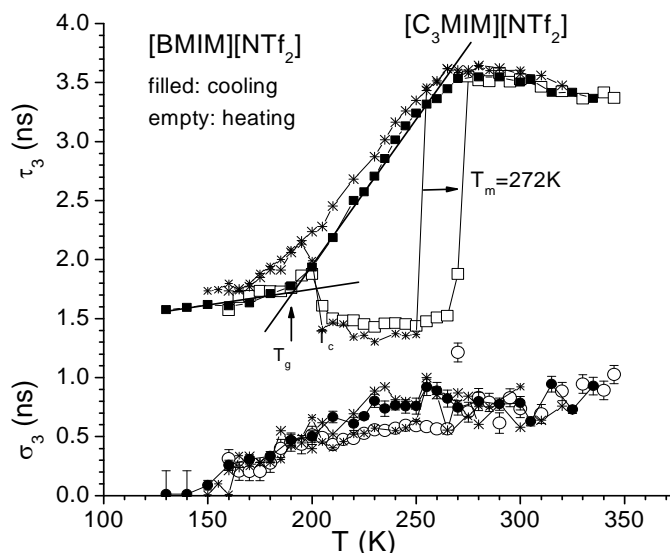
Figure 7.14 Comparison of the mean, $<\tau_3>$ (squares), and the standard deviation, σ_3 (spheres) of the o-Ps lifetime distribution for [C$_3$MIM][NTf$_2$] (Ref. [13]) with [BMIM][NTf$_2$].

PALS parameters of ionic liquid [C$_3$MIM][NTf$_2$] from our previous work [13], which has the same anion but one CH$_2$ group less than [BMIM][NTf$_2$] are compared to [BMIM][NTf$_2$] in figure 7.14. $<\tau_3>$ and σ_3 exhibit very similar behavior. The clearest difference is that, melting is shifted from 253 K for the former sample to 270 K for the later one.

The VFT fit from the dielectric spectroscopy data (figure 7.16) yields the parameter: $\log_{10}\tau_0$ is -11.22, B' is 317.65, and T_0 is 156.44. So the temperature $T(\tau_\alpha = \tau_{\text{max\_o-Ps}} = 3.5 \text{ ns}) = 271 \text{ K} \approx T_k$.

During cooling, $<v_h>$ linearly decreases with temperature from 240 Å³ to 60 Å³ with a slope change at T_g and levels off at T_k like positron lifetime behaviour.

A linear fit between the specific total volume from the PVT experiment under 0 MPa and the mean hole volume from PALS experiment gives the specific hole density $N_h' = 0.179 \times 10^{21}$ g^{-1} and occupied volume $V_{occ} = 0.6405$ cm³/g. The Sanchez-Lacombe fitting of PVT experiment gives V_{occ} with the value 0.6421 cm³/g, in agreement with the value obtained from PALS.
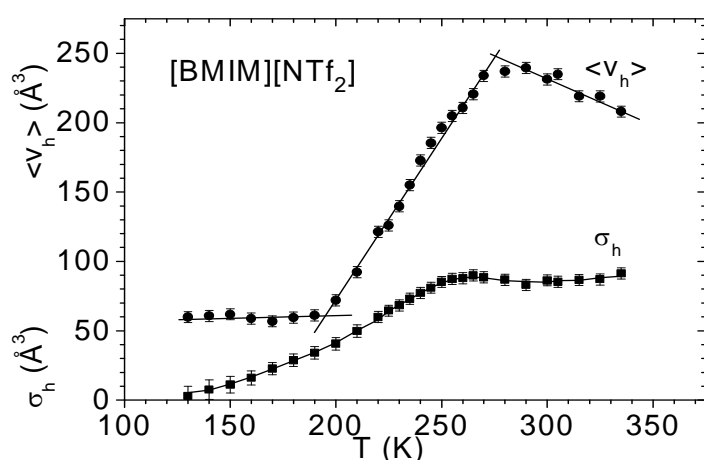
Figure 7.15 Number-weighted mean $<v_h>$ and standard deviation σ_h of the hole size calculated from positron lifetime.
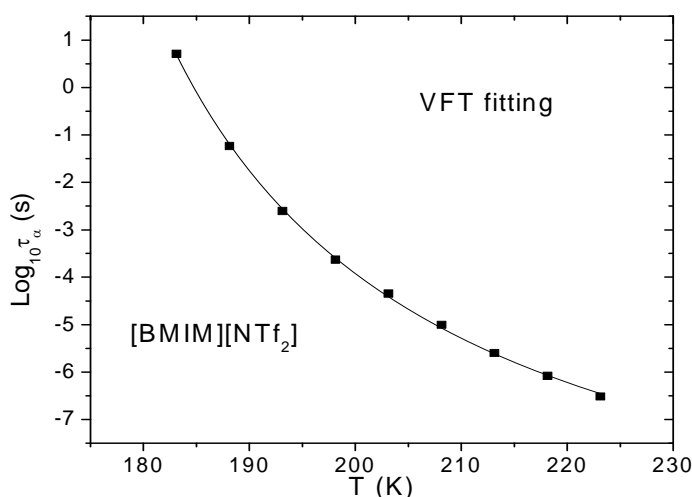
Figure 7.16 VFT fits to the α-relaxation for [BMIM][NTf$_2$] of dielectric spectroscopy experiment data.
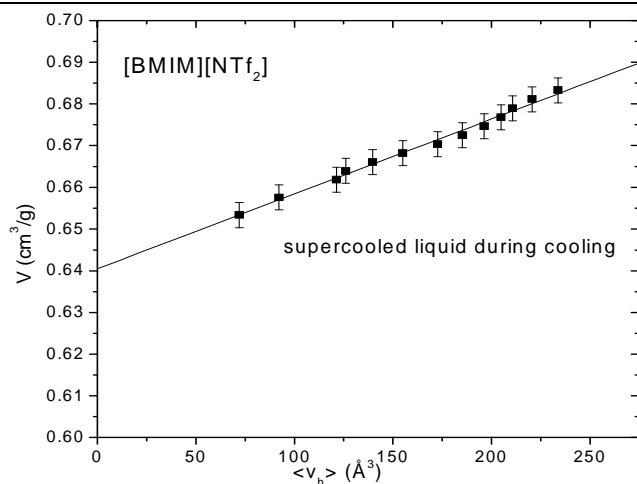
Figure 7.17 Plot of the specific volume from PVT experiment under 0 MPa vs the mean hole volume at supercooled liquid state (between T_g and T_k). The line is a linear fit of the data.

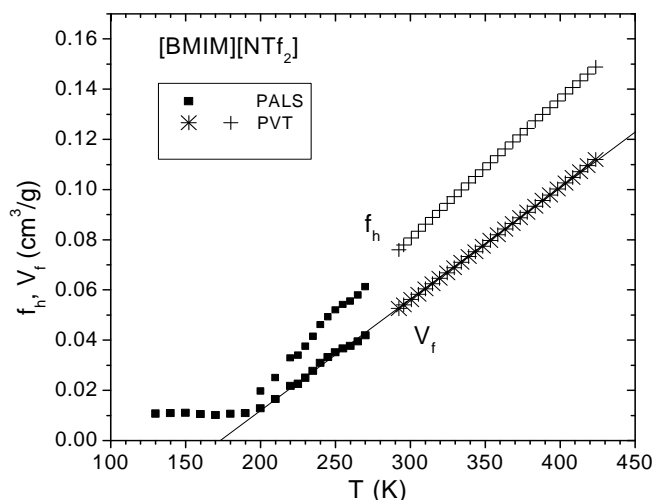The Schottky equation fit of f_h with the data in figure 7.18 delivers $A = 0.72517$ and $H_h = 5.54$ kJ/mol.

Figure 7.18 Temperature dependence of specific free volume V_f and free volume fraction f_h.

7.3.3 1-Butyl-3-methylimidazolium trifluoromethanesulfonate [BMIM][OTf]

[BMIM][OTf] ([OTf] = [triflate] = [CF$_3$SO$_3$]) shows a rather simple phase behavior, as can be observed in figure 7.19. Following the DSC experiments (rate of 10 K/min) of Fredlake et al. [8], it crystallizes during cooling at 254 K, melting occurs during heating at 286 K [8].

Choudhury et al. [14], however, detected in DSC heating scans of crystallized samples a phase transition at 251 K before melting occurred at 279 K. The [BMIM][OTf] was crystallized by cooling to 253 K, and single-crystal X-ray diffraction data were collected at 200 K. The ions are packed in the lattice via ionic interaction between CF$_3$SO$_3$– and the imidazolium cation. Further, several C-H···O hydrogen bonds (H···O $\leq$ 2.6 Å)

connect adjacent cations to anions to build the lattice. The [BMIM][OTf] forms a monoclinic lattice with the parameters a = 10.222 Å, b =12.534 Å, c= 22.541 Å, α = 90.0°, β = 93.28°, γ = 90.0 °, V_{cell} = 2883.2 Å^3, ρ_{calc} = 1.33 g/cm^3 and M = 288.3.
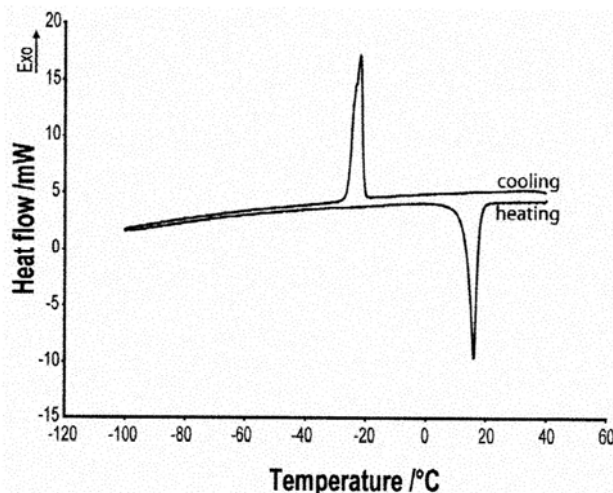

Figure 7.19 DSC-plot for [BMIM][OTf]. The data were recorded on a Setaram DSC131 instrument with a scanning rate of 5 K/min [15].
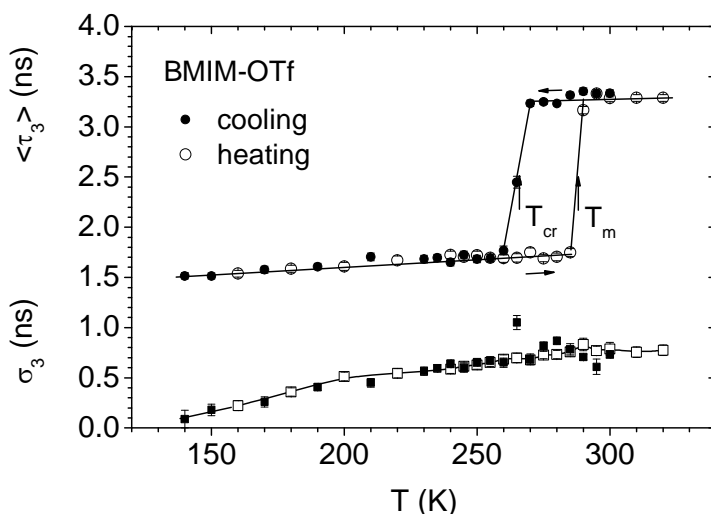

Figure 7.20 The mean, $<\tau_3>$, and the standard deviation, σ_3, of the o-Ps lifetime distribution as a function of temperature T during cooling and heating of [BMIM][OTf]. T_{cr} and T_m show the temperatures (half step) of crystallization (during cooling) and melting.

The lifetime parameters behave as simple as expected from the DSC experiments (figures 7.20 – 7.22). During cooling, the mean o-Ps lifetime $<\tau_3>$ stays almost constant at 3.25 ns. The material is in the liquid state. Between 270 K and 260 K, $<\tau_3>$ drops down to 1.70 ns indicating the crystallization of the sample. During further cooling $<\tau_3>$ decreases slightly to 1.50 ns at 140 K. The heating reproduces completely the lifetime parameters of the cooling curve for the crystallized sample up to T_{cr} and continuous to increase linearly

up to 285 K. Between 285 K and 290 K the parameters jump to the values of the liquid state indicating melting. As discussed previously, the differences of the *o*-Ps lifetime mirror the different packing density and different sizes of the local free volume in the crystallized and liquid sample. Other than for [BMIM][NTf$_2$], the dispersion parameter σ_3 shows no differences for the crystallized and molten states. The extraordinary large value of σ_3 in the cooling curve at 265 K is due to the two-phase character of the sample at this point (partially crystallized).

The *o*-Ps intensity I_3 stays constant at 13% in the liquid state. It has distinctly higher values in the crystalline state which vary between 19% (140 K) and 33% (285 K). Crystallization and melting lead to a sharp increase or decrease, respectively, of I_3. As discussed for [BMIM][NTf$_2$], the low value of I_3 in the liquid state can be attributed to the solvation of spur electrons e^- and/or thermalized positrons e^+ by the ions of the liquid which decreases the Ps formation reaction $e^- + e^+ \rightarrow$ Ps. This Ps inhibition effect is strongly reduced in crystals due to the regular arrangement of ions and due to the formation of the C-H···O hydrogen bonds.
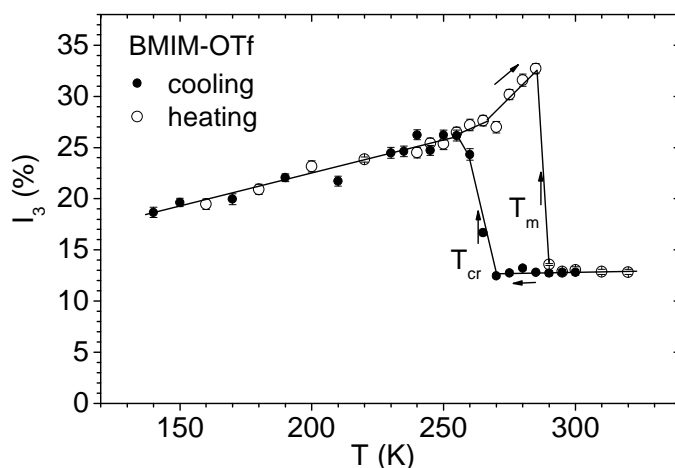

Figure 7.21 As for figure 7.20, but the *o*-Ps intensity I_3.

Finally, we look to the positron lifetime parameters $<\tau_2>$ and σ_2. Both parameters behave analogously to $<\tau_3>$. The decrease during crystallization and increase during melting show that e^+ also feels in crystals a higher packing density than in the liquid state of [BMIM][OTf].
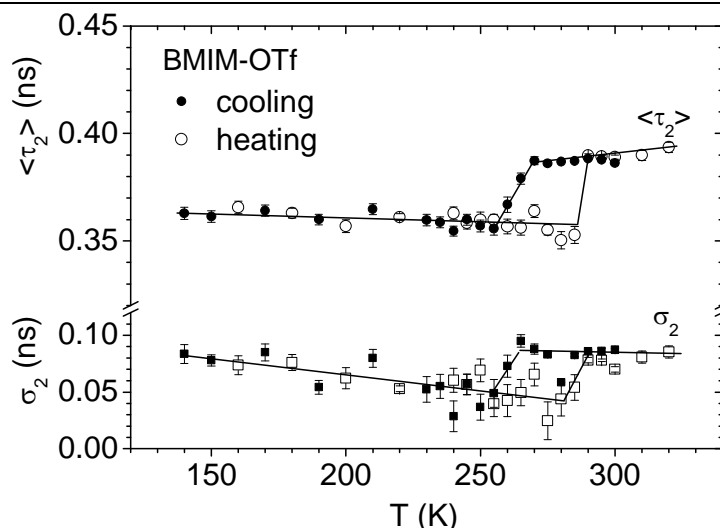
Figure 7.22 As for figure 7.20, but the mean, $<\tau_2>$, and the standard deviation, σ_2, of the e^+ lifetime distribution.

7.3.4 1-Butyl-3-methylimidazolium hexafluorophosphate [BMIM][PF$_6$]

[BMIM][PF$_6$] shows a more complex phase behavior than many other ILs including polymorphism in the crystalline state. This IL was investigated by quasi-adiabatic, continuous calorimetric measurements, X-ray and neutron diffraction by Triolo et al. [16, 17] and other authors [10, 14, 18-20]. Figure 7.23 shows the DSC plot from Freiburg [15]. During cooling (with a rate of 5 K/min) the IL stays in the amorphous state and shows indications of the glass transition around 190 K. During heating an exothermic peak mirrors the crystallization, followed by a more complex behavior due to crystalline transition. Melting occurs at 283 K.
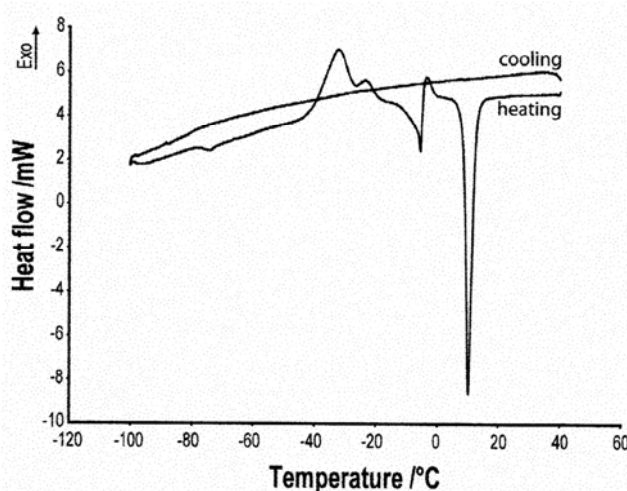

Figure 7.23 DSC-plot for [BMIM][PF$_6$]. The data were recorded on a Setaram DSC131 instrument with a scanning rate of 5 K/min [15].

Triolo et al.[17] found from quasi-adiabatic DSC and scattering experiments the following processes: Upon heating the amorphous glass from 160 K, one

can observe (i) the glass-liquid transition at 194 K (191 K in Ref. [18]), (ii) the crystallization event (cr-II formation) with an onset temperature of 220 K. Indications of a crystal to crystal transition (cr-II to cr-I, i.e., from the low-temperature stable phase to the high-temperature one) upon further heating can be observed around 252 K. The cr-I and cr-II are different crystalline phases.

The cr-I phase is triclinic with the structural parameters: a = 8.774 Å, b = 8.944 Å, c = 9.032 Å and α = 95.95°, β = 114.93°, and γ = 101.01° at 180 K [14]. The unit cell contains two molecules. Each $[PF_6]^-$ ion is involved in six different C$-$H$\cdots$ F interaction connecting four different imidazolium cations in the lattice. The structure of the cr-II phase seems not yet resolved.

Endo et al. [20] performed recently experiments with calorimetric and Raman spectroscopy techniques. In heating experiments they identified three crystalline phases. The conformations of the butyl group for these crystalline phases are assigned to gauche-trans (GT), trans-trans (TT), and gauche'-trans (G'T) conformations in lower-energy order. It has been shown that these three conformers coexist in the liquid, supercooled liquid, and glass states. In calorimetric heating experiments with a rate of 5 mK/s, transitions were observed at 192 K (glass transition), 226.5 K (crystallization of crystal α, *GT* conformation, peak-top), 250.3 K and 276 K (two crystal-crystal transitions α to β (*TT* conformation) and β to γ (*G'T* conformation)), and 285.3 K (melting, all of the three conformations appear). The transition at 276 K is hardly to observe since it appears close to the melting peak.

Since the structure of this IL is more complicated and depends on the thermal history of the sample, different PALS cooling and heating runs were performed. As previously, first the cooling run was started at 300 K. Again, each PALS measurement at the given temperature lasted 5 - 6 hours. In the following part the most important lifetime parameters will be discussed.

a) First cooling (c1)

The *o*-Ps lifetime τ_3 decreases almost linearly from 3.0 to 2.35 ns when decreasing the temperature from 300 K to 235 K (figure 7.24). Between 235 and 230 K a sharp jump to 1.50 ns occurs which is linked with an increase of I_3 from 15% to 27% (figure 7.25). At temperatures below the jump, τ_3 shows only

a slight decrease to 1.40 ns at 150 K while I_3 decreases linearly to 21%. This jump of the lifetime parameters at $T = 233 \pm 3$ K can be attributed to the crystallization of the supercooled liquid. The low value of τ_3 mirrors the dense packing of the crystalline state and the high value of I_3 can be interpreted as an indication of the reduced solvation of e^+ due to formation of hydrogen bonds C–H··· F in the crystal.

b) First heating (h1, after the cooling run)

The parameters τ_3 and I_3 remain on the level of the crystallized sample up to a temperature of 235 K. Between 235 K and 250 K a transition occurs and the positron lifetime spectrum shows indications of an additional, longer component. A four-term analysis was performed, but σ_3 and σ_4 must be fixed to zero to reduce the statistical scatter of the analyzed parameters. The results are the following. In this temperature interval, τ_3 decreases from 1.50 ns to 1.20 ns while I_3 drops off from 29% to 17%. The second, longer o-Ps lifetime has values τ_4 between 3.2 ns and 4.3 ns (with a mean of 3.8 ns at 280 K, figure 7.24) and a weak intensity of 1.9 – 2.5% (figure 7.25). In the temperature range between 250 K and 280 K τ_3 stays constant at 1.20 ns while I_3 shows an increase from 16% to 22.5%. Between 280 K and 285 K the lifetime parameters jump back to the values of the liquid, $\tau_3 = 3.0$ ns and $I_3 = 13.5\%$, and remain here. This is in agreement with the melting temperature from DSC, $T_m = 282$ K [10].
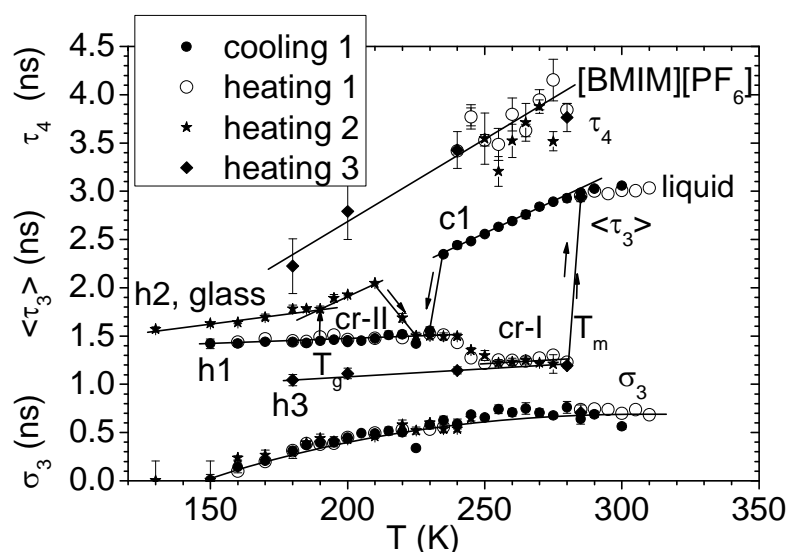

Figure 7.24 The mean, $<\tau_3>$, and the standard deviation, σ_3, of the o-Ps lifetime distribution as a function of temperature T during cooling and heating of [BMIM][PF$_6$]. τ_4 shows an additional o-Ps lifetime, which appears after transformation of the cr-II into the cr-I phase.

c) Second heating (h2, after fast cooling the sample from 300 K to 130 K)

The cooling of the sample inside the PALS device from the liquid state at 300 K to 130 K took about 30 minutes (5 K/min). The lifetime spectrum shows at 130 K three components with τ_3 = 1.57 ns being slightly larger than that for the crystallized state (1.42 ns). I_3 =14.0% corresponds to the value of the liquid and is clearly smaller than in the crystallized state (21.5%). The small I_3 values can be attributed to the reduced Ps formation as consequence of the solvation of e^+ by anions. From this observation one can conclude that the sample remains amorphous and is in the glassy state at 130 K as has been found also in DSC cooling experiments (figure 7.23). When increasing the temperature, τ_3 shows a slight rise with an increase in the slope at the glass transition temperature of T_g(PALS)= 188 $\pm$ 3 K in agreement with DSC experiments (T_g(DSC) = 191 $-$ 194 K [10, 17, 18]).

Between 210 K and 225 K, τ_3 and I_3 go down and up respectively to the level of the crystallized sample (1.50 ns, 27%). This change can be attributed to cold crystallization of the sample in agreement with T_{onset} = 220 K from DSC [17] (230 K in Ref. [10]). The lifetime parameters stay at their level up to 240 K and exhibit between this temperature and 255 K the transition to the state observed already in the first heating run (τ_3 = 1.20 ns, I_3 = 28%).
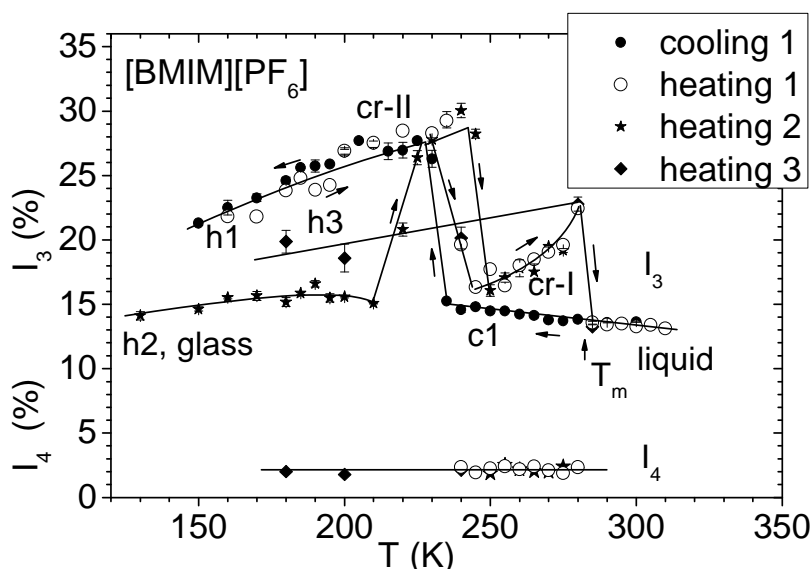

Figure 7.25 As for figure 7.24, but the two *o*-Ps intensities I_3 and I_4.

Following the work of Triolo et al. [17], the phase which is formed during cold crystallization of the quenched sample at 210 - 225 K is cr-II. It is characterized by τ_3 = 1.50 ns and I_3 = 27% (230 K). Obviously, this phase is also formed

during the crystallization in the cooling run at 225 to 230 K. This process was not observed before. During heating the cr-II phase transforms at temperatures between 240 - 255 K to the crystalline phase cr-I ($T_{transition}$(DSC) = 252 K [17]). τ_3 lowers to 1.20 ns and a longer o-Ps lifetime of ~3.8 ns with a small intensity of ~2% appears. This lifetime component can be attributed to larger vacancy-type defects, such as voids and/or grain-boundaries, which can appear due to the internal deformation of the sample during the cr-II to cr-I transition. As shown by Triolo et al.[17], the cr-I phase is also formed when holding the liquid sample for a longer period at 260 K, that is above the cr-II to cr-I transition.

There are two possible interpretations of the lowering of the lifetime τ_3 from 1.50 ns to 1.20 ns at the cr-II to cr-I transition at 210 – 255 K. The low τ_3 may mirror the more dense crystalline packing in cr-I than in cr-II, $\tau_3 = \tau_{Ps,cr-I} = 1.2$ ns. In this case it is assumed that the fourth component τ_4 comes from o-Ps directly formed at vacancy defects. The alternative explanation is that o-Ps particles are first formed in the crystalline phase cr-I. A fraction of them may diffuse to the vacancy defects and get trapped there and annihilates. In this case the third lifetime can be expressed by

$$\tau_3 = 1/(1/\tau_{Ps,cr-I} + \kappa_{Ps,tr}) \qquad (7.4)$$

where $\tau_{Ps,cr-I}$ is the true o-Ps lifetime in the cr-I crystal and $\kappa_{Ps,tr}$ is the trapping rate of Ps by vacancy defects. Usually, it is assumed that Ps trapping is diffusion-limited, then the trapping rate is given by $\kappa_{Ps,tr} = 4\pi D_{Ps} \times r_{trap} \times N$ [21]. Here r_{trap} is the radius of the trap, N is its volume concentration, and D_{Ps} is the Ps diffusion coefficient. In crystals D_{Ps} has a value of 0.2 cm^2/s while in amorphous materials it is only 10^{-4} cm^2/s [21]. The important point is that now $\tau_3 < \tau_{cr-I}$. The value of τ_4 is characteristic of the vacancy trap and does not depend on $\kappa_{Ps,tr}$, but I_4 would increase with increasing $\kappa_{Ps,tr}$.

It is important to notice that the lowering of τ_3 and the appearance of the extra o-Ps lifetime τ_4 is not observed for crystallized [BMIM][NTf$_2$]. Obviously, these effects are caused by the crystalline-crystalline transition, which does not occur in the latter material.

d) Third heating (h3, after fast cooling the sample from 275 K to 180 K)

The second heating run stopped at 275 K, i.e. before the solid-liquid

transition and the sample was cooled to 180 K. The next heating h3 occurred in large temperature steps. The lifetime parameters τ_3 and I_3 remain on the level of the cr-I phase and no transition to the cr-II phase was observed, which is in agreement with X-ray diffraction data [17]. The o-Ps lifetime τ_4 shows strong temperature dependence and increases from 2.2 ns (180 K) to 3.8 ns (280 K). The nature of this variation is not yet clear. Between 280 K and 285 K the cr-I to liquid transition can be observed as a jump of τ_3 (I_3) to larger (smaller) values.

The dispersion parameter σ_3 of the o-Ps lifetime distribution is shown in figure 7.24. This value decreases with decreasing temperature and disappears at 150 K. The data fixed to $\sigma_3 = 0$ are not plotted in this figure. Surprisingly, there is no clear difference in σ_3 between the supercooled liquid and glassy state on the one side and the cr-II state on the other side. In this respect [BMIM][PF$_6$] differs from [BMIM][NTf$_2$] and [C$_3$MIM][NTf$_2$] (Ref.[13]).
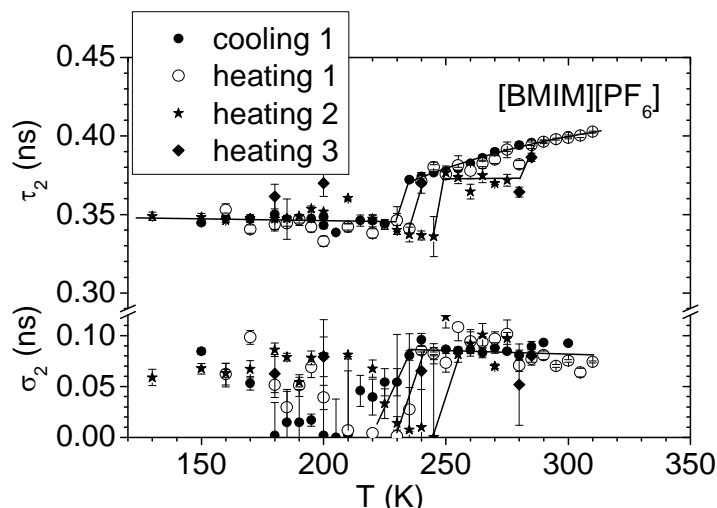
Figure 7.26 As for figure 7.24, but the mean, $<\tau_2>$, and the standard deviation, σ_2, of the e^+ lifetime distribution.

Figure 7.26 shows the e^+ lifetime parameters τ_2 and σ_2. Due to the large statistical scatter the behavior of these parameters is not so clear, however the transitions of supercooled liquid to cr-II (c1) and cr-II to cr-I (h1 and h2) have also a clear effect on these parameters.

In summary, we found that [BMIM][PF$_6$] stays in the amorphous, supercooled liquid or glassy state when cooling quickly from the liquid at 300 K to 130 K. During heating the o-Ps lifetime shows the glass transition at T_g(PALS) = 188 K and a cold crystallization at 210-224 K by an abrupt lowering

of the o-Ps lifetime τ_3 and increase of the o-Ps intensity I_3. The low lifetime mirrors the dense packing of the crystal compared with the amorphous state. The increased I_3 is due to the reduction of the solvation of e^+ [20], the Ps precursor, as consequence of hydrogen bond formation in the crystal [14]. The formed phase is interpreted as cr-II crystal. This phase is also formed in the cooling run at 230 – 235 K. The transformation of the cr-II to the cr-I phase is observed as a further lowering of the o-Ps lifetime τ_3 from 1.50 ns to 1.20 ns and the appearance of a second, longer o-Ps lifetime τ_4 of ~3.8 ns. This lifetime is attributed to vacancy-type defects and/or grain boundaries which may be formed during the crystalline phase transition.
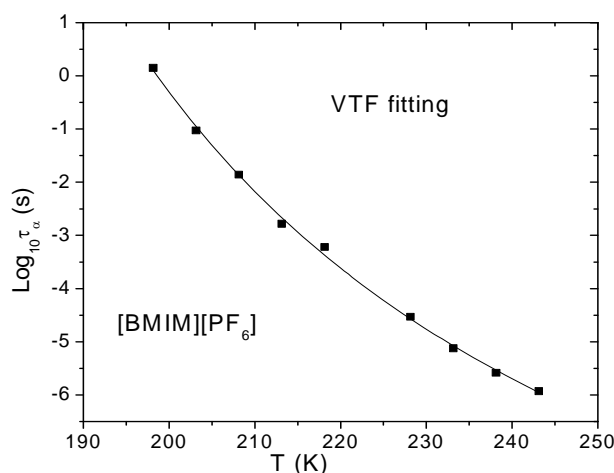
Figure 7.27 VFT fits to the α-relaxation for [BMIM][PF$_6$] of dielectric spectroscopy experiment data.

A VFT fit from dielectric spectroscopy data (figure 7.27) delivers the parameter $\log_{10}\tau_0$ = -14.78, $B' = 977.12$ and $T_0 = 132.49$. So the temperature $T(\tau_\alpha = \tau_{max\_o\text{-Ps}} = 3$ ns) = 288 K, about 5 K higher than T_k.
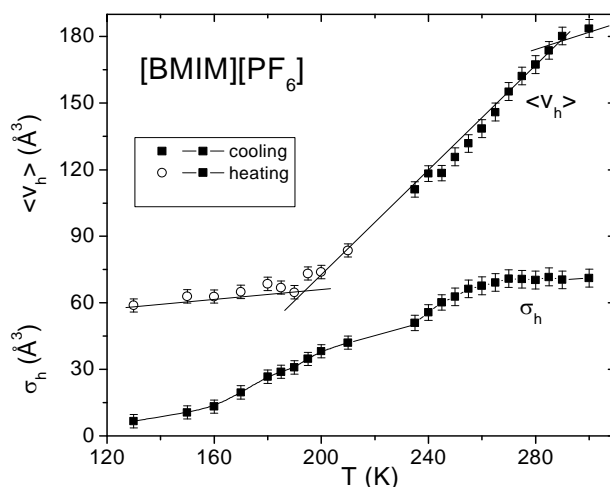

Figure 7.28 Number-weighted mean $<v_h>$ and standard deviation σ_h of the hole size calculated from positron lifetime.

The temperature dependence of $<v_h>$ and σ_h in amorphous state (glass, supercooled liquid and true liquid) is exhibited in figure 7.28. The $<v_h>$ linearly changes with temperature from 65 Å^3 to 180 Å^3 with a slope change at T_g and levels off at T_k like positron lifetime.

Comparison between the specific total volume from PVT experiment under 0 MPa and the mean hole volume from PALS experiment gives a specific hole density $N_h' = 0.376 \times 10^{21}$ g^{-1} and the occupied volume V_{occ} 0.6670 cm^3/g. The Sanchez-Lacombe fitting of the PVT experiment gives V_{occ} with the value 0.6880 cm^3/g, in agreement with the value obtained from PALS.
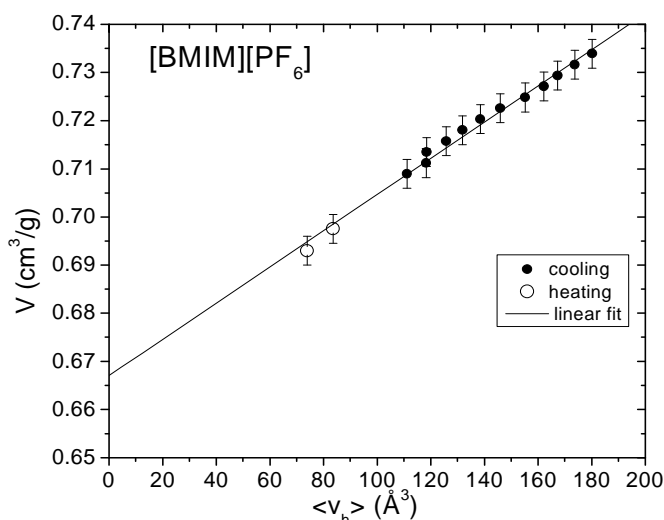
Figure 7.29 Plot of the specific volume from PVT experiment under 0 MPa vs the mean hole volume at supercooled liquid state. The line is a linear fit of the data.

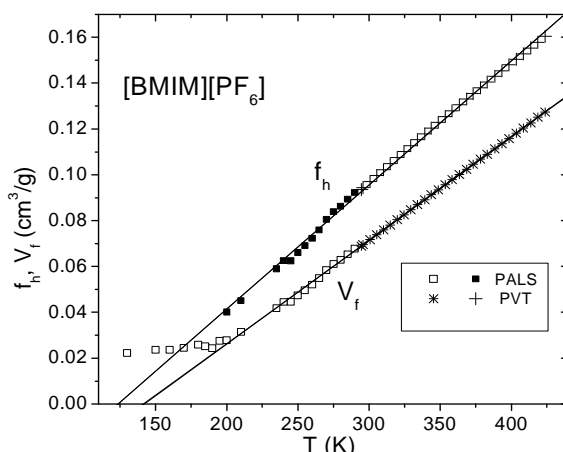A Schottky equation fit of f_h with the data in figure 7.30 delivers $A = 0.55247$ and $H_h = 4.36$ kJ/mol.

Figure 7.30 Temperature dependence of specific free volume V_f and free volume fraction f_h.

7.3.5 1-Butyl-3-methylimidazolium chloride [BMIM][Cl]

[BMIM][Cl] is a prototype ionic liquid with a melting point above room

temperature. This material shows crystal polymorphism [22-27]. Two polymorphs are designated as Crystal (1) and (2). Usually the more stable Crystal (1) phase is formed. Figure 7.31 shows the behavior of the molar heat capacity for the glass-liquid and Crystal (1) phase derived from adiabatic calorimetry [26]. The glass phase was produced by cooling the liquid at a rate of ca. 2 K/min down to 5 K. During heating a glass transition appeared around $T_g = 225$ K. The Crystal (1) was produced by cooling the sample down to 200 K and then annealing it for a day at around 290 K. This phase fused at $T_m = 341$ K accompanying a long low-temperature tail starting from ca. 240 K. The low-temperature tail was attributed to the gradual change of conformation of the butyl-group. The transitions follow the $T_g/T_m = 2/3$ law.
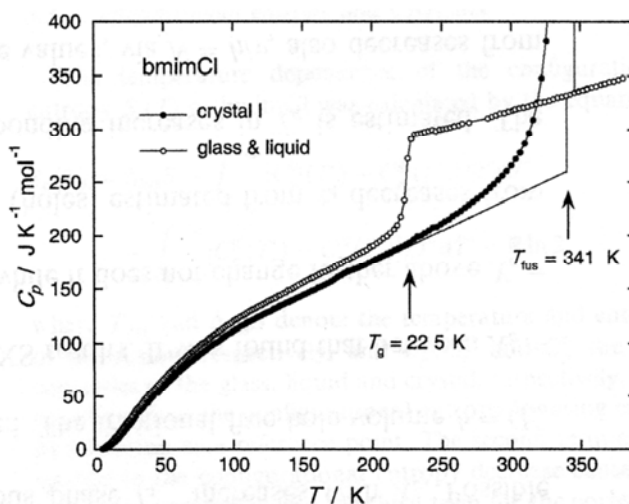

Figure 7.31 Molar heat capacity of the glass-liquid phase (open circles) and Crystal (1) phase (close circles) of [BMIM][Cl](Ref.[26]).

Raman spectroscopy showed that two types of crystals denoted as Crystal (1) and Crystal (2) are formed when cooling the liquid to 255 K and keeping it for 48 h [22]. Crystal (2) dominated in this procedure, but was converted to Crystal (1) when leaving the sample for more than 24 h at dry-ice temperature. Therefore it was concluded that Crystal (2) is a metastable form and Crystal (1) is the stable form at dry-ice temperature. Using X-ray powder diffraction investigation it was shown that both modifications have distinct crystal structures. It was also noted that the continuous background in the X-ray powder pattern is higher in Crystal (2) than in Crystal (1), indicating that Crystal (2) contains more disordered structures than Crystal (1). The [BMIM]$^+$ cation may appear in two rotational isomers: in the trans-trans configuration and in the gauche-trans configuration [24]. It was found that in Crystal (1) only the

trans-trans configuration occurs. In the melt of [BMIM][Cl], like for [BMIM][BF$_4$] (Ref. [24]), both rotational isomers appear, which explains the disorder of the liquid.

Single crystal X-ray diffraction has been used to determine the structure of the crystal polymorphs. Saha et al.[23] determined the structure of Crystal (1) grown from the melt at room temperature to be monoclinic with a = 9.982 Å, b= 11.590 Å, c = 10.077 Å, β = 121.80 °, V= 990.8 Å^3, Z = 4, and ρ_{calc} = 1.17 g/cm^3. The chemical formula is C$_8$H$_{15}$N$_2$Cl and M = 174.67.

Nishikawa et al.[27] studied in detail the melting and freezing behavior of Crystal (1) and Crystal (2), where Crystal (2) was found to have an orthorhombic structure. This structure was studied by single crystal X-ray diffraction by Holbrey et al.[25], but denoted as form (*I*). It has the lattice parameters a = 10.113 Å, b = 11.411 Å, c = 8.3285 Å, V= 961.1 Å^3 (at T = 171 K), and Z = 4. The cation has four close anions at, or below, the van der Waals distance, and three further with slightly larger distances, forming C-H⋯Cl bonds. The shortest contact, to the C(2)-H hydrogen, results in an almost linear hydrogen bond (2.57 Å, 161°). DSC shows melting of this crystal at 339 K.
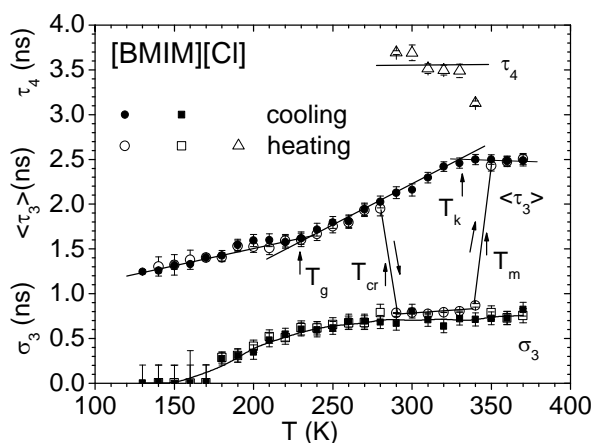

Figure 7.32 The mean, <τ_3>, and the standard deviation, σ_3, of the o-Ps lifetime distribution as a function of temperature T during cooling and heating of [BMIM][Cl]. τ_4 shows an additional o-Ps lifetime which appears after crystallization.

Figures 7.32 to 7.34 show the results of the PALS experiment. During cooling [BMIM][Cl], the mean o-Ps lifetime <τ_3> shows a behavior which is typical for amorphous materials (figure 7.32). From this behavior one may conclude that the sample remains in the amorphous state although the cooling rate is rather small (6 h per measured point). The <τ_3> decreases from 2.50 ns

at 370 K to 1.25 ns at 130 K. The glass transition appears at T_g(PALS) = 230 ± 5 K in agreement with calorimetry [26]. Analogously to the o-Ps lifetime $<\tau_3>$, the mean e^+ lifetime $<\tau_2>$ shows the glass transition at the same temperature, while the width of the e^+ lifetime distributions, σ_2, goes continuously down (figure 7.34). The intensity of the o-Ps lifetime component, I_3, is almost constant at 13% (figure 7.33).

The same behaviour as during cooling can be observed in the heating run, performed after cooling, up to a temperature of 280 K. Between 280 K and 290 K a sharp transition can be observed in all parameters. The $<\tau_3>$ drops down from 2.50 ns to 0.80 ns. A similar effect also occurs for $<\tau_2>$. As previously, this behaviour can be attributed to the cold crystallization of the supercooled liquid.
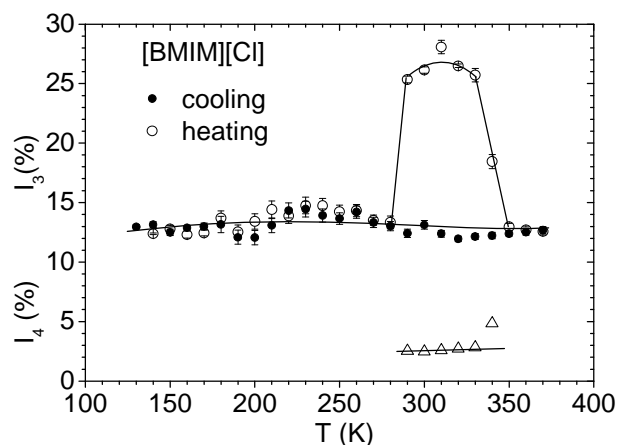

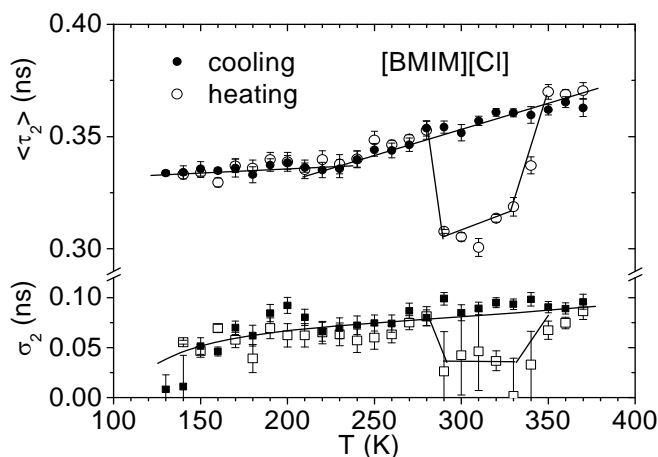**Figure 7.33 As for figure 7.32, but the two o-Ps intensities I_3 and I_4.**

Figure 7.34 As for figure 7.32, but the mean, $<\tau_2>$, and the standard deviation, σ_2, of the e^+ lifetime distribution.

As found for [BMIM][PF$_6$], the fit of the lifetime spectra was sufficient only when allowing four lifetime components. During the fits the dispersion parameters σ_3 and σ_4 were set to zero to reduce the scatter in the analysed

parameters. A second, longer *o*-Ps lifetime appeared with τ_4 = 3.55 ns in the average and an intensity of I_4 = 2.5%. This component can be attributed to *o*-Ps annihilation at voids and/or grain boundaries. Holbrey et al. [25] discussed that, because both crystalline polymorphs of [BMIM][Cl] have distinct and non-mixing crystal lattices, their formation of an eutectic liquid region below the melting points of both polymorphs might be anticipated from the competition between the two crystalline forms. $<\tau_3>$ = 0.80 ns is a rather low *o*-Ps lifetime. As for [BMIM][PF$_6$], it can be explained by very dense packing of ions in the Crystal (1) phase, and/or by the trapping of *o*-Ps, formed in the crystal, to the vacancy defects (compare equation (7.4)). The decreases of $<\tau_2>$ and σ_2 during crystallization may indicate the rather dense packing of this crystal phase.

The low value of I_3 = 13% in the true and supercooled liquid including the glass can be attributed to a solvation of e^+ by the Cl$^-$ anions, which reduces the Ps formation probability. In the crystallized material the anions are fixed in C-H···Cl bonds, which reduces or nullifies the solvation and increases the Ps formation. This leads to the increase of I_3 from 13% to 25%. In the temperature range between 330 and 350 K all parameter change to the values of the liquid.

In summary, the PALS data show that [BMIM][Cl] remains in the amorphous state (supercooled liquid, glass) during slowly cooling. During heating, it shows the glass transition at 230 K and cold crystallization at 280 - 290 K. The *o*-Ps lifetime drops down, and a second, longer *o*-Ps lifetime τ_4 appears, which can be attributed to vacancy-type defects. The melting occurs at 330 - 350 K where all lifetime parameters recover to the values of the liquid.
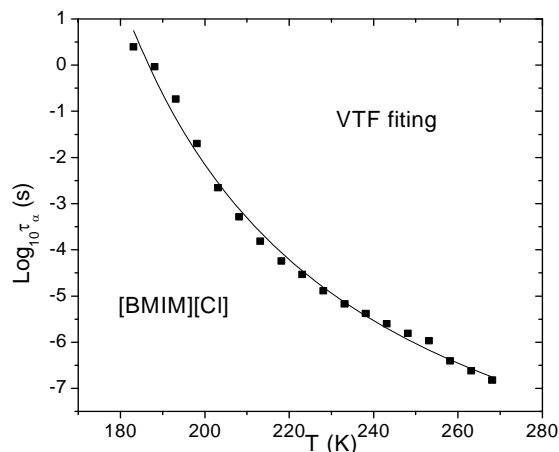

Figure 7.35 VFT fits to the α-relaxation for [BMIM][Cl] of dielectric spectroscopy experiment data.

A VFT fit from dielectric spectroscopy data (figure 7.35) delivers the parameter $\log_{10}\tau_0$ = -11.60, B' = 677.80 and T_0 = 128.23. So the temperature $T(\tau_\alpha = \tau_{\text{max\_o-Ps}} = 2.5$ ns) = 354 K is about 10 K higher than T_k.

The temperature dependence of $<v_h>$ and σ_h in amorphous state (glass, supercooled liquid and true liquid) during cooling is exhibited in figure 7.36. The $<v_h>$ linearly decrease with temperature from 115 Å^3 to 47 Å^3 with a slope change at T_g and levels off at T_k like positron lifetime.

Comparison between the specific total volume from PVT experiment under 0 MPa and mean hole volume from PALS experiment gives the specific hole density N_h' = 0.584 × 10^{21} g^{-1} and the occupied volume V_{occ} = 0.8822 cm^3/g. The Sanchez-Lacombe fitting of PVT experiment gives V_{occ} with the value 0.9055 cm^3/g, in agreement with the value obtained from PALS.
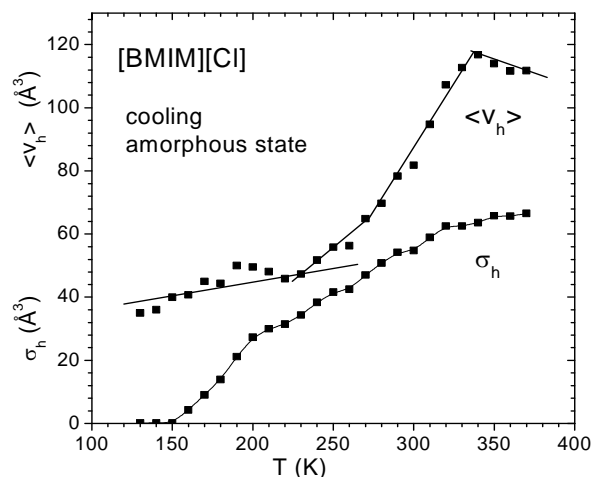

Figure 7.36 Number-weighted mean $<v_h>$ and standard deviation σ_h of the hole size calculated from positron lifetime.
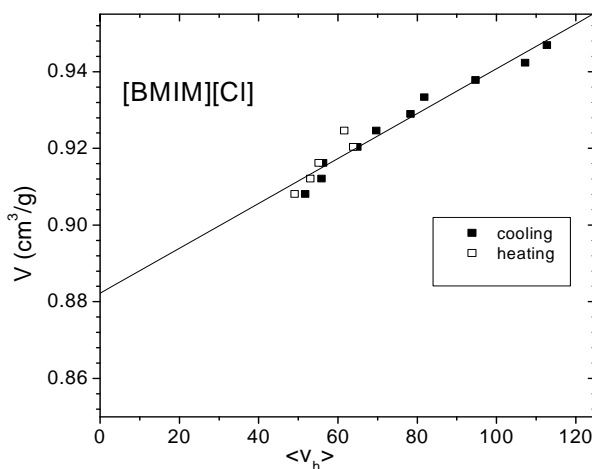

Figure 7.37 Plot of the specific volume from PVT experiment under 0 MPa vs the mean hole volume at supercooled liquid state. The line is a linear fit of the data.
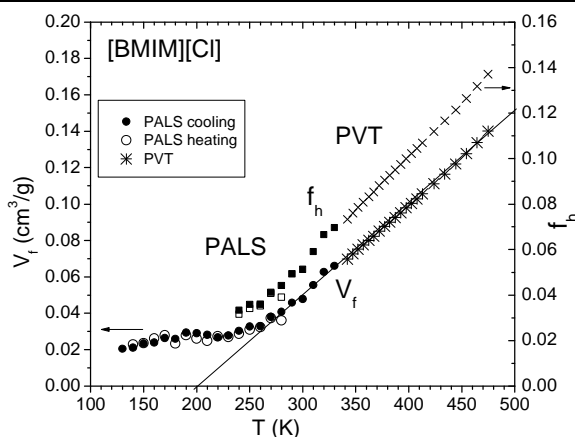
Figure 7.38 Temperature dependence of specific free volume V_f and free volume fraction f_h.

The Schottky equation fit of f_h with the data in figure 7.38 delivers $A = 0.65748$ and $H_h = 6.23$ kJ/mol.

7.3.6 1-Butyl-3-methylimidazolium tetrakis(hexafluoroisopropoxy)borate [BMIM][B(hfip)₄]

The phase transition process for [BMIM][B(hfip)$_4$] is rather simple in the PALS experiment. Lifetime parameters are reversible during cooling and heating. Melting and crystallization occur at 327 ± 3 K. During cooling $<\tau_3>$ drops sharply from 4.35 ns to 2.0 ns at crystallization temperature, and slightly decrease after that in the crystalline solid state. σ_3 shows steadily linear change with temperature and drops a little in true liquid state. $<\tau_3>$ levels off at true liquid and corresponds to a volume of 340 – 350 Å^3.

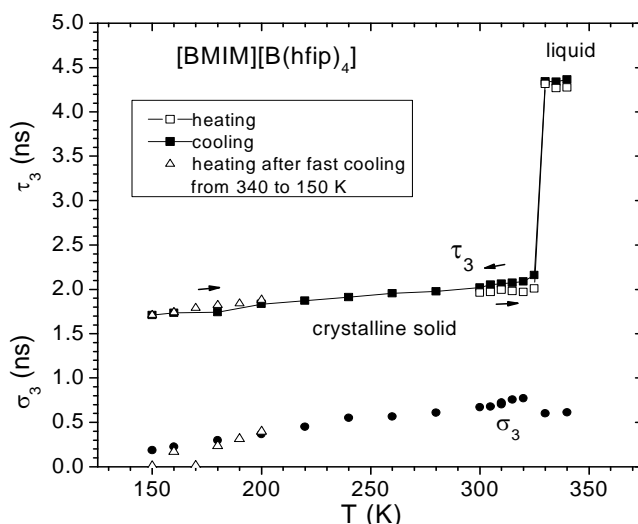**Figure 7.39 The mean, $<\tau_3>$, and the standard deviation, σ_3, of the o-Ps lifetime distribution as a function of temperature T during cooling and heating of [BMIM][B(hfip)₄].**

All the parameters obtained from DSC, PALS, PVT, and dielectric spectroscopy experiments are summarized in table 7.1. The parameters in this table are: T_g(K)(DSC), T_m/T$_{cr}$(DSC): glass transition, melting and crystallization

temperature from DSC; T_g(PALS), T_k: glass transition and "knee" temperature from PALS; V_{occ_sp}(cm^3/g) (PALS): specific occupied volume from PALS (compare with PVT); N_f(10^{21} g^{-1}): specific number density of hole volume; M_A(g/mol): molecular weight; N_M (10^{21}g^{-1}): specific number density of molecule (=N_A/M_A, N_A: Avogadro number); V_{occ}(Å^3): molecular occupied volume (=V_{occ_sp}/ N_M); log(τ_0)(s), T_0(K), B'(DS_VFT): parameters from VFT fitting of dielectric spectroscopy data; A, H_h(kJ/mol) (Schottky): parameters from fitting hole fraction data with Schottky equation; $f_h(T_g)$, $f_h(T_k)$: hole fraction at glass transition and "knee" temperature.

Table 7.1 Summarized parameter from experiment result for the ionic liquids.

[BMIM]$^+$	[Cl]$^-$	[BF$_4$]$^-$	[PF$_6$]$^-$	[OTf]$^-$	[NTf$_2$]$^-$	[B(hfip)$_4$]$^-$
T_g(K)(DSC)	225	188-190	190-194		186	
T_m/T_{cr} (DSC)	341/290		283/220	286/254	271/232	
T_g(PALS)	230 ± 5 K	190±3 K	188 ± 3 K		190±5K	
T_k	335 ± 5 K	280±5 K	285 ± 5 K		270±5 K	
T_g/T_k	0.687	0.679	0.660		0.704	
V_{occ_sp}(cm^3/g) (PALS)	0.8822	0.7574	0.6670		0.6405	
N_f(10^{21} g^{-1})	0.584	0.442	0.376		0.179	
M_A(g/mol)	174.67	226	284.18	288.29	419.37	818.153
V_{occ}(Å^3)(PALS)	256	284	315		446	
N_M (10^{21}g^{-1})	3.4465	2.66372	2.11838		1.43549	
N_f/N_M	0.1694	0.1659	0.177		0.125	
log(τ_0)(s) T_0(K) B' (BDS_VFT)	-11.6 128.23 677.80	-12.89 140.8 581.72	-14.78 132.49 977.12		-11.22 156.44 317.65	
A H_h(kJ/mol) (Schottky)	0.65748 6.23	0.61709 4.78	0.55247 4.36		0.72517 5.54	
$f_h(T_g)$	0.025 (230)	0.030 190	0.034 188		0.022 190	
$f_h(T_k)$	0.070 (335)	0.079 (280)	0.088 (285)		0.061 (270)	

7.4 Hole volumes and their distributions

In this section the results from PALS experiment are compared with the molecular and ionic volumes calculated from X-ray diffraction data in order to clear up whether both data sets show a systematic correlation. For a 1:1 salt $[A]^+[X]^-$ the molecular volume V_m is defined as the sum of the ionic volumes $V([A]^+)$ and $V([X]^-)$. From the experimental unit cell dimensions of X-ray crystal structures, V_m, and the ionic volumes are calculated by [15, 28]:

$$V_m = V([A]^+) + V([X]^-) = V_{cell}(A^+X^-)/Z. \tag{7.5}$$

here V_{cell} is the volume of the unit cell of the crystal and Z is the number of formula units in the cell. If the ionic volume of one of the ions is known, (e.g. halide anions or alkaline metal cations), it may be used as a reference ion to determine the ionic volume of the other ion in the structure. The volumes V_m, $V([A]^+)$ and $V([X]^-)$ are taken from Refs. [15, 28, 29]. $V([A]^+) = V([BMIM]^+) = 196$ Å^3 and the $V([X]^-)$ vary between 47Å^3 ($[Cl]^-$) and 556 Å^3 ($[B(hfip)_4]^-$). The molecular volumes $V_m = V(A^+X^-)$ change from 240 Å^3 to 759 Å^3.

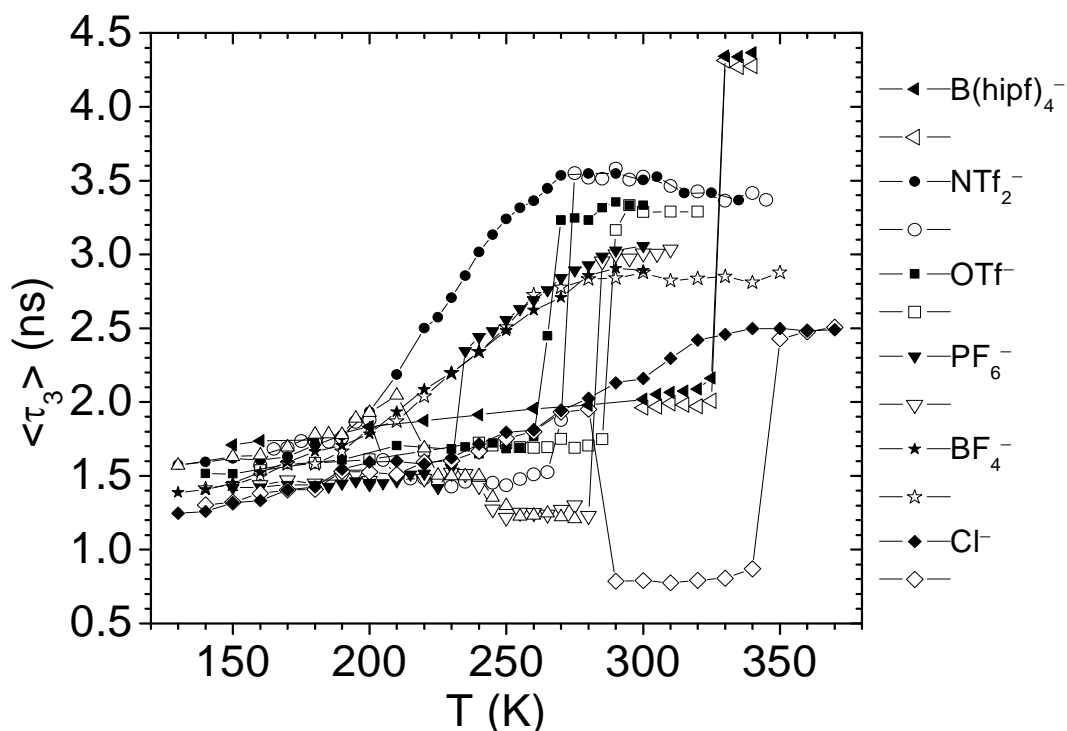**Figure 7.40 Comparison of the mean o-Ps lifetime $<\tau_3>$ for the ionic liquids under investigation. Filled symbols: cooling, empty symbols: heating.**

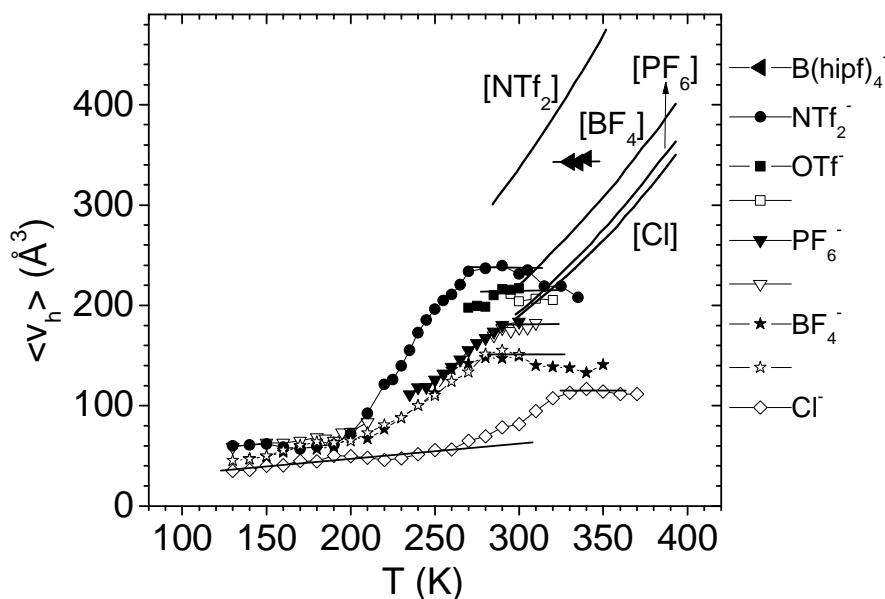**Figure 7.41 Comparison of the mean hole volumes <v_h> for the liquid or supercooled liquid and glassy states of the ionic liquids under investigation. Filled symbols: cooling, empty symbols: heating. Free volume calculated by Fürth theory [30] is shown as line in the graph.**

Figure 7.40 and 7.41 show the PALS results: the mean o-Ps lifetime <τ_3> and the (number weighted) mean local free or hole volume <v_h>. The hole volume was calculated only for those data points where the sample is in disordered states, these are the liquid, supercooled liquid and glassy states. Only for these states it is certain that the hole model can be applied. Table 7.2 includes the mean o-Ps lifetime, <τ_3>, and the mean hole volume, <v_h>, for the liquid (maximum values from figure 7.40 and 7.41), for the glass at 140 K, and for the crystalline solid.

Table 7.2 X-ray molecular volumes $V_m = V(A^+X^-)$ and from these derived anion volumes $V(X^-)$ for a series of [BMIM]-based (crystallized) ionic liquids (top part). The volume of the cation is $V([BMIM]^+) = 196\pm21$ Å^3 (From the collection given in Refs. [15, 28]. The ion volumes for [Cl]$^-$, [BF$_4$]$^-$, and [PF$_6$]$^-$ were taken from Ref. [29]). The bottom part shows the PALS results: the mean o-Ps lifetime, <τ_3>, and the mean hole volume, <v_h>, for the liquid (maximum values from figure 7.40 and 7.41), for the glass at 140 K, and for the crystalline solid. Molecular occupied volume V_{occ} were taken from Table 7.1.

[BMIM]$^+$	[Cl]$^-$	[BF$_4$]$^-$	[PF$_6$]$^-$	[OTf]$^-$	[NTf$_2$]$^-$	[B(hfip)$_4$]$^-$
$V_m = V(A^+X^-)$ (Å^3)	240	269±30	305±29	327±36	428±36	759
$V([X]^-)$ (Å^3)	47±13	73±9	107±10	129±7	232±15	556
liquid (<τ_3>, ns; <v_h>, Å^3) [1]	2.50 115±5	2.85 150±5	3.03 180±5	3.28 215±5	3.505 240±5	4.35 340±5
glass, 140 K (τ_3, ns ; <v_h>, Å^3)) [1]	1.25 36±3	1.40 47±3	1.60 61±3		1.60 61±3	
crystal (<τ_3> ns) [1]	0.78	-	1.50/1.25	1.70	1.45	1.70 - 2.00
V_{occ}(Å^3) (PALS)	256	284	315		446	

1) The lifetimes have all a mean error of not more than ±0.05 ns.

Free volume calculated by Fürth's theory [30] (section 4.2) from surface tension [31, 32] is also displayed in figure 7.41 as line for the ionic liquids. For [BMIM][NTf$_2$], the hole volume from Fürth's theory fits well with the result of PALS experiment. For [BMIM][Cl] the deviation from the two method is quite large, but still in the same dimension.

It can be observed that $<\tau_3>$ and $<v_h>$ grow systematically with the volumes V_m and $V([X]^-)$, respectively. For a more quantitative discussion figure 7.42 plots the hole volume $<v_h>$ in the liquid and in the glass states (empty circles) as function of the molecular volume $V_m = V(A^+X^-)$. The data can be roughly fitted by straight lines constrained to pass zero, with slopes of $d<v_h>/dV_m = 1.00\pm0.07$ and 0.33 ± 0.026, respectively. The hole volume of [BMIM][B(hfip)$_4$] deviates mostly from the straight line and is lower than the fit. A better fit is obtained by a quadratic function. Figure 7.43 shows the same hole volumes as a function of the anionic volume $V([X]^-)$. Here linear fits are worse, and quadratic fits to the data are shown.
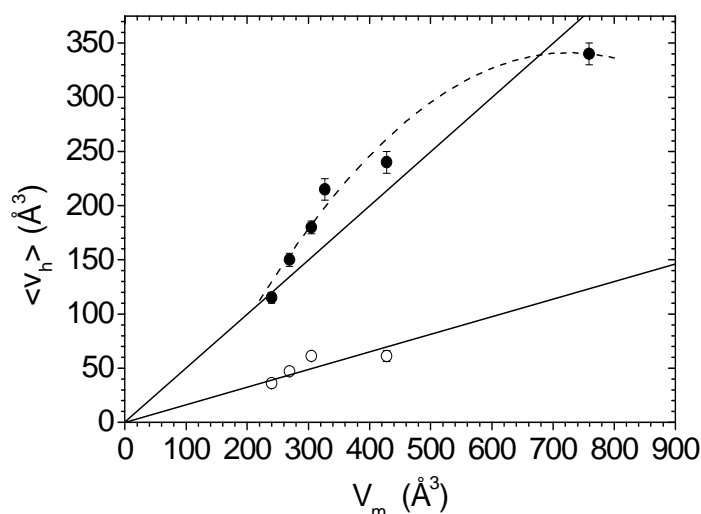

Figure 7.42 The hole volumes of various ILs in the liquid (filled circles) and in the glass (140 K, empty circles) states as function of the molecular volume $V_m = V(A^+X^-)$. The straight lines are linear fits constrained to pass zero, the dashed line shows a quadratic fit.

The correlation between the mean volume of gaps between the particles, in the disordered state of the ionic liquids, $<v_h>$, and the size of particles forming the material, $V([X]^-)$ and V_m ($V_m/2$ can be considered as mean volume of both particles (cation and anion) forming the IL), can be discussed as follows. All ions of the ionic liquids of our work have a more or less three dimensional shape. In a dense packing the gaps between the ions grow with the

geometrical size of the ions. The gaps are small in the glassy state of the ionic liquids ($<v_h>$ at 140 K) and show an only small size distribution (small or disappearing width parameter σ_3 and σ_h). The particle movement (primary relaxation) is frozen. Above the glass transition, particles show a mobility with increasing frequency (analysed by dielectric spectroscopy, for example) and amplitude (analysed by neutron scattering as mean square displacement) resulting in the thermal density fluctuation. Consequently, the empty spaces (holes) between the particles show a size (and shape) fluctuation in space and time. The o-Ps probe makes snap-shots of this fluctuating hole structure and mirrors this as quasi-static hole size distribution. Its mean value, $<v_h>$, and width, σ_h, grow with increasing temperature. At the so-called knee-temperature T_k, which is close to the melting temperature T_m, the frequencies of molecular motion become very high and the hole walls move significantly during the lifetime of o-Ps. This results in an apparent smearing of the hole size and the almost constant behaviour of the o-Ps lifetime. PVT experiments show that the free volume increases continuously with T.
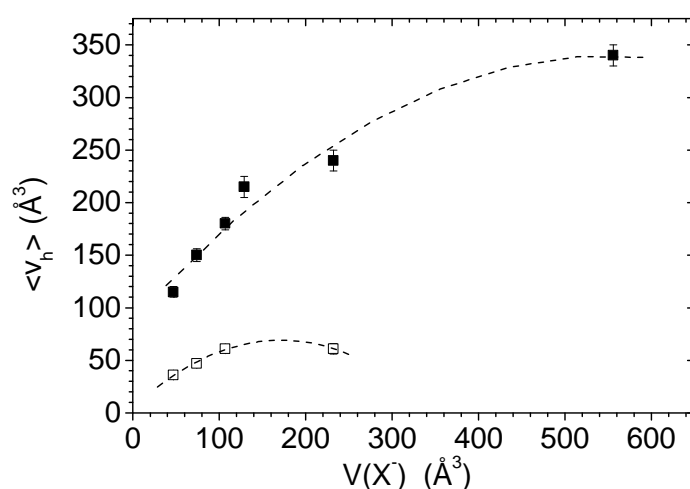

Figure 7.43 The hole volumes of various ILs in the liquid (filled circles) and in the glassy (140 K, empty circles) states as function of the volume of the anion molecular volume $V([X]^-)$. The dashed lines are quadratic fits to the data.

Some of the ionic liquids under investigation cannot be undercooled or show crystallization in the heating run. In the lifetime spectra the formation of the crystalline state is indicated mainly by the distinct lowering of o-Ps lifetime. This shows generally that o-Ps feels a structure which exhibits a more dense packing than the disordered, supercooled state of the same material. Unfortunately, the quantitative description of Ps annihilation in organic crystals

is less developed.

There are different possible types of annihilation sites for Ps in crystalline matter: (i) Ps is in a delocalized Bloch state and moves in the empty spaces between the lattice; Ps is localized (ii) in channel-like free spaces of the lattice, (iii) in interstitial sites of the lattice (octahedral and tetrahedral holes), and (iv) in vacancy-type lattice defects or at interfaces of the crystallites.

From the low value of the *o*-Ps lifetime in crystals, one may conclude that the case (iv) does not play a major role in effecting the value of $<\tau_3>$. However, if the fourth lifetime τ_4 (the second, larger *o*-Ps lifetime) appears, like observed for [BMIM][PF$_6$] and [BMIM][Cl], this lifetime can be attributed to larger vacancy defects and grain boundaries. A lifetime of $\tau_4 = 3.5$ ns ([BMIM][Cl]) and 4.0 ns ([BMIM][PF$_6$]) would correspond to spherical hole size of volume 260 Å^3 and 320 Å^3. This is larger than the holes in the liquid of the corresponding ionic salts. As mentioned earlier, the small lifetime τ_3 for crystals (0.80 ns for [BMIM][Cl], 1.20 ns for [BMIM][PF$_6$] may be the result for trapping of o-Ps formed in crystals at vacancy defects and grain boundaries with a rate $\kappa_{Ps,tr}$. Then τ_3 mirrors not directly the bulk free volume ($\tau_{Ps,cr}$) but is given by $\tau_3 = 1/(1/\tau_{Ps,cr} + \kappa_{Ps,tr})$.

The other ILs do not show the τ_4 component. That means that the formed crystallites seem to be sufficiently perfect, the volume fraction of grain boundaries appears negligibly small, and no thermal vacancies are detected in the crystal before melting. One has also to remark that the *o*-Ps lifetime in the crystalline state is smaller than in the glass of the same material, which shows the compact packing of the crystalline structure.

7.5 Conclusion

Important information of the local free volume in the amorphous (glass, supercooled liquid, true liquid) and crystalline phases of ionic liquids as well as the corresponding phase transitions can be obtained from PALS. The *o*-Ps mean lifetime $<\tau_3>$ and its dispersion σ_3 show different behaviour indicating different phases (smaller values in crystalline phase due to dense packing of the material). The parameters I_3 and e^+ lifetime also respond to phase transition by sharp value change.

The local free volume from PALS displays a systematic relationship with molecular volume and ionic volume and is in good agreement with the Fürth theory [30].

7.6 Reference

1.   Lee, B.S., et al., *Imidazolium Ion-Terminated Self-Assembled Monolayers on Au: Effects of Counteranions on Surface Wettability.* Journal of the American Chemical Society, 2003. **126**(2): p. 480-481.

2.   Rogers, R.D. and K.R. Seddon, *Ionic Liquids--Solvents of the Future?* Science, 2003. **302**(5646): p. 792-793.

3.   Seddon, K.R., *Ionic liquids: A taste of the future.* Nature Materials, 2003. **2**(6): p. 363-365.

4.   Wang, P., et al., *A Binary Ionic Liquid Electrolyte to Achieve ⩾7% Power Conversion Efficiencies in Dye-Sensitized Solar Cells.* Chemistry of Materials, 2004. **16**(14): p. 2694-2696.

5.   Xu, W. and C.A. Angell, *Solvent-Free Electrolytes with Aqueous Solution-Like Conductivities.* Science, 2003. **302**(5644): p. 422-425.

6.   Wasserscheid, P., M. Sesing, and W. Korth, *Hydrogensulfate and tetrakis(hydrogensulfato)borate ionic liquids: synthesis and catalytic application in highly Bronsted-acidic systems for Friedel-Crafts alkylation.* Green Chemistry, 2002. **4**(2): p. 134-138.

7.   Bonhôte, P., et al., *Hydrophobic, Highly Conductive Ambient-Temperature Molten Salts†.* Inorganic Chemistry, 1996. **35**(5): p. 1168-1178.

8.   Fredlake, C.P., et al., *Thermophysical properties of imidazolium-based ionic liquids.* Journal of Chemical and Engineering Data, 2004. **49**(4): p. 954-964.

9.   Tokuda, H., et al., *Physicochemical properties and structures of room temperature ionic liquids. 1. Variation of anionic species.* Journal of Physical Chemistry B, 2004. **108**(42): p. 16593-16600.

10. Jin, H., et al., *Physical properties of ionic liquids consisting of the 1-butyl-3-methylimidazolium cation with various anions and the bis(trifluoromethylsulfonyl)imide anion with various cations.* Journal of Physical Chemistry B, 2008. **112**(1): p. 81-92.

11. Dlubek, G., et al., *Temperature dependence of the free volume from positron lifetime experiments and its relation to structural dynamics: Phenylphthalein-dimethylether.* Physical Review E, 2008. **78**(5): p. -.

12. Schottky, *Über die Drehung der Atomachsen in festen Körpern.* Physik. Zeitschr, 1922. **XXIII**: p. 448.

13. Dlubek, G., et al., *Free volume in imidazolium triflimide ([C₃MIM][NTf₂]) ionic liquid from positron lifetime: Amorphous, crystalline, and liquid states.* The Journal of Chemical Physics, 2010. **133**(12): p. 124502-10.

14. Choudhury, A.R., et al., *In situ Crystallization of Low-Melting Ionic Liquids.* Journal of the American Chemical Society, 2005. **127**(48): p. 16792-16793.

15. Krossing, I., et al., *Why Are Ionic Liquids Liquid? A Simple Explanation Based on Lattice and Solvation Energies.* Journal of the American Chemical Society, 2006. **128**(41): p. 13427-13434.

16. Triolo, A., et al., *Relaxation Processes in Room Temperature Ionic Liquids: The Case of 1-Butyl-3-Methyl Imidazolium Hexafluorophosphate.* The Journal of Physical Chemistry B, 2005. **109**(46): p. 22061-22066.

17. Triolo, A., et al., *Thermodynamics, Structure, and Dynamics in Room Temperature Ionic Liquids: The Case of 1-Butyl-3-methyl Imidazolium Hexafluorophosphate ([bmim][PF6]).* The Journal of Physical Chemistry B, 2006. **110**(42): p. 21357-21364.

18. Kabo, G.J., et al., *Thermodynamic properties of 1-butyl-3-methylimidazolium hexafluorophosphate in the condensed state.* Journal of Chemical and Engineering Data, 2004. **49**(3): p. 453-461.

19. Christopher, H. and et al., *Liquid structure of 1, 3-dimethylimidazolium salts.* Journal of Physics: Condensed Matter, 2003. **15**(1): p. S159.

20. Endo, T., et al., *Phase Behaviors of Room Temperature Ionic Liquid Linked with Cation Conformational Changes: 1-Butyl-3-methylimidazolium Hexafluorophosphate.* Journal of Physical Chemistry B, 2010. **114**(1): p. 407-411.

21. Mogensen, O.E., *Positron Annihilation in Chemistry.* Springer, Berlin, Heidelberg 1995.

22. Hayashi, S., R. Ozawa, and H.-o. Hamaguchi, *Raman Spectra, Crystal Polymorphism, and Structure of a Prototype Ionic-liquid [bmim]Cl.* Chemistry Letters, 2003. **32**(6): p. 498-499.

23. Saha, S., et al., *Crystal Structure of 1-Butyl-3-methylimidazolium Chloride. A Clue to the Elucidation of the Ionic Liquid Structure.* Chemistry Letters, 2003. **32**(8): p. 740-741.

24.   Ozawa, R., et al., *Rotational Isomerism and Structure of the 1-Butyl-3-methylimidazolium Cation in the Ionic Liquid State.* Chemistry Letters, 2003. **32**(10): p. 948-949.

25.   Holbrey, J.D., et al., *Crystal polymorphism in 1-butyl-3-methylimidazolium halides: supporting ionic liquid formation by inhibition of crystallization.* Chemical Communications, 2003(14): p. 1636-1637.

26.   Yamamuro, O., et al., *Heat capacity and glass transition of an ionic liquid 1-butyl-3-methylimidazolium chloride.* Chemical Physics Letters, 2006. **423**(4-6): p. 371-375.

27.   Nishikawa, K., et al., *Melting and freezing behaviors of prototype ionic liquids, 1-butyl-3-methylimidazolium bromide and its chloride, studied by using a nano-watt differential scanning calorimeter.* Journal of Physical Chemistry B, 2007. **111**(18): p. 4894-4900.

28.   Preiss, U.P.R.M., J.M. Slattery, and I. Krossing, *In Silico Prediction of Molecular Volumes, Heat Capacities, and Temperature-Dependent Densities of Ionic Liquids.* Industrial & Engineering Chemistry Research, 2009. **48**(4): p. 2290-2296.

29.   Jenkins, H.D.B., et al., *Relationships among Ionic Lattice Energies, Molecular (Formula Unit) Volumes, and Thermochemical Radii.* Inorganic Chemistry, 1999. **38**(16): p. 3609-3620.

30.   Fürth, R., *On the theory of the liquid state.* Mathematical Proceedings of the Cambridge Philosophical Society, 1941. **37**(03): p. 252-275.

31.   Klomfar, J., M. Souckoká, and J. Pátek, *Surface tension measurements with validated accuracy for four 1-alkyl-3-methylimidazolium based ionic liquids.* The Journal of Chemical Thermodynamics, 2010. **42**(3): p. 323-329.

32.   Ghatee, M.H. and A.R. Zolghadr, *Surface tension measurements of imidazolium-based ionic liquids at liquid-vapor equilibrium.* Fluid Phase Equilibria, 2008. **263**(2): p. 168-175.

Erklärung

Hiermit erkläre ich an Eides Statt, dass ich die vorliegende Arbeit selbständig und ohne fremde Hilfe verfasst und nur die angegebenen Quellen und Hilfsmittel verwendet habe. Ergebnisse anderer wissenschaftlicher Arbeiten wurden als solche gekennzeichnet. Diese Arbeit wurde bisher weder im In- noch im Ausland in gleicher oder ähnlicher Form in einem Prüfungsverfahren vorgelegt. Ich erkläre hiermit, dass ich mich bis zu dem jetzigen Zeitpunkt noch nie um einen Doktorgrad beworben habe.

Halle (Saale), July 2011   Yu, Yang

Curriculum vitae

Family name: Yu

Given name: Yang

Date of birth: 13/07/1982

Place of birth: Changchun, China

Marital status: Single

1989 – 1995: Primary school

1995 – 1998: Junior high school

1998 – 2001: High school

2001 – 2005: University of Science and Technology of China
Bachelor Major of Nuclear and Particle Physics
Modern Physics Department

July 2005: Bachelor of Science in Physics

2005 – 2007: University of Science and Technology of China
Master Major of Nuclear and Particle Physics
Modern Physics Department

2007 – 2009: Positron Annihilation Laboratory
Scientific Department II-Chemistry and Physics
Martin-Luther-University Halle-Wittenberg
Diplom Major of Physics

June 2009: Diplom of Physics

2009 – 2011: Positron Annihilation Laboratory
Scientific Department II-Chemistry and Physics
Martin-Luther-University Halle-Wittenberg
Doctor Major of Physics

Acknowledgement

Publication List:

1. Yang Yu et al., *Phase Transitions in Polymers Containing Long Self-Assembled CH2 Sequences in the Side Chain: A Psitron Lifetime Study.* Materials Science Forum, 2010. **666**: p. 71-74.

2. Dlubek, G., Yu, Yang et al., *Free volume in imidazolium triflimide ([C$_3$MIM][NTf$_2$]) ionic liquid from positron lifetime: Amorphous, crystalline, and liquid states.* The Journal of Chemical Physics, 2010. **133**(12): p. 124502-10.

3. Dlubek, G., Pionteck, J., Yu, Yang et al., *The free volume and its recovery in pressure-densified and CO2-swollen heterocyclic-ring-containing fluoropolymers.* Macromolecular Chemistry and Physics, 2008. **209**(18): p. 1920-1930.